Nonlinear phenomena in ecology

Competition in mixing water and discrete state population dynamics

István Scheuring

Budapest, 2006.

To the memory of my father..

Contents

Chapter 1

Introduction

1.1 The brief history of dynamics

Possibly the development of calculus was one of the most important mathematical inventions in the natural sciences. Working with infinitesimal values Isaac Newton was the first scientist who used differential equations to handle dynamical processes in the mid 17th century. He demonstrated the solution of the problem of calculating the motion of earth around the sun. However extending the analytical method used in this two-body problem to the three-body system is hopelessly difficult. While generations of physicists and mathematicians have tried to solve the three-body problem analytically it became clear that the only analytically tractable problems (with the exception of some special cases) are linear or the nearly so. Consequently, till the end of 19th century, textbooks of physics concentrated on the linear or closely linear phenomena, suggesting indirectly that the world is at least closely linear and the dynamics can be described quantitatively.

Henri Poincaré's pathbreaking work changed the attitude. Poincaré focused on the qualitative nature of the motion rather than finding a quantitative solution to the three-body problem. He did not want to determine the exact positions and velocities of planets at all times (quantitative description), but rather he asked whether the three-body system is stable or can bodies fly off to infinity. He introduced a new geometric approach to handle this question. He was able to show that the motion can be aperiodic and depends sensitively on the initial conditions in this deterministic model, so that the motion is complex and potentially unpredictable (Poincaré 1894). Poincaré's methods were extended by Birkhoff (Birkhoff 1913) and later by Kolmogorov, Arnol'd and Moser. Papers by Kolmogorov Arnol'd and Moser have proven that the unpredictable random motion is general in all non-linear

mechanical system (Kolmogorov 1957; Arnold 1963; Moser 1962). Beside these important mathematical results, the qualitative analysis of nonlinear dynamical systems has become increasingly widespread in physics and have been used in theoretical ecology since the beginning of the last century. For example, Alfred John Lotka and Vito Volterra, the most prominent founders of mathematical ecology, used this method to analyse dynamics of interacting populations (Lotka 1925; Volterra 1925).

The emergence of computers in the mid of 20th century gave the opportunity to study dynamical systems "experimentally", that is to solve numerically any kind of dynamical system. Studying a simplified model of atmosphere dynamics numerically, Edward Lorenz realized that the solution never tends to some simple motion such as fixed point or some periodic attractor - instead variables fluctuate in an irregular manner. However, as he pointed out the motion is not totally random: there is a typical geometric structure of the motion in the phase space of the system (Fig. 1.1). Further, he has shown that the motion is inherently unpredictable - beginning simulations with slightly different initial conditions result totally different states after a very short time (Lorenz 1963).

Lorenz's experiment generated exploring evolution in this field. Numerous computer simulations and experiments conducted in the 70's showed that low dimensional deterministic dynamical systems can behave in a complicated random manner. Deterministic chaos – as this complex behavior is named – (Li & Yorke 1975) dramatically changed the approach in several fields of science, noteably hydrodynamics and in ecology. Ruelle and Takens studied the onset of turbulence based on chaos theory in 1971 (Ruelle & Takens 1971). Some years later Robert May wrote several keystone papers about the possibility of chaos in simple deterministic models of population biology (May 1976). Since then it has became clear that chaos is common in hydrodynamics, and an increasing number of traces also imply chaotic dynamics in ecology.

1.2 Characteristics of nonlinear dynamics

In the previous historical introduction we used many terms – such as dynamical system, linear vs. nonlinear system, phase space, chaos, etc. This can not be problem for an expert of nonlinear dynamics, but are likely unfamiliar to the general reader. So in this section we briefly explain the most important notions without mathematic accuracy and summarize some general characteristics of nonlinear dynamical systems.

When we speak about dynamics we think about the time evolution of

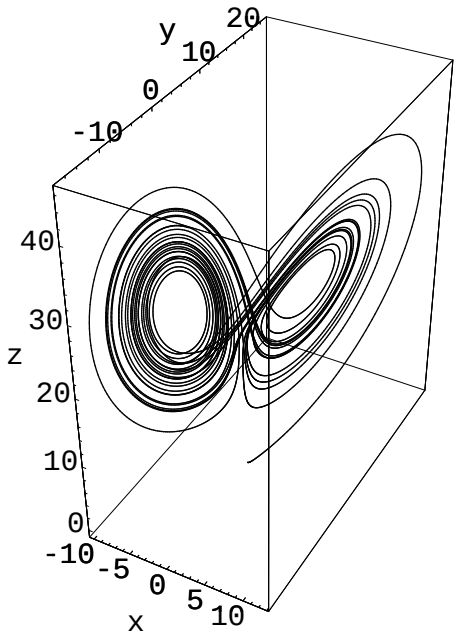

Figure 1.1: The strange attractor of the Lorenz model in the phase space of the variables denoted by x, y and z.(The variables generated by the following differential equation system: $\dot{x} = -3(x-y)$, $\dot{y} = -xz+26.5x-y$, $\dot{z} = xy-z$, $x(0) = y(0) = z(0) = 1$)

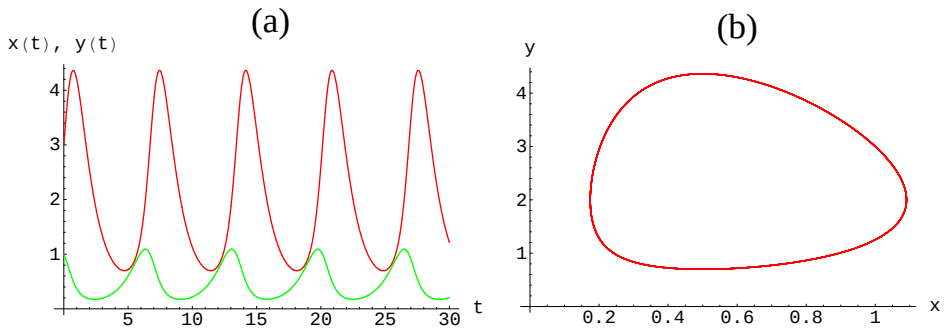

Figure 1.2: Time evolution of a dynamical system defined by variables $x(t)$ (green), $y(t)$ (red) visualized by variables vs time plot (a), and by the phase space method (b). The dynamics is periodic as can be seen in figure (a) or the motion follows a limit cycle as indicated by figure (b).(We used the classical Lotka-Volterra system for demonstration, that is $\dot{x} = x(a - by)$, $\dot{y} = y(-c + dx)$, where $a = 1$, $b = 0.5$, $c = 1$, $d = 2$, $x(0) = 1$, $y(0) = 3$.)

some defined variables. So our main question is how the state of the system changes in time: does it tend to a rest (fixed) point, does it move periodically along a limit cycle or does it follow a complex chaotic motion, etc.? Differential and difference equations are typical examples of dynamical systems, or more precisely they are well-known mathematical tools for describing dynamics observed in Nature. So in the following when we use the term dynamical systems we identify them with differential or difference equations, although for example cellular automata are dynamical systems too. In linear dynamical systems the changes of the variables (e.g. the time derivatives in differential equations) depend only on the linear combinations of the variables. In *every other* cases we speak about nonlinear dynamical systems.

When we are interested in the behavior of a defined dynamical system we might ask the exact state of the system at every time assuming that we knew the initial state of the system. This is the case when we analyse the system quantitatively, or simply when we "solve" the differential equation by integration. However, as mentioned earlier only linear and some other specific nonlinear dynamical system can be solved analytically, thus a quantitative description is generally impossible. Qualitative characterization focuses on the long term behavior of the system, and we are interested in only the generic features of the motion. To visualize dynamical behavior, the motion is depicted in the space of the variables, that is in the phases space of the motion (Fig. 1.2). There are typical attracting objects in the phase space of nonlinear systems. There can be stable fixed points which attract the system

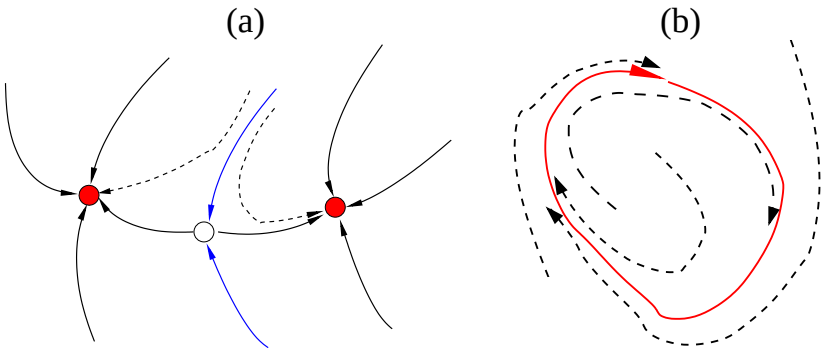

Figure 1.3: Schematic pictures of some typical type of attractors. (a) The system tends to one of the stable fixed points (red circles) depending on the initial conditions. Stable fixed points' basin of attractions are separated by the stable manifold (blue line) of the unstable (or hyperbolic) fixed point (empty circle). Dashed lines denote typical trajectories, solid lines are the invariant manifolds of the fixed points. (b) A limit cycle (red line) with some typical trajectories (dashed lines) approximate to this attractor .

from their basin of attraction (Fig. 1.2 a). The attractor of the motion can be a limit cycle (Fig. 1.2 b), or the motion can be chaotic by following a so called strange attractor in the phase space (Fig. 1.1). (Naturally there are other type of attractors, but we mention here only some common ones.) The stability and the presence of the attractors can depend on the parameters of the dynamical system, thus the same system can behave in qualitatively different ways depending on the parameters of the system. These parameters which influence the dynamical behavior are the control parameters of the systems, and thus it is very informative to depict the stable and unstable attractors as a function of the control parameters (Fig. 1.2). The parameter value(s) where attractors loss their stability and new stable attractors emerge (or previously unstable attractors become stable ones) are called bifurcation points of the diagram. This is the point where the system's behavior changes qualitatively.

As we mentioned above, chaos is a typical characteristic of nonlinear dynamical systems. Since chaos has a keystone role in the present monograph too, I discuss it in more detail, but without using mathematical formalism. Chaos concerns to the time evolution of dynamical systems. We speak about chaos if the system is nonlinear, deterministic (or weakly noisy) and has only a few variables. Chaotic motion has the following main characteristics (Tél 2002):

1. The motion of the long-term steady-state of the system is *irregular*.

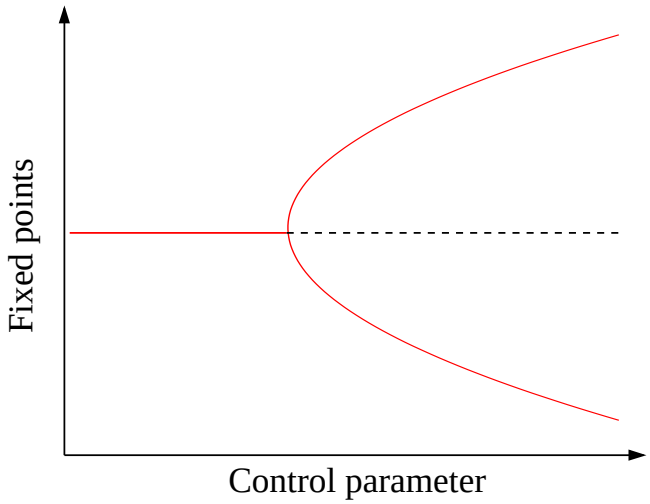

Figure 1.4: A diagram of stable (solid line) and unstable (dashed line) attractors (fixed points in this case) as a function of the control parameter of the system.(Here we used the so called pitchfork bifurcation for demonstration, but many different types of bifurcation are known see e.g. (Strogatz 1994).

2. The motion sensitively depends on the initial conditions, consequently it is impossible to predict the state of the system for a long time. This sensitivity follows from the *permanent instability* present in the course of motion.

3. The motion has some order in the phase space: the so called *strange attractor* of the motion is a fractal set (see Fig. 1.1).

Finally I discuss the consequence of permanent instability, since *Lyapunov exponents*, a central measure of chaos are closely correlated with them. If a state is unstable then a local perturbation nearby this state increases exponentially. So if two states, aer close to each other and an unstable state at the same time then they diverge from each other exponentially. The speed of divergence can be measured along the whole attractor, and the average of this speed describes the level of instability (or stability), and is called the Lyapunov exponent λ. Consequently, if $\lambda > 0$ then the motion is on average unstable, so the motion is chaotic; if $\lambda < 0$ it indicates that convergence of adjacent points is the typical nature of the motion, so the motion is regular.

1.3 Nonlinearity in ecology and in hydrodynamics

The intra- and inter-specific interactions are typically nonlinear in ecology. The reproductive success and death rate of an individual is determined by the probability of encounters with other individuals within the population as well as the probability of encounters with individuals of different populations. Consequently, both the reproductive success and death rate must be some nonlinear function of the densities of individuals.(Since interaction among individuals is generally local, and the mixing is rather low, the dynamics is determined by local densities.) Since the time evolution of populations depends on their reproduction and death rates, the mathematical models describing the dynamics of interacting populations are nonlinear too. Therefore it is not surprising that numerous nonlinear phenomena (e.g. limit cycle, bifurcation and chaos) can be observed in mathematical models of interacting populations (Takeuchi & Adachi; Hastings & Powell 1991; McCann et al. 1998; Koi & Boer 2003). Ever since Robert May's seminal paper (May 1976), it has been known that complicated nonlinear dynamics (including chaos) can emerge in most ecological models (Hastings & Powell 1991; Costantino et al. 1997; Clodong & Blasius 2004) etc. However, it is difficult to detect these nonlinear phenomena in field communities or even in lab experiments. There are at least three reasons for this difficulty: firstly the inherent noise present in almost every ecological system masks the observable nonlinear phenomenon; secondly the dynamics is generally too slow to detect complicated dynamics so there is a typically a shortage of ecological time series; and thirdly communities generally contain many dozens of interacting populations while mathematical models focus on small systems of only two or three species. Thus elementary nonlinear phenomena can be demonstrated in such lab experiments where environmental conditions are constant, generation times of populations are short, and only a few populations interact. Microbial populations and insects often fit these conditions.

Although population cycles have been known to occur in both field (see e.g. Elton & Nicholson 1942) and laboratory experiments (e.g. Luckinbill 1973) for some time, only recently has it been possible to connect the experimental observations with the predictions of mathematical models (Fussmann et al. 2000). Fussmann and his coworkers (Fussmann et al. 2000) have studied a predator-prey system with a planktonic rotifer (*Brachionus calyciflorus*) feeding on a green algae (*Chlorella vulgaris*). They cultured these species in a chemostat and monitored their population dynamics under

different conditions. At the same time they studied the dynamical model of the populations. The mathematical model predicts that depending on the nitrogen concentration and dilution rate (control parameters), the predator alone or both species may become extinct, or the two species may coexist at a stable equilibrium or on a stable limit cycle. They run the experiments with different nitrogen concentrations and dilution rates to scan the behavior of this predator-prey system predicted by the model. They found a very strong quantitative concordance between experiment and theory (Fussmann et al. 2000). Another recent work has studied the dynamics of a one-predator (a ciliate) two-prey (bacteria) system in a chemostat experiment (Becks et al. 2005). While it was know earlier that one-predator two-prey model systems can show many different nonlinear behavior (including chaos) (Takeuchi & Adachi 1983; Koi & Boer 2003), Becks and his coworkers could show experimentally that the dynamics of a three species system can be triggered by the dilution rate. Populations achieve constant densities at higher dilution rates. If the dilution rate decreased densities follow aperiodic oscillations, Lyapunov exponent estimations indicate that system is chaotic in this range of dilution rate. Stable limit cycles were established at even smaller dilution rate, although the three species still remained in coexistence.

Despite the fact that chaos can be detected at certain parameter ranges in most ecological models, there are only a few examples where the chaotic dynamics, forecasted by the model were pointed out experimentally as well (Cushing et al. 2003). Cushing and collaborators set up a stage structured model for the dynamics of the flour beetle (*Tribolium castaneum*) and analyzed its dynamics in a very accurate manner. Among others they have shown that the system can follow a quasiperiodic cycle or can be chaotic at different parameter ranges. At the same time they started a long-term experiment on this population. According to the mathematical model they manipulated the populations to set up stable equilibrium, quasiperiodic cycle and chaos in the different experiments. Data analysis and comparisons with the dynamical model provided convincing evidence of transitions to chaos in this experiment (Costantino et al. 1997; Cushing et al. 2001; Cushing et al. 2003).

Some years later this group raised an interesting problem: because individuals in populations are discrete units, mathematical models should consider population densities as discrete variables instead of continuous ones, as assumed in most models. This difference can have a significant effect on dynamics: while continuous state systems can be chaotic, deterministic discrete state systems *can not*. So, they re-analyzed their chaotic data series assuming that it was generated by a deterministic discrete state dynamical system with additional demographic noise. They found on one hand those fragments

of cycles in the data series wich are present only in discrete state model. On the other hand, other characteristics of the data series can be explained by the continuous state model (Henson et al. 2001; Henson et al. 2003). I highlight this peculiar nonlinear phenomenon here because the second part of this monograph focuses on the dynamics of noisy discrete state population dynamical models and analyzes the *Tribolium castaneum* data series assuming noisy discrete state dynamics.

However, the prevalence of chaotic dynamics in model ecosystems contrasts with the rarity of reliable reports for chaos in real systems. One of the plausible reason for this discrepancy is that the difficulties in detecting nonlinear behavior are the most pronounced if the dynamics is chaotic. The other reason might be that the simplifications generally used in modeling population dynamics increase the dynamical instability, and consequently the appearance of chaos. Thus it is possible that chaos is really much rare in real than in model ecosystems (Berryman & Milstein 1989; Scheuring 2001).

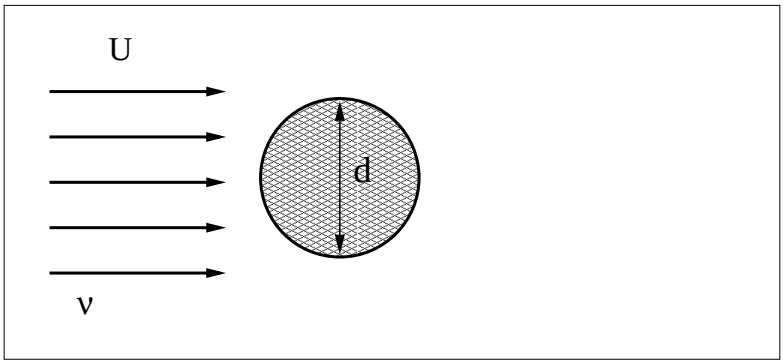

Figure 1.5: The cylinder in a flow.

Hydrodynamics is a field of physics where nonlinearity effects are central. The Navier Stokes equation (the equation of motion of hydrodynamics) is inherently nonlinear because of viscous dissipation among the neighboring fluid parcels. If dissipation can not be neglected, then depending on the characteristic speed of motion a great variety of nonlinear phenomena might emerge. A rich variety of nonlinear phenomena can be demonstrated by the following simple experiment: Put a cylinder into a flow and study the characteristics of the streams emerging around the cylinder. It is known that only one dimensionless number, the so called Reynolds number (R_e), determines the characteristics of the flow. In our case $R_e = \frac{Ud}{\nu}$, where U is the upstream velocity, d is the diameter of the cylinder and ν is the dynamic viscosity of the fluid (Fig. 1.5). For very low Reynolds numbers ($R_e \ll 1$) the flow is symmetrical upstream and downstream (Fig. 1.6 a).

This symmetry disappears for higher Reynolds number ($R_e < 4$), but the flow remains laminar without any circulation. If $4 < R_e < 40$, re-circulations appear behind the cylinder, but the wake is completely laminar, and the vortices act like rollers over which the main stream flows (Fig. 1.6 b). The eddies get longer as R_e is increased.

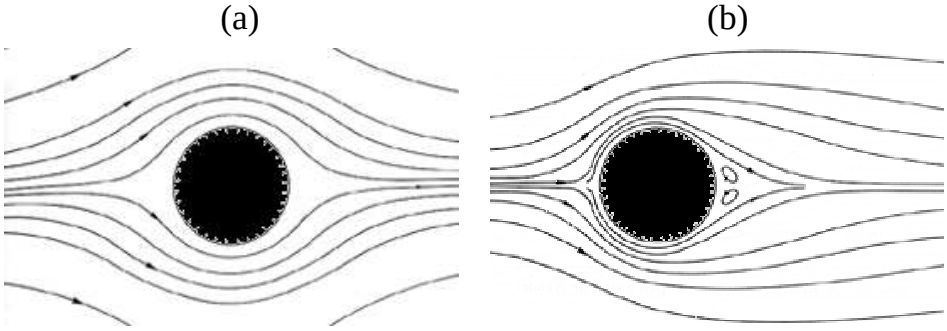

Figure 1.6: The velocity field of the flow around a cylinder at different Reynolds numbers (R_e). a: $R_e \ll 1$ b:$4 < R_e < 40$.

Up to $R_e \approx 40$ the vortices start to break away from the cylinder. The vortices appear and then are shed alternatively at a constant frequency (Fig. 1.7). This is the well know von Kármán vortex street. While the flow is time periodic and relatively simple, tracers follow a transient chaotic motion in the wake of the cylinder (Fig 1.8) (Ott 2002). (Among others we used this type of open chaotic flow as a model system, so we explain it in detail later.) The flow changes again by the time we get to $R_e \approx 400$. The von Kármán vortex street disappears and the flow becomes turbulent, that is there are regions behind the cylinder where the vector field changes randomly in time. Naturally, the focus on the nonlinearity in hydrodynamics is not accidental since the next chapter concentrates on ecological communities where the hydro- and population-dynamical processes closely connected, so in order to explain population dynamics it is important to take hydrodynamics into consideration. Typical examples are the phytoplankton communities: phytoplankton live in aquatic habitat, individuals are generally small single-celled organisms without any active moving capabilities. So their motion controlled mainly by physical laws, that is hydrodynamics has a central role in explaining plankton population dynamics.

In the following section we study the dynamics of species competing for the same sort of material in open chaotic flow. Then the dynamics of passively advected competitors are modeled in a mesoscale turbulent flow. In section 2.3 the dynamical behavior of non-hierarchical competitive systems is treated in closed chaotic flows. As mentioned earlier, the last chapter before the

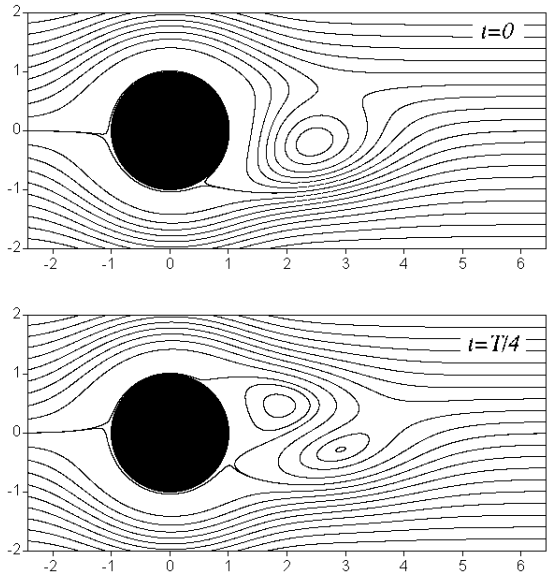

Figure 1.7: The velocity field of the flow around a cylinder at R_e is about 250. Snapshots from $t = 0$ and from $t = T/4$, where T is the period of the motion. (At $t = T/2$ the field is identical with the vector field mirrored to the horizontal symmetry axle, and at $t = 3T/4$ field looks like as the mirror of vector field being at $t = T/4$.)

summary and outlook deals with the dynamics of discrete state population dynamical models. In the first section we compare the deterministic and noisy discrete and continuous state models. The second section of this chapter reviews our time series analyzes from the *Tribolium castaneum* data series based on dynamical behavior of discrete state dynamical systems.

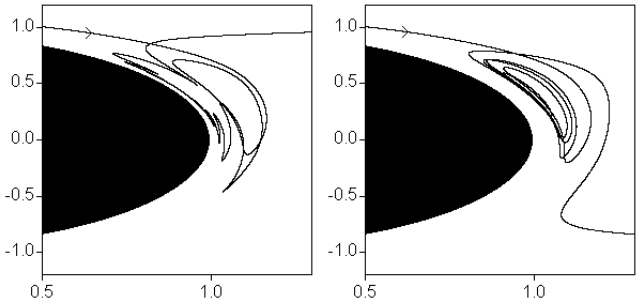

Figure 1.8: Transient chaos in the wake of the cylinder. Trajectories of two tracers started from adjacent positions from upstream. The motion of tracers is complicated transiently in the wake of cylinder, and the motion is highly sensitive to the initial position.

Chapter 2

Competition in the moving water

2.1 Coexistence of competitors in open chaotic flow

2.1.1 The paradox of plankton

The problem of coexistence of competing species is a classical question of theoretical ecology. In most natural habitats numerous competing species are able to coexist, while generally only few resources (niches) limit these communities. This fact contradicts the classical theoretical and empirical studies predicting competitive exclusion of all but the most perfectly adapted species for each limiting factor (Gause & Witt 1935; Hardin 1960).

This puzzle, originally presented by Hutchinson (1961), is most strikingly present in phytoplankton communities. Hutchinson asked the question: "How is it possible for a number of species to coexist in a relatively isotropic or unstructured environment, all competing for the same sorts of materials?" To solve this so called "paradox of plankton", he put forward the idea that seasonal environmental changes prevent competitive exclusion in natural phytoplankton communities. Thus the species of the community, at least on the time scale of ecological observation, are in nonequilibrium coexistence.

Since then numerous investigations reinforced that many different mechanisms, including spatial and temporal heterogeneity of habitat, predation, disturbance, coevolution, etc., might increase the probability of competitive coexistence. Naturally, under the word competition many different biological phenomena are collected together, which influence the coexistence of

species in different ways. Thus the original problem changed into finding the most relevant mechanisms which maintain diversity in particular situations (Connell 1978; Huston 1979; Wilson 1990; Tilman & Pacala 1993; Bartha et al. 1997). Despite the vivid debate in this field of ecology, there is by now a consensus that climatic periodicities and fluctuations play the main role in causing species' persistence in phytoplankton communities (Gaedeke & Sommer 1986; Reynolds 1993; Sommer et al. 1993). Freshwater ecologists frequently argue that an intermediate disturbance (Connell 1978) is the most adequate hypothesis for the explanation of high diversity in aquatic systems (cf. Reynolds 1998). According to this view the environmental fluctuations (e.g. wind blows and storms) disturb ecosystems in a spatially and temporally nonuniform manner. If this disturbance is neither too intense and frequent nor too weak and rare, the community behaves as a complex mosaic of different nonequilibrium subsystems. This qualitative argumentation is convincing and supported by microcosm (Gaedeke and Sommer, 1986) and field experiments (Reynolds 1986) (and references therein). However, to determine the relevant spatiotemporal scales of disturbance and community dynamics is still a great methodological challenge for ecologists (Collins & Glenn 1997; Bartha et al. 1997).

My aim here is to show that a pure hydrodynamical phenomenon, *chaotic advection* (Ottino 1989; Jana et al. 1994; Aref 1994), ensures a peculiar small-scale spatial heterogeneity that allows the *coexistence* of competing species. For phytoplankton populations, this provides a novel possibility for explaining coexistence. In fact, the mechanism proposed by me could also be a consequence of some intermediate disturbance. Frequent, but moderately blowing winds may drive the water sufficiently in order to generate chaotic advection, thus supporting coexistence.

My model of competition and its interaction with hydrodynamics is chosen deliberately to simulate a realistic mixing situation: in a perfectly mixed environment the competition dynamics allow for the survival of the most fit species only, while in flows with nonchaotic advection, the coexistence of two species is possible but in spatially separated patches only, without real competition. It is thus the flow induced *imperfect mixing* (Epstein 1995) which can maintain coexistence in aquatic systems.

It is worth to mention here that one can meet a similar problem in *early evolution of life*. Since life evolves from the simple structured entities to the most complex ones, there must have been a stage in the evolution, when life was essentially no more complex than what a collection of self-replicating nucleic acids present (Maynard Smith & Szathmáry 1995). They were competing for a few limiting resources (such as mononucleids and energy rich chemicals) and making copies of themselves without any spe-

cific enzyme. Without enzymes the copying accuracy could not be very high. Estimating the selective superiority of the best replicator and the copying accuracy per nucleotide, it is concluded that the maximum length of these molecules is about 100 nucleotides (Eigen 1971). However, if the prebiotic ocean was (as the models assumed directly or indirectly) on long time-scales well-mixed, there would have been only a few winners of the selection, namely the most fit macro-molecule surrounded by its closest mutants (Eigen 1971; Eigen & Schuster 1979). But how can we surmount the gap between these primitive replicators with 100 nucleotides and the most simple RNA viruses with 4000–5000 nucleotides? Specific replicase enzymes are needed to increase the copying fidelity, and thus the length of the replicator, but these replicators are too short to code specific enzymes. This is the "Catch 22" of the prebiotic evolution (Maynard Smith 1983): no genome without an enzyme, however no enzyme without genomes. This problem can be resolved if some mechanism maintains the coexistence of several different replicator molecules, and therefore the information necessary for coding a replicase enzyme can be stored by the union of smaller information carriers. In this situation the replication error does not grow exponentially as in the case of a base-by-base copying, it grows only linearly with the number of smaller carriers.

Current theories point out coexistence of replicators moving on a surface (Boerlijst & Hogeweg 1991; Czárán & Szathmáry 2000), preferring thus the concept of "prebiotic pizza" against the concept of "prebiotic soup" (Wächtershäuser 1994). In these models, however, some replicator molecules either catalyze each others replication directly (Boerlijst & Hogeweg 1991), or indirectly operate on a common metabolism (Czárán & Szathmáry 2000; Károlyi et al. 2002), consequently they are not completely competitive. An alternative explanation assumes that both the replicative and enzymatic functions were co-evolved, thus the length of the replicators and the accuracy of enzymatic functions increased together (Poole et al. 1999; Scheuring 2000; Szabó et al. 2002).

In both problems (i.e., in the paradox of plankton and in the Catch 22 of prebiotic evolution) the traditional population dynamical equation for two species B_1, B_2 competing for the resource A read:

$$\frac{dN_1}{dt} = \alpha_1 N_1 - \delta_1 N_1, \tag{2.1}$$

$$\frac{dN_2}{dt} = \alpha_2 N_2 - \delta_2 N_2. \tag{2.2}$$

Here N_i is the instantaneous number of individuals of species B_i in a given range of a well stirred region. The instantaneous parameters α_i, δ_i are posi-

Figure 2.1: SEAWIFS image of a phytoplankton bloom at Shetland Islands, May 12, 2000, from the NASA archive. Plankton individuals (light gray) move along a fractal-like set.

tive and depend, in general, on the concentration of the resource material A, too.

Independently of the particular form of this dependence and the dynamical equation of A, *no* fixed points can exist in the system in which both species would be in a steady state with nonzero values of $N_i = N_i^*$ (Gurney & Nisbet 1998). The coexistence might, however, be possible in *imperfectly stirred environments*. As numerous remote sensing images demonstrate phytoplankton are distributed along fractal filaments in the oceans indicating a strong but imperfect mixing environment (Fig. 2.1).

2.1.2 Passive advection in open flows

Chaotic advection in open hydrodynamical flows is an ubiquitous phenomenon. A flow is considered locally open if there is a net current flowing through the observation region (Lamb 1932). It became clear in the last decade that passive advection even in simple time-dependent flows is typically chaotic (Péntek et al. 1996; Sommerer et al. 1996; Károlyi & Tél 1997) and possesses

complicated particle trajectories. These flows, characterized by strong *imperfect* mixing, lead to a fractal spatial distribution of advected particles in a finite region of the flow. This region is called the *mixing region*. In our terminology, a flow is chaotic if the advection dynamics generated by the flow is chaotic.

In the case of several (three or more) types of passively advected tracers, distinguished for example by their color, it was shown (Toroczkai et al. 1997, and references therein) that their distribution may follow a rather non-trivial topology on the fractal, a property called the Wada property: every point *on* the fractal is lying on the boundary of at least three colors. There is, however, poor mixing elsewhere.

It is worth emphasizing that a complicated flow field (turbulence) inside the mixing region is not required for the flow to be chaotic, (i.e., for complex advection dynamics or for the appearance of fractal patterns). Even simple forms of time dependence, e.g. a periodic repetition of the velocity field with some period T, is sufficient (Aref 1994). Thus, for sake of simplicity, we examine advection in time-periodic open flows.

The complicated form of trajectories implies a long time spent in the mixing region. In other words, advected particles can be temporarily trapped there. It is even more surprising, however, that there is an *infinity* of special non-escaping orbits. The simplest among these orbits are the periodic ones with periods that are integer multiples of the flow's period T. All the non-escaping orbits are highly unstable, of saddle type, and possess a strictly positive local Lyapunov exponent (which is the expanding eigenvalue of the unstable periodic orbit). Another important feature of these orbits is that despite their infinite number they are rather exceptional so that they cannot fill a finite portion of the phase space. Indeed, the union of all non-escaping orbits forms a fractal "cloud" of points on any snapshot. This fractal cloud moves periodically with the flow and never leaves the mixing region.

Typical advected particle trajectories are not in the set of the non-escaping orbits, but are, nevertheless, influenced by them. They follow closely some periodic orbit for a while and later turn to follow others. This wandering amongst periodic (or, more generally, non-escaping) orbits results in the chaotic motion of passively advected particles. Indeed, as long as the particles are in the mixing region, their trajectories possess a positive average Lyapunov exponent λ. Hence the union of all non-escaping orbits is called the *chaotic saddle*. The flows relevant from our point of view can be considered to be incompressible. This results in a time-reversal invariant, area preserving particle dynamics. Therefore, the negative average Lyapunov exponent is exactly $-\lambda$, and it characterizes the compression towards the chaotic saddle.

While many of the particles spend a long time in the mixing region, the

overwhelming majority of them leaves this region sooner or later. The decay of their number in a fixed frame is typically *exponential* with a positive exponent κ ($< \lambda$), which is independent of the frame, i.e., $N(t) = N(0)\exp(-\kappa t)$. This quantity κ is the *escape rate* from the saddle (or from the mixing region). The reciprocal of the escape rate can be considered as the average lifetime of chaos, and therefore the chaotic advection of passive particles in open flows is a kind of *transient chaos* (Tél 1990).

The chaotic saddle is the set of non-escaping orbits which advected particles may follow for an arbitrarily long time. Each orbit of the set, and therefore the set as a whole, has an inflow and an outflow curve, also called in the mathematical jargon of chaos theory the stable and unstable manifolds, respectively. The *inflow curve* is a set of points along which the saddle can be reached after an infinitely long time. The *outflow curve* is the set along which particles lying infinitesimally close to the saddle will eventually leave it in the course of time. By looking at different snapshots of these curves we can observe that they move periodically with the period T of the flow. Their fractal dimension D_0 ($1 < D_0 < 2$ in two-dimensional flows) is, however, independent of the snapshot. (The inflow and outflow curves have identical fractal dimension due to the advection dynamics' time reversal invariance.)

There is a unique relation between the fractal geometry and the advection dynamics, expressed by the relation (Kamtz & Grassberger 1985; Hsu et al. 1988; Tél 1990):

$$D_0 = 2 - \frac{\kappa}{\lambda}. \tag{2.3}$$

(By characterizing the dynamics by one single dimension D_0, we have assumed that the advection process has a monofractal geometry. In reality, a set of dimensions D_q is required for the full description of the fractal aspects. It is for the $q = 1$ dimension, the so-called information dimension, D_1, for which (2.3) is an exact equality. In practice, however, the relative difference between D_0 and D_1 is on the order of a few percents and therefore the use of a single dimension is justified for practical purposes.) It says that the deviation of the dimension from that of the plane is given by the ratio of two quantities characterizing the global and the local instability of the dynamics. Relation (2.3) shows that out of the three basic characteristics (κ, λ and D_0) only two are independent. When speaking about population numbers in what follows, we shall use the escape rate and the fractal dimension as independent parameters. In the local dynamics (see next section), however, only the average Lyapunov exponent appears.

The outflow curve plays a special role since it is the only set which can be directly observed in an experiment. Let us consider a droplet (ensemble) of a large number of particles which initially overlaps with the inflow curve. As

the droplet is advected into the mixing region its shape is strongly deformed, but the ensemble comes closer and closer to the chaotic saddle as time goes on. Since, however, only a small portion of particles can fall very close to the inflow curve, the majority does not reach the saddle and starts flowing away from it along its outflow curve. Therefore, in open flows droplets of particles trace out the outflow curve of the chaotic saddle after a sufficiently long time of observation Next, I illustrate the above observations in the simple case of a *time-periodic* flow around a cylinder. The flow is considered two-dimensional, i.e., the velocity field does not depend on the third coordinate, the depth. Its incompressibility can always be assumed for velocities much below the speed of sound. A uniform inflow velocity can lead to a periodic detachment of vortices in the wake with a period T, which forms the so-called von Kármán vortex street (Shariff et al. 1991; Jung & Ziemniak 1992; Jung et al. 1993; Ziemniak et al. 1994; Péntek et al. 1996; Sommerer et al. 1996; Toriczkai et al. 1997). For numerical simplicity we use an analytic model of this flow introduced by Jung et al. (1993).

Figure 2.3 shows the unstable manifold in the wake at a given instant of time. Its complicated winding fractal structure is striking. Three stagnation points on the surface of the cylinder, denoted by Q, R and S, are also shown. The front stagnation point S acts as a saddle point separating the upper and lower part of the cylinder. It has its own stable manifold but this is a *smooth* curve lying close to the symmetry (x) axis. It leads tracers towards the cylinder's surface, thus they can penetrate into the boundary layer. This stable manifold is a kind of watershed between fluid particles moving around the disc of the cylinder along its upper or lower semicircle.

I emphasize that the qualitative features of the fractal patterns and of the boundary layer, which are essential for our study, are robust and can be found in any open time-dependent flow. The shape of the obstacle, two-dimensionality, time periodicity and even incompressibility of the flow are only considered for convenience and easy presentation.

2.1.3 Dynamics of a single species in open chaotic flow

In this section I briefly repeated the mathematical derivation of the dynamics of a single population living in an open chaotic flow (for more details see Toroczkai et al. 1998; Károlyi et al. 1999; Tél et al. 2000). Replication, competition for the limiting resources, and spontaneous decay are taken into account in our population model, while stage and age structure is neglected for simplicity. The discrete and continuous-time models are derived as well.

First it is assumed that the intake of resource, multiplication and decomposition are instantaneous and take place at integer multiples of a time lag τ.

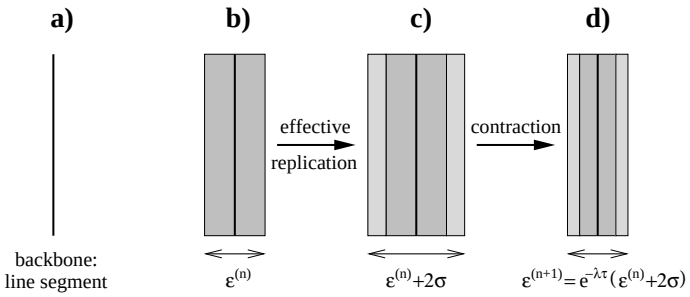

Figure 2.2: Schematic diagram of the individuals' distribution along the a line segment of the outflow curve. (b) The average width of of stripes is $\varepsilon^{(n)}$. (c) The net effect of replications and decays increase the width with 2σ. (d) Then the contraction perpendicular to the line segment decreases the width with $e^{-\lambda\tau}$.

Here τ acts as an average time-scale on which the reproduction takes place.

The basic observation is that after a sufficiently long time the filaments of the outflow curve are covered in narrow stripes by individuals of species B due to their replication (Toroczkai et al. 1998; Károlyi et al. 1999). Individuals are thus distributed on a fattened-up fractal set. On linear scales larger than an average width ε^* the distribution of B is a fractal of the same dimension D_0 as the outflow curve of the chaotic saddle. Let $\varepsilon^{(n)}$ denote the *average* width of these stripes right before replication and decomposition takes place. It is worth measuring this width in the unit of a characteristic length scale of the flow (e.g. in the cylinder radius in the example of Fig. 2.3). Thus, $\varepsilon^{(n)}$ is a dimensionless variable. Since material A is available outside of these stripes, replication increases the width with some constant distance γ, the replication range, while spontaneous decay due to death of individuals decreases it with a distance μ. Naturally individuals die everywhere within the filaments, but there is no resource for reproduction within them. However, the strong contraction towards the outflow curve rapidly fills in the "holes" appearing after death of individuals. The net effect of the replication and spontaneous decay can then be modeled by a broadening of the width by an amount proportional to the difference $\sigma = \gamma - \mu$, the effective replication range. Thus, $\varepsilon^{(n)} \to \varepsilon^{(n)} + c\sigma$. Here c is a dimensionless number expressing geometrical effects. If the fattened-up filaments do not overlap, then replication does occur on both sides of the stripes leading to $c = 2$ (see Fig. 2.2(a), (b), (c)). If there is overlapping of some of the fattened-up filaments, like in case of a fractal, then $c \neq 2$. This *geometrical factor* turns out to be slightly time dependent due to the pulsation of the flow, but for simplicity it can be considered to be constant from the point of view of the qualitative behavior

of the population (Toroczkai et al. 2001).

In the next period of length τ there is no replication and decomposition, just contraction towards the outflow curve. The average contraction factor is $\exp(-\lambda\tau)$, where $(-\lambda)$ is the negative average Lyapunov exponent of the advection dynamics (Fig. 2.2 (d)). Therefore, the width $\varepsilon^{(n+1)}$ right before the next replication can be given as

$$\varepsilon^{(n+1)} = (\varepsilon^{(n)} + c\sigma)e^{-\lambda\tau}. \tag{2.4}$$

This is a recursive map for the actual width of the B-stripes on snapshots taken with multiples of the time lag τ. The solution of (2.4) converges for $n \to \infty$ to the fixed point

$$\varepsilon^* = \frac{c\sigma}{e^{\lambda\tau} - 1}. \tag{2.5}$$

In the time-continuous limit $\tau \to 0$, $\sigma \to 0$, but keeping $\sigma/\tau \equiv v_r$ constant, one obtains the differential equation:

$$\frac{d\varepsilon}{dt} = cv_r - \lambda\varepsilon, \tag{2.6}$$

which has a steady-state solution given by:

$$\varepsilon^* = \frac{cv_r}{\lambda}\ . \tag{2.7}$$

Here v_r can be interpreted as the net speed of replication.

Knowing the ε-dynamics and that the individuals accumulate on a fractal set in the mixing region, the time evolution of the number N of B individuals in that region can be calculated. First, note that the area $\mathcal{A}$ occupied by species B scales as $\mathcal{A} \approx \epsilon^{2-D_0}$, with D_0 as the fractal dimension of the outflow curve, for any box size ϵ not smaller than the width ε of the B-stripes. We can thus choose

$$\epsilon = \varepsilon \approx \mathcal{A}^{1/(2-D_0)}. \tag{2.8}$$

(In general, (2.8) also contains a proportionality constant, called the Hausdorff volume. Since this only rescales the constant q (see below), for clarity we took the Hausdorff volume to be unity.)

If the linear size of the area occupied by a single individual is ϵ_0, we have $N = \epsilon_0^{-2}\mathcal{A}$, and therefore we can rewrite (2.4) or (2.6) so that it represents an equation for the individuals in discrete and continuous cases, respectively:

$$N^{(n+1)} = e^{-\kappa\tau}\{[N^{(n)}]^{1/(2-D_0)} + q\sigma\}^{(2-D_0)}, \tag{2.9}$$

and

$$\frac{dN}{dt} = -\kappa N + q(2 - D_0)v_r N^{-\beta}, \tag{2.10}$$

with

$$q = c\,\epsilon_0^{-2/(2-D_0)}. \tag{2.11}$$

Here (2.3) has been used, and

$$\beta \equiv \frac{D_0 - 1}{2 - D_0} \tag{2.12}$$

appears as a nontrivial exponent. (For multifractal flows one can show (Tél et al. 2000) that exponent β is that given by (2.12) with D_0 replaced by the information dimension D_1.) Since the fractal dimension of the outflow curve lies between 1 and 2, exponent β is positive. For $D_0 = 1$ the differential equation (2.10) describes a classical surface reaction along a line with front velocity v_r in the presence of escape. For $1 < D_0 < 2$ it represents a novel form of dynamical equations containing a fractality-enhanced biological activity term with a negative power of the individual number of B. The less B individuals are present, the more effective the reproduction is, because the resolved perimeter is larger. Consequently, in a competitive situation the subordinate species has an advantage if it becomes rare compared to the dominant species. This balancing mechanism can make coexistence possible, as shown in the the next sections. The dimension D_0 can approach 2 if the flow becomes closed, when the outflow curves become space filling. This happens for vanishing escape rate $\kappa \to 0$, see (2.3). In this limit, therefore, both terms of the right hand side of (2.10) go to zero, corresponding to a space-filling steady state, without any more activity.

As one can see from Eqs. (2.9,2.10), in both the discrete and continuum pictures a steady state is reached after a sufficiently long time if the geometrical factor c (and therefore also q) is constant (Toroczkai et al. 2001). In this case, the steady-state number of individuals in the mixing region is $N^* = \epsilon_0^{-2}(\varepsilon^*)^{2-D_0}$ where ε^* is given by (2.5) and (2.7) for the discrete and continuum cases, respectively.

2.1.4 Competing species in open chaotic flow

A model of competition

As in the single species case, we consider a simple model of replication and competition with passively advected point like individuals of type B_1 and B_2, multiplying themselves instantaneously. The resource material A which the different species B_1 and B_2 compete for is uniformly distributed on the surface of the flow. Therefore two auto-catalytic processes $A + B_1 \to 2B_1$, $B_1 \to A$ and $A+B_2 \to 2B_2$, $B_2 \to A$ represent the replication and competition process in our model in an imperfectly mixed environment. Similarly to the single

species case, the parameters γ_i and μ_i $(i = 1, 2)$ are defined as the increase and decrease of the B_i stripe width due to replication and decomposition, respectively, so that the effective replication distances are $\sigma_i = \gamma_i - \mu_i$.

As before, an important feature of the advection dynamics is its deterministic nature. Concerning the population dynamics, this implies that we work in the limit of weak diffusion and assume that the mutual diffusion coefficients between any pair of the constituents is small.

Prior to discussing the consequences of the imperfect mixing generated by the chaotic flow to this dynamics, it is worth briefly giving the traditional equations governing the above defined auto-catalytic processes in a well-mixed environment. In a fixed region of observation they are:

$$\frac{dN_1}{dt} = \gamma_1 A N_1 - \mu_1 N_1, \tag{2.13}$$

$$\frac{dN_2}{dt} = \gamma_2 A N_2 - \mu_2 N_2, \tag{2.14}$$

where N_i denotes the number of individuals of species B_i, and A is the instantaneous amount of the resource material in the same region. Note that the meaning of the replication and death rates are slightly different here from those in the discrete model (thus e.g., μ_i in eqs. (2.13), (2.14) is of dimension frequency, while the same quantity in the discrete version is a distance). If the dynamics of resource is much faster than the dynamics of competing species, then the former can be considered to be in a quasi-stationary state: $dA/dt = 0$. The equation for resource A is then

$$\frac{dA}{dt} = 0 = l - \gamma_1 A N_1 - \gamma_2 A N_2, \tag{2.15}$$

and l is the constant inflow of resource A into the region of observation. Equations (2.13), (2.14) correspond to the general scheme (2.1) and (2.2) given in the Introduction by identifying μ_i with δ_i and $\gamma_i A$ (where A is given by the right hand side of (2.15)) with α_i.

After analyzing (2.14) and (2.15), one can easily see that species with lower ratio γ_i/μ_i of replication and death rates would be outcompeted, and thus stable coexistence is impossible. However, the above equations are not valid in an imperfectly mixed media like an open chaotic flow is.

Numerical simulations

The competitive dynamics starts with the full surface occupied by the background material A. Initially, we place two droplets of individuals from species B and C into the flow in front of the cylinder with C being the weaker

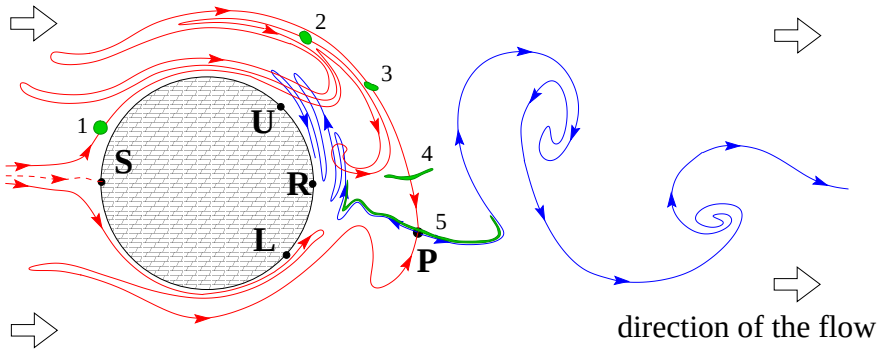

Figure 2.3: The topology of in and outflow curves and their relation to a passively advected droplet. Schematic drawing of the in and outflow curves of a period-one orbit P at a given instant of time. They are very similar to the in and outflow curves of the full chaotic set. The outflow curve (blue line marked by outgoing arrows) is a complicated winding fractal curve extending downstream to infinity. The inflow curve of this orbit (red line entering P) foliates regions around the cylinder and upstream to it. The time evolution of a green droplet overlapping initially with the inflow curve of P is also indicated. Its shape is shown after integer multiples of the flow's period. Note the convergence towards the outflow curve.

competitor. The fixed region of observation is a rectangle containing the cylinder and the wake. We monitor the number of individuals present in this region during the competition process. After an initial rapid increase the number of B and C cells becomes *synchronized* with the flow (see inset of Fig. 2.4a). I emphasize that species B and C coexist in spite of their very different γ/δ ratio. The filamental structure shown in Fig. 2.4 is reminiscent of the patterns found in mesoscale plankton models (Spall & Richards 2000; López et al. 2001; Bees et al. 1998) which do not study competition, and in remote sensing images of chlorophyll concentration in the wake of islands (Arístegui et al. 1997), Field observation in the same region (Barton et al. 1998) indicate increase of biomass belonging to *Cyanobacteria* and *Phytoflagellates* taxa in monthly averages. The explanation of the coexistence of species is based on concepts of the theory of chaotic advection. In order to have an intuitive understanding of the complexity of the advection dynamics, let us first imagine how a droplet of dye behaves in a simple uniform flow when it is advected past an obstacle of small spatial extent like a fixed needle. The dye particles which touch the needle remain attached, but the bulk of the droplet moves further downstream. As the droplet flows past the needle, its shape starts to change, developing tongues on both sides of the needle. These tongues are becoming ever longer and narrower and asymptotically

the droplet traces out a line extending downstream to infinity. It is the so called *outflow curve*. Geometrical points of the fluid surface from where dye particles can reach the needle form another straight line, the *inflow curve*, extending upstream. If the needle is oscillating perpendicularly to the direction of the flow, both the in and outflow curves become bent and take on a wavy shape. Having infinitely many needles, all moving in a complicated manner in a finite region of the flow, the in and outflow curves of all these needles form a complicatedly interwoven striation of the fluid.

If a circular cylinder is placed in a moderately fast uniform flow, there is a periodic detachment of vortices from the upper and the lower segments UR and RL, respectively (c.f. Fig. 2.3). The periodic vortex shedding generates never escaping *periodic paths* in the wake, i.e., particle motions which return to their original positions after the full period of the flow, or an integer multiple of it.

Naturally these paths are unstable. Each such periodic orbit plays the role of a moving needle: they can be reached along some inflow curves (red lines in Fig. 2.3), particles can remain hung up on them, and droplets flow away from them along their outflow curves (blue lines in Fig. 2.3). A close analysis shows that there is an *infinity* of different periodic paths, all unstable arranged in a fractal set in the wake. Therefore their in and outflow curves are complicatedly winding in the wake, and can even intersect each other at a given time, as indicated schematically in Fig. 2.3. Since the particle motion around the infinitely many periodic orbits is irregular, chaotic, the union of all the periodic orbits is called the *chaotic set* of the advection dynamics. The bundle of inflow and the outflow curves (called stable and unstable manifolds in the jargon of dynamical system theory) provides a *fractal* foliation of the fluid surface.

The physical relevance and observability of the outflow curve is due to the fact that a droplet of particles initially overlapping with the inflow curve traces out the outflow curve as it is advected past the cylinder (Jung & Ziemniak 1992; Sommerer et al. 1996). (shown in green in Fig. 2.3). This implies that if the tracers are chemically or biologically active, the active process mainly takes place along the outflow curve since it is there where the particles spend a long time in the wake (c.f. Fig. 2.4). The fractal filaments on which reactions accumulate are in fact filaments of the outflow curve.

If the initial droplets of both species overlap with the inflow curve of the chaotic set, they are trapped in the wake, and accumulate along the filaments of the fractal outflow curve (c.f. Fig. 2.4). This leads to an enhancement of their activity, since the continuous stretching and folding action of the underlying flow provides them with increased access to the background A for which they compete. Consequently, in the steady state, filaments of B

and C along the outflow curve are *separated* efficiently by narrow bands of material A (see Fig. 2.4b).

In analogy with chemical reactions, it is found that species with low concentration replicate with an increased efficiency. Thus *the rare species has an advantage over the common one*. Spatial separation and increased replication activity of the rare species results in the coexistence of the competing species for a wide range of the parameter values.

The boundary layer surrounding the cylinder's surface also plays an important role. The species populating the boundary layer is in a favorable position, since it acts as a stable source for generating offsprings into the wake without being subject to mixing and competition. To underline this argument we placed a droplet C upstream close to the cylinder followed by a droplet B further upstream. We find with my coworkers that in spite of B being the stronger competitor, it is unable to outcompete C from the boundary layer. On the other hand, if the B droplet is placed closer to the cylinder than C, B populates the boundary layer acting as a strong B source in the wake. In spite of this favorable position, the weaker species C still survives in the wake, provided the initial droplet also intersects the inflow curve of the chaotic set (c.f. Fig. 2.4). The initial conditions thus determine which organisms occupy the boundary layer after a long time, but they do *not* change the fact that both organisms can survive. Different species can occupy different niches simply by appearing at different places in the flow. Both niches of both species are narrow bands along the unstable curve. This underlines again that in open chaotic flow the *traditional picture of well-mixed systems is broken*: the weaker competitor can even become dominant over the stronger one due to the advection dynamics.

To check the generic nature of these results, similar numerical experiments were performed with *three* different competitors, competing for the same unique limiting resource A. We found that in a wide range of the reproduction abilities of the competitors the coexistence was robust, even if randomly mixed species were starting from the same initial droplet in front of the cylinder. It was also checked whether coexistence is possible without the effect of the boundary layer by carrying out further simulations with the so-called "baker map". The baker map is the paradigm of mixing exemplified by its successive stretching and folding actions (Ottino et al. 1988; Ott 2002) (see the inset of Fig. 2.5 and a detailed description in the following section). If green (B) and red (C) regions are covered by nonreproducing individuals, by successive actions of the baker map the density of species decays in the unit square with equal rates, and the individuals staying in the unit square forever cover a fractal set (like in the wake).

If, however, the reproducing B and C species are allowed to occupy neigh-

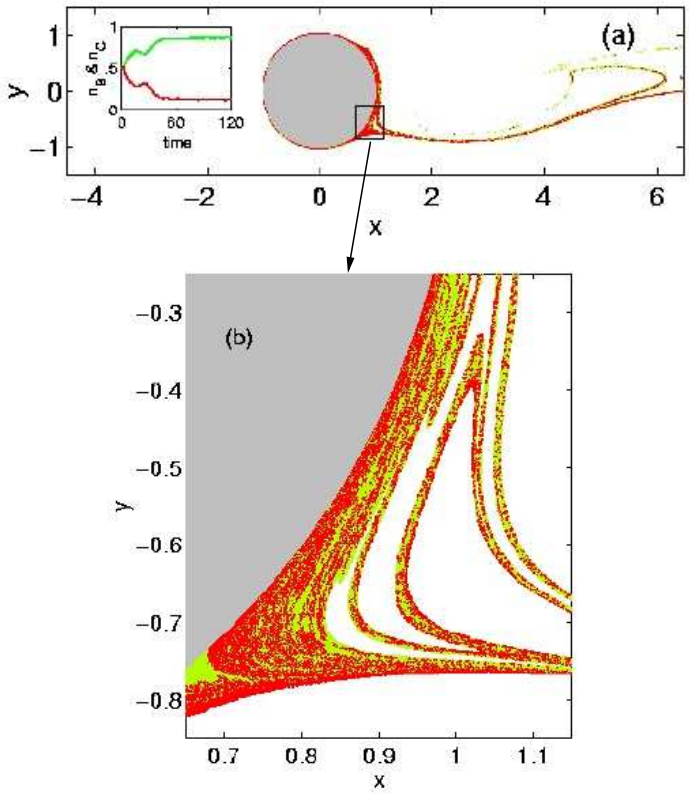

Figure 2.4: (a) Spatial distribution of species B (green) and C (red) are shown on a snapshot taken after 24 periods T of the flow. They both cover a fractal curve, and are present at all times in the wake of the cylinder. The initial position of species B and C is a rectangle of linear size 0.07×0.76 centered around $x = -1.36$, $x = -1.10$ and $y = 0$, respectively. (The length is measured in units of cylinder radius R.) In the inset of a) the percentage n_B (n_C) of species B (C) present in the wake is shown by green (red) line as a function of time, measured in units of T. Note the steady time-periodic behavior reached after about 40 time units. The simulation was performed on a rectangular grid of size $\varepsilon = 2 \cdot 10^{-3}$ times the cylinder radius. Species B and C are passively advected during time lags $\tau_B = 0.6T$, and $\tau_C = 0.8T$, respectively, then they reproduce instantaneously, with new individuals being "born" within a distance $\sigma_B = \sigma_C = 1/500$ of the "parent" if there is resource A available there [$\gamma_B \sim \sigma_B/\tau_B = 1/(300T)$, $\gamma_C \sim \sigma_C/\tau_C = 1/(400T)$]. Additionally, at each time lag τ_B (τ_C) B (C) individuals die with a probability $\tau_B\delta_B$ ($\tau_C\delta_C$) [$\delta_B = \delta_C = 1/(10T)$]. (b) A high resolution image of the small rectangular region from a) indicates self-similarity. The grid size is $\varepsilon = 8 \cdot 10^{-4}$. The total area covered by B and C in the wake follows a fractal scaling with dimension $D \approx 1.6$, the same as in the autocatalytic chemical model (Toroczkai et al. 1998).

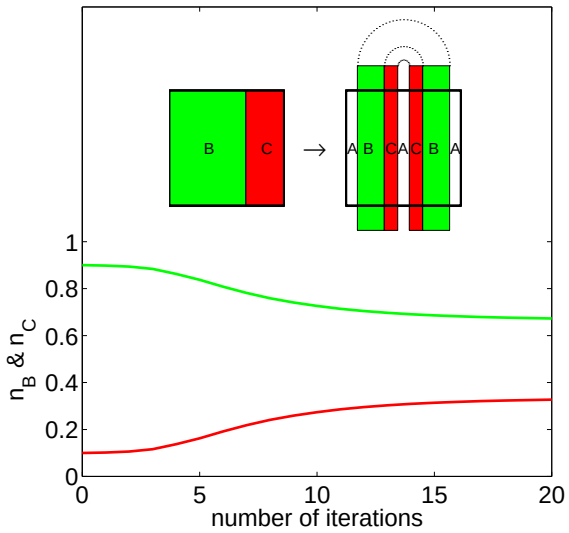

Figure 2.5: Time evolution of the competitor densities in a baker map mixing model. The percentage n_B (green line) and n_C (red line) of B and C, respectively vs. the number of iterations of the baker map on the unit square. Species B and C occupy neighboring regions of A within a distance $\sigma_B = 2\sigma_C = 1/500$, and have mortality rates $\delta_B = \delta_C = 1/5$. In spite of C being outnumbered 9:1 at the beginning of the simulation, C can coexist with B in the long time limit. In the inset, the stretching and folding action of one step of the baker map is illustrated. First, the unit square (shown in bold lines) is compressed by a factor a (= 0.4) in horizontal direction and stretched by $1/a$ in the vertical direction while keeping the area constant. Next this stretched rectangle is folded in two over the unit square. This process is then iterated several times. Note that the "flow" described by the baker map is *open* since at each iteration of the map a portion $(1 - 2a)$ of particles leaves the unit square and is being replaced by regions of the background material A.

boring regions covered by A within certain different distances, then they compete for this only limiting resource. The time evolution of the percentage of species B and C is shown for such a case in Fig. 2.5. These simulations were repeated for various parameter regimes and initial conditions and showed a *robust* coexistence of the competitors. The boundary layer is thus not necessary for coexistence, but its presence certainly enhances the effect.

A mathematical model for the competition dynamics

As numerical simulations indicate after sufficiently long time, both species B_1 and B_2 will be distributed in narrow stripes along the chaotic saddle's outflow curve as follows from the passive advection dynamics. Due to the replication and decomposition, however, the stripes have finite widths (cf. Fig. 2.4) which might depend on time. Let ε^n denote the dimensionless average width of the stripes right before an instantaneous replication takes place. These stripes are defined by the fact that outside of them there is only background material A available. Inside the stripe of width $\varepsilon^{(n)}$ there might be several narrow B_1 or B_2 filaments. The background material A is eaten up sooner or later in the inside of any stripe, therefore, for the sake of an easier presentation, we assume that this is the case and only material B_1 and B_2 are present. Let us denote the total widths of all the filaments of a given material within an $\varepsilon^{(n)}$ stripe by $\varepsilon_i^{(n)}$ with $i = 1, 2$ corresponding to B_1 and B_2, respectively. The sum of these partial widths is of course the total one $\varepsilon_1^{(n)} + \varepsilon_2^{(n)} = \varepsilon^{(n)}$. Our aim is to build up the dynamics of the partial widths based on plausible assumptions, from which the dynamics of the different populations follows.

We assume, that the boundaries are occupied by species B_1 or B_2 with *probabilities* p_1 and p_2, respectively. In other words, a stripe-boundary picked at random from the many filaments of the outflow curve will have a probability p_i to be of type B_i, $i = 1, 2$. If mixing of the two species were perfect along the fractal set, these probabilities would be equal to their relative densities. This is not the case, however. The relative position of the species in the initial distribution to the inflow curve determines which individual or patch of individuals will be trapped by which orbit of the chaotic saddle. The rest, i.e., the untrapped individuals will drift out of the mixing region. The trapped individuals, however, will stay there forever, and follow their specific trapped orbit. In the course of time, individuals give birth to others of the same species, and patches of individuals are stretched along the outflow curve specific to the trapping orbit of the chaotic saddle. In either cases, we end up with long stripes of the two species lined up along each other in an alternating manner, tracing out the outflow curve. Then the probability of

one species to be on the edge of these lines, and thus to be capable of reproduction, depends on which trapping orbit will produce the filament of outflow curve being on the edge of the stripe, on the order in which the species are lined up across one stripe, and on the actual width of the coverage of the filaments. In other words, it is the complex chaotic dynamics which makes the introduction of probabilistic concepts—on a somewhat phenomenological level—unavoidable.

The probabilities p_i depend on what the distribution of the species inside the stripes is. Thus, the simplest possible assumption is that the probabilities depend on the partial widths $\varepsilon_i^{(n)}$. Their actual functional form might also contain parameters of the flow and of the biological activity.

Naturally the probabilities fulfill $0 \leq p_1^{(n)} \leq 1$ and $p_2^{(n)} = 1 - p_1^{(n)}$. They might have a general dependence on the partial widths $\varepsilon_i^{(n)}$, $i = 1, 2$: But due to dimensional reasons they can only depend on the ratio $z^{(n)} \equiv \varepsilon_1^{(n)}/\varepsilon_2^{(n)}$, and $p_i^{(n)} = p_i^{(n)}\left(z^{(n)}\right)$. Thus we write

$$p_1^{(n)} = g\left(z^{(n)}, \omega\right), \qquad p_2^{(n)} = 1 - g\left(z^{(n)}, \omega\right). \tag{2.16}$$

Here $\omega > 0$ is a parameter of the distributions, and incorporates the dependence on the replication rates. We also made the plausible assumption, that g has no explicit n (or time) dependence. A general property of g is that it vanishes in the origin $g(0, \omega) = 0$ since this expresses the obvious fact that if species B_1 is missing, then the probability to find it in the filaments is zero. Similarly for infinitely large values of z it must be unity: $g(\infty, \omega) = 1$ which corresponds to the absence of B_2. Also, due to the fact that p_1 and p_2 are probabilities, we must have $0 \leq g(z, \omega) \leq 1$ for all $z \geq 0$. Furthermore, the functional form must be symmetric by interchanging the role of the species. This implies that one must have $g'(0, \omega) \geq 0$, where the prime denotes derivation with respect to the argument. This implies

$$p_2^{(n)} = g\left(1/z^{(n)}, 1/\omega\right), \tag{2.17}$$

where the appearance of $1/\omega$ means that an interchange of the species index brings the parameter in its reciprocal value, as e.g. in the case when $\omega = \sigma_1/\sigma_2$ (the dependence on the ratio of the replication distances follows from dimensional reasons). The normalization of the probability implies

$$g(z, \omega) + g(1/z, 1/\omega) = 1 \tag{2.18}$$

This is a functional equation for g. With the above properties and boundary conditions one can find that a family of solutions is given by the form:

$$g(z) = \frac{z^\alpha}{z^\alpha + \omega}, \tag{2.19}$$

with α and ω as two positive parameters. In the range of $0 < \alpha < 1$ the smaller population is less probable on the boundary but yet with a weight which is weaker than linear in the widths. For $\alpha = 0$ there is no width-dependence at all, the probabilities p_i are constant. The case $\alpha = 1$ and $\omega = 1$ corresponds to a homogeneous mixing within the stripe of width ε. For $\alpha > 1$ a superdominance is described. In the following I show that the form (2.19) of $g(z)$ is indeed in good agreement with numerical simulations, and determine values for parameters α and ω.

The broadening of the average widths is then $c\sigma_1 p_1^{(n)}$ and $c\sigma_2 p_2^{(n)}$ due to species B_1 and B_2, respectively. Here the geometrical factor c and parameter $\sigma_i = \gamma_i - \mu_i$ have the same meanings as in the single species problem defined previously.

Thus, similar to (2.4) the partial width of B_i after the $(n+1)$st step is

$$\varepsilon_i^{(n+1)} = \left[\varepsilon_i^{(n)} + c\sigma_i p_i^{(n)}\right] e^{-\lambda\tau} \tag{2.20}$$

for $i = 1, 2$. Note that in our theory, cp_1 and cp_2 can also be interpreted as re-normalized geometric factors for each species, due to the screening effects at the boundaries of the stripes. As a consequence, the total width of the stripes changes at a replication as

$$\varepsilon^{(n+1)} = \left[\varepsilon^{(n)} + c(\sigma_1 p_1^{(n)} + \sigma_2 p_2^{(n)})\right] e^{-\lambda\tau}. \tag{2.21}$$

For simplicity, the explicit width-dependence (2.16) of the probabilities has not been written out. For $\sigma_1 = \sigma_2$ we recover the width dynamics of the single species problem, see (2.4).

Next I turn to the dynamics of the number of individuals. On scales larger than or equal to $\varepsilon^{(n)}$, the total number of individuals $N = N_1 + N_2$ occupied by stripes appears to be a fractal of the same dimension D_0 as the outflow curve. For simplicity of writing we assume that individuals of both species have the same size ε_0 (an extension for different sizes is straightforward).

Since the relation between the $\varepsilon^{(n)}$ and the number of individuals $N^{(n)}$ is the same as in the single species model, we can use (2.8). Thus (2.21) implies a recursion for the area right before replication as

$$N^{(n+1)} = e^{-\kappa\tau}\left\{\left[N^{(n)}\right]^{1/(2-D_0)} + q\left[\sigma_1 p_1^{(n)} + \sigma_2 p_2^{(n)}\right]\right\}^{2-D_0} \tag{2.22}$$

with q given by (2.11). Next, we derive the dynamics of the number of individuals $N_i^{(n)}$ for species i contained in the stripes. The number of individuals of species i is the portion of the total number $N^{(n)}$ proportional to the partial widths:

$$N_i^{(n)} = N^{(n)} \frac{\varepsilon_i^{(n)}}{\varepsilon^{(n)}}. \tag{2.23}$$

This is due to the fact that there is no fractal scaling below $\varepsilon^{(n)}$. Since $\varepsilon^{(n)} = [\epsilon_0^2 N^{(n)}]^{1/(2-D_0)}$, Eq. (2.23) leads to

$$\varepsilon_i^{(n)} = N_i^{(n)} \epsilon_0^{2/(2-D_0)} \left[N^{(n)}\right]^{\beta}. \tag{2.24}$$

As another consequence of (2.23), the ratio of the partial widths is the ratio of the population numbers:

$$z^{(n)} \equiv \frac{\varepsilon_1^{(n)}}{\varepsilon_2^{(n)}} = \frac{N_1^{(n)}}{N_2^{(n)}}. \tag{2.25}$$

From Eqs. (2.20) and (2.24) we therefore obtain the dynamics of the population numbers as

$$\begin{aligned} N_i^{(n+1)}[N^{(n+1)}]^{\beta} = e^{-\lambda\tau} \Big\{ & N_i^{(n)} \left[N^{(n)}\right]^{\beta} \\ & + q\sigma_i p_i^{(n)} \left(N_1^{(n)}/N_2^{(n)}\right) \Big\} \end{aligned} \tag{2.26}$$

for $i = 1, 2$. Here exponent β is the same expression (2.12) as in the case of the single species problem, and q is given by (2.11).

The time continuous limit is obtained by letting both the time lag and the effective replication ranges go to zero so that their ratios remain finite. Thus we define replication velocities

$$v_i = \lim_{\tau \to 0} \frac{\sigma_i}{\tau}, \tag{2.27}$$

with $i = 1, 2$ for species B_1, B_2, respectively. In the continuous time limit, the differential equations obtained for the partial widths from (2.20) read as

$$\frac{d\varepsilon_i}{dt} = -\lambda\varepsilon_i + cv_i p_i(\varepsilon_1/\varepsilon_2) \tag{2.28}$$

where $p_1 = g$, $p_2 = 1 - g$.

The differential equation for the number of all individuals follows from (2.22) as

$$\frac{dN}{dt} = -\kappa N + q(2 - D_0) v N^{-\beta}. \tag{2.29}$$

Here

$$v \equiv p_1 v_1 + p_2 v_2 \tag{2.30}$$

is an average velocity, but note that it is not a constant since the p_i depend on the population numbers, and q is given by (2.11). If one of the species, say B_2, is not present, then $p_1 = 1$, $N_2 = p_2 = v_2 = 0$ and hence $v = v_1 = v_r$,

$N = N_1$ and Eq. (2.29) becomes equivalent to (2.10). The same happens if both species are equivalent, i.e., for $v_1 = v_2$ when $v = v_r$.

The differential equation for the number N_i of individuals of the two species can be derived from (2.28) and the continuum version of (2.24), i.e., $\varepsilon_i = \epsilon_0^{2/(2-D_0)} N_i N^\beta$. The result is

$$\frac{dN_i}{dt} = -\kappa N_i - q(D_0 - 1) v N^{-\beta-1} N_i + q v_i p_i \left(N_1/N_2\right) N^{-\beta}, \tag{2.31}$$

with $N = N_1 + N_2$. Here (2.3) and (2.12) have been used. By summing over i in (2.31) one recovers Eq. (2.29).

An equivalent form is obtained after rearranging terms and taking into account the definition of the average replication velocity (2.30). It reads

$$\frac{dN_1}{dt} = -\kappa N_1 + q N^{-\beta-1} \left[(2 - D_0) v N_1 + (v_1 p_1 N_2 - v_2 p_2 N_1)\right], \tag{2.32}$$

and an analogous expression for the second species obtained from (2.32) by interchanging the indices 1 and 2. It can be clearly seen that the first term of the bracket corresponds to the growth of the total population, while the second describes the effect due to a weighted difference in the population numbers. Expression (2.31) or (2.32) represents a strongly coupled set of nonlinear equations with a novel type of power-law behavior (with negative exponent $-\beta$). This set of equations is the central result of this session since it can be considered as a population dynamics describing the coupling of two populations mixing on a fractal, and as we show below, opens up the possibility to have a nontrivial coexistence.

A simple further equivalent form can be derived by using relative densities $c_i \equiv N_i/N$. The equations describing the populations then become (by using (2.32) and (2.29):

$$\frac{dc_1}{dt} = q N^{-\beta-1} (v_1 p_1 c_2 - v_2 p_2 c_1) \tag{2.33}$$

with $c_1 + c_2 = 1$. The temporal change of the densities is determined by the weighted relative difference in the densities. Note that they are *multiplicatively* coupled to $N^{-\beta-1}$ which is proportional to the average width of the filament covering. For $D_0 = 1$ this is just $1/N$ and it is the spatial concentration or the density of the total population. For $2 > D_0 > 1$ (fractals), this factor is the *fractal* spatial density of the population as a whole. According to the detailed stability analysis (see Appendix A) the coexistence of competitors is stable if $0 < \alpha < 1$, and one of the species excludes the other one if $\alpha > 1$.

In the next section we analyze dynamics of competing species in a simple chaotic dynamical system, the Baker map. Since my theory contains some nontrivial assumptions our aim in the following section is to verify the results. Here we show that $g(z)$ is given by Eq. (2.19) in this process, find a perfect agreement with the stability criterions, and determine the parameters α and ω from numerical experiments.

Numerical verification

In this section we present numerical verification of the new type of population dynamical equation we introduced before. We have already shown that coexistence in open flows is possible as is shown before (Scheuring et al. 2000; Károlyi et al. 2000), so we deal with the *quantitative* verification of the theoretical results.

For computational simplicity, we use the so-called *baker map* to model the flow (Toroczkai et al. 2001). This can be considered as a simplified model of stretching and folding in a chaotic flow observed periodically after specified time-intervals. Thus, in this case τ, the time lag between instantaneous multiplications of the species, is an integer number denoting the number of snapshots taken of the flow between two consecutive multiplications. The baker map, acting on the unit square, gives the new location (x', y') of an individual starting at point (x, y):

$$\begin{array}{ll} x' = ax + (1-a)\theta(y-1/2), & x \in [0,1], \\ y' = \frac{1}{a}y - (\frac{1}{a}-1)\theta(y-1/2), & y \in [0,1], \end{array} \tag{2.34}$$

where $a < 1/2$ is the parameter of the baker map, and $\theta(x)$ is the Heaviside step function. The action of the baker map is shown schematically in Fig. 2.6. The area preserving property of this baker map models the incompressibility of realistic hydrodynamical flows, while outflow is modeled by neglecting the area hanging over the edge of the unit square. Starting with any initial conditions, after a few steps of iterations both species will be distributed along narrow filaments parallel to the y axis.

After τ baker steps, individuals of species B_i multiply and give birth into a vertical stripe of width σ_i covered by resource A, lying along the borderline of the previously occupied region of species B_i parallel to the y axis. In the numerical experiments, we used $\tau = 1$, that is, the species multiplied after each baker-step. Regions which are invaded by both species after instantaneous multiplication are divided between them in a ratio of σ_1/σ_2. It is expected that (2.26) describes the time-evolution of the species, reaching the fixed-point (4.14) evaluated in Appendix B. Figure 2.7 shows in a typical case how the equilibrium state with coexistence is reached after about

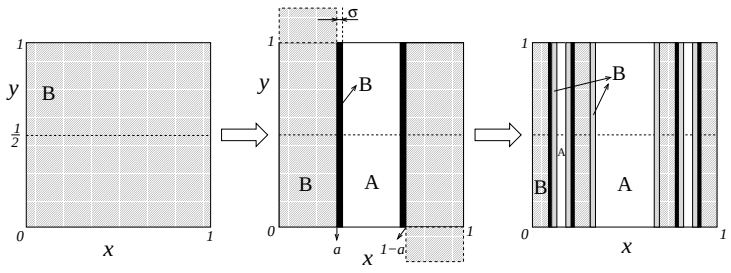

Figure 2.6: Two consecutive steps of the baker map and two replications ($\tau = 1$) for the single species model. The bands of width σ become occupied by B in each replication. The material hanging over the unit square is discarded.

18 baker steps. Similar results were obtained with various other parameter settings, in accordance with the theoretical results. We checked the validity of the form (4.14) against the numerical results in steady states. N_i^* is the fixed-point number of individuals of species B_i. The fixed point values are found to fulfill (4.14), see Fig. 2.8.

Next we check the validity of (2.26) for the time-evolution before reaching the steady state. We measure the population numbers in discrete time n and use relation (4.13) to extract the form of the probability distribution g (see Appendix B). Figure 2.9 shows p_1 as a function of N_1/N_2 for fixed parameter values, but for various initial conditions. There is a single function covering the measured points which can well be fitted by the form $g_1(z) = z^\alpha/(z^\alpha+\omega)$. In all cases $\alpha < 1$ was measured indicating that the coexistence fixed point is stable. Also note that $\omega \approx (\sigma_1/\sigma_2)^\alpha$ was found in all experiments, which implies that (2.18) holds.

We also measured how α depends on the parameter of the baker map, or, on the fractal dimension D_0 of the outflow curve of the chaotic saddle. We found that $\alpha = 0.79 \ln a + 1.54$, see Fig. 2.10. Using the fact that $D_0 = \ln 2/\ln(1/a)$, we obtain $\alpha = 1.54 - 0.55/D_0$.

2.1.5 Discussion

We derived a novel type of coupled population dynamic equations for two populations competing on a fractal set provided by open chaotic flows. The equation for the number of species in a given fixed range of the flow can be written in the general scheme (cf. 2.32)

$$\frac{dN_1}{dt} = \alpha_1 \left(\frac{N_1}{N}\right) N_1^{-\beta} - \kappa N_1, \tag{2.35}$$

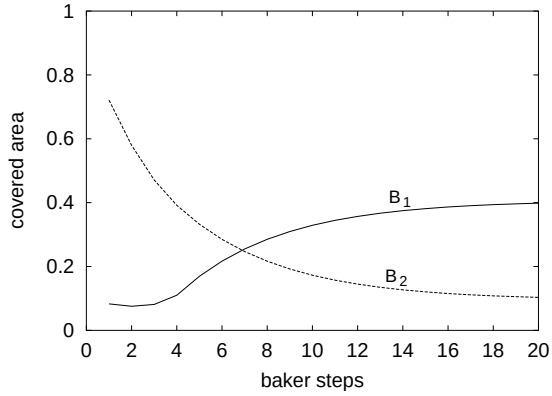

Figure 2.7: Reaching the equilibrium states with the coexistence of two species is shown. Initially, two patches of species were placed, one patch of B_1 in $x \in [0; 0.1]$, $y \in [0; 1]$, and another patch of B_2 at $x \in [0.1; 1]$, $y \in [0; 1]$. The parameter values are $a = 0.4$ for the baker map, and $\sigma_1 = 0.003$ $\sigma_2 = 0.001$ for the competing species. The areas covered by the species are shown right after the multiplications taking place. After an initial transient (time-steps 1–4), we have a rapid convergence to the fixed point (time-steps 5–18), after that we have an equilibrium setting in (time-steps 18–20).

$$\frac{dN_2}{dt} = \alpha_2 \left(\frac{N_2}{N}\right) N_2^{-\beta} - \kappa N_2. \tag{2.36}$$

The coefficients α_i of the replication terms depend on the relative densities (denoted by $N_i/N \equiv c_i$) only. Their explicit form follows from (2.32). For example,

$$\alpha_1 \left(\frac{N_1}{N}\right) = q \left(\frac{N_1}{N}\right)^{\beta} \left[(1 - D_0) v \frac{N_1}{N} + v_1 p_1\right]. \tag{2.37}$$

The structure of these equations is similar to that of (2.1, 2.2) or (2.13, 2.14). The time derivative is the sum of a gain term and a loss term, but now the gain term contains a nontrivial negative power of the population number and is coupled to the other population in a nonlinear way. These equations describe the population dynamics in an imperfectly mixed environment of dimension $1 < D_0 < 2$. The fractality D_0 of the mixing region (in our case of the outflow curve) appears in the power $\beta = (2 - D_0)/(D_0 - 1)$. In this set of equations a phenomenological function (p_1) is also present characterizing the probability that a given population is on the surface of the fractal support with free access to the single available resource. Based on general arguments and a simple model, this function turned out to be a normalized power law

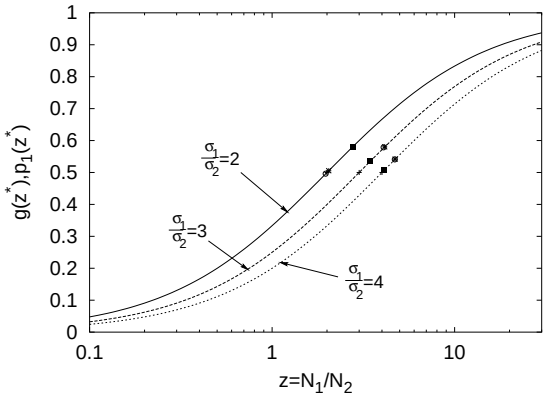

Figure 2.8: The dependence of the probabilities p_1 on N_1/N_2 in the nontrivial fixed points. The initial positions do not influence the fixed point reached. The curve $h(z) = z/(z + \sigma_1/\sigma_2)$ is shown with solid line for $\sigma_1 = 0.002$, $\sigma_2 = 0.001$, with dashed line for $\sigma_1 = 0.003$, $\sigma_2 = 0.001$, and with dotted line for $\sigma_1 = 0.004$, $\sigma_2 = 0.001$. All the measured fixed point values fulfill $g(z^*) = z^{*^\alpha}/(z^{*^\alpha} + \omega) = h(z^*) = z^*/(z^* + \sigma_1/\sigma_2)$. The fixed points are marked by crosses ($a = 0.25$), black squares ($a = 0.3$), stars ($a = 0.35$), and circles ($a = 0.4$ as the baker parameter).

distribution of the type of (2.19). This form expresses a kind of "advantage of rarity" principle: for exponent $0 < \alpha < 1$ the derivative is infinite in the origin, a very small increase in the size of the weaker population leads to a drastic increase of the probability for being on the free surface and hence to grow. On the contrary, for $\alpha > 1$, only a relatively large population size has considerable growing probability, in this case the weaker population dies out. With exponents larger than unity this form does not allow for coexistence. The presented mathematical forms and the conditions for coexistence remain valid if $m > 2$ species live in open chaotic flow, a numerical evidence for which has been reported by (Károlyi et al. 2000). It is natural to expect that the probabilities p_i, $i = 1, ..., m$ appear in the generalized form of $p_i = (\omega_i \varepsilon_i^\alpha)/(\sum_{i=1}^m \omega_i \varepsilon_i^\alpha)$, where ε_i are the partial width of the species and ω_i are phenomenological constants.

Although in the numerical simulation, based on the baker map as a model flow, we only found stable coexistence, we also carried out simulations where the biological process was not based on parallel stripes filled out homogeneously with individuals, as assumed in our theory. In these cellular automaton-like simulations the replication and competition process is carried out on a uniform rectangular grid of lattice size ϵ_0. This ϵ_0 can be considered as the smallest distance between the individuals, or the linear size of a

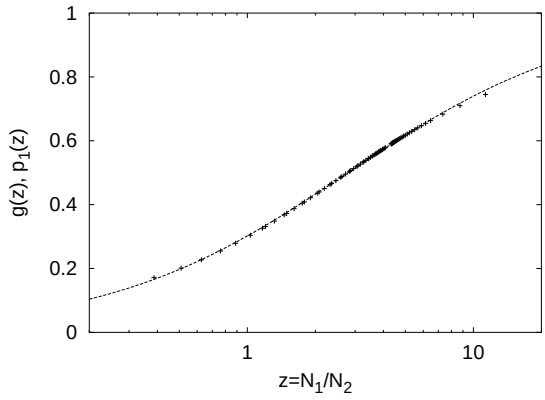

Figure 2.9: The dependence of the probabilities p_1 on N_1/N_2 with $\sigma_1 = 0.003$, $\sigma_2 = 0.001$ values, and with five different initial conditions. The parameter of the baker map was $a = 0.4$. The initial positions do not influence the fixed point reached. Solid line shows the function $g(z) = z^\alpha/(z^\alpha + \omega)$ with $\alpha = 0.818 \pm 0.002$ and $\omega = 2.312 \pm 0.006$. The parameter of the baker map was $a = 0.4$.

single individual below which there is hard-core exclusion among them. Individuals of each species can occupy the center of each grid-cell. When they are advected by the flow into another grid-cell during the time τ, they are instantaneously placed to the center of that grid-cell. During reproduction, they give birth to new individuals in the surrounding empty grid-cells, whose centers are within a distance σ_i. If more than one species tries to give birth into the same grid-cell, only one of them will be able to do so according to one of the following rules: *rule I:* both species can win this competition in each cell with equal probability, or *rule II:* both species can win this competition in each cell with probability proportional to the number of individuals of the same species intending to give birth there, or *rule III:* always the better competitor (with higher σ) wins. Our results show that the coexistence depends on which rule has been applied. In some cases one of the populations was competed out, but even in such cases the distribution function was found to be of the shown form, with an exponent $\alpha > 1$, in full harmony with the theory. We may conclude that the exponent α is determined by the flow (see Fig. 2.10) and the biological process (see the different competition rules). It is worth mentioning that with the same rules on a lattice, in previous simulations (Károlyi et al. 2000) for the more realistic fluid dynamical case of a flow around an obstacle we always found coexistence. This indicates that the boundary layer present around the obstacle enhances the chances of survival.

Our theory does not describe the effects of diffusion. Besides the fact that

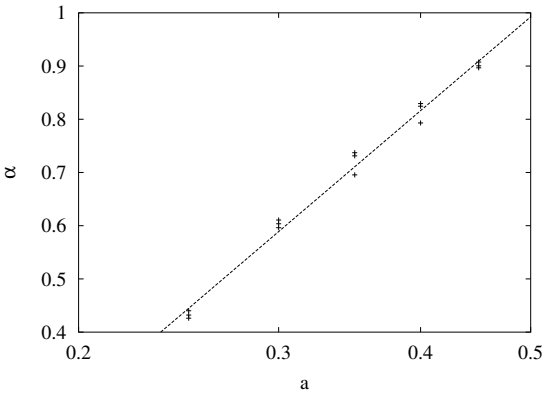

Figure 2.10: Dependence of α on the parameter a of the baker map. Various points are measured values for multiple σ_1/σ_2 ratios. The dashed line is the function $\alpha(a) = 0.79 \ln a + 1.54$.

for individuals of small but macroscopic mass and size, like eg. phytoplankton, diffusion is not believed to be important, it can be shown (Tél et al. 2000) that weak diffusion in such models only renormalizes the replication rates. As a consequence, the cut-off scale below which fractality cannot be observed is somewhat increased, but the population dynamical equations remain unchanged.

In this theory the location dependence of the death and replication rates is not taken into account. Such effects is studied in numerical simulations (Károlyi et al. 2000; Santoboni et al. 2002) and are not expected to change the essence of our findings.

In conclusion, we have shown that a particle-like (microscopic) model of individuals competing for a single resource around a fractal outflow curve of a chaotic flow leads, on the level of the total number of individuals, to dynamical equations with unusual singular terms. These describe enhanced intra- and decreased inter-species competition due to inhomogeneous mixing. The appearance of unusual population dynamical equations can be expected in general in all cases where the individual dynamics is not taking place on full compact regions of the space but are restricted to fractal subsets of it.

On the basis of numerical simulations and mathematical analysis we conclude that the coexistence of competing species is a generic feature expected to be found in open flows exhibiting chaotic advection. I emphasize that the qualitative features of the fractal patterns (and of the boundary layer), which are essential for this study, are robust and can be found in any open time-dependent flow. The shape of the obstacle and the time periodicity of the flow are only considered for convenience and easy presentation.

Although stratifiation of aquatic systems often ensures the two- dimensional nature of the flow, I briefly comment on possible effects of the third dimension. It has been shown that in the advection by stationary three-dimension flows third dimension plays an analogous role to that of the time in time-dependent two-dimensional flows (Sagdeev et al. 1992).

This implies that the concept of inflow and outflow curves should be replaced by that of inflow and outflow surfaces. In flows with chaotic advection these are a bundle of highly convoluted, nested sheets. A periodic time dependence of the three dimensional flows makes these sheets to oscillate. The coexistence of competing advected species is expected along these outflow surfaces. Any planar intersection of them exhibits the same filamental structure as in the two dimensional models discussed above.

Typical fluid motions are rarely time-periodic. In a broad class of flows, however, when the flow field is chaotic in time but exhibits a kind of structural stability (like in the example of randomly driven or chaotically moving vortices (Jacobs et al. 1997; Neufeld & Tél 1998) the topology of the advection patterns remains unchanged. This means that although the inflow and outflow surfaces move in a non-periodic, chaotic fashion, their fractal dimension and the escape rate of the open flow remains well defined (Jacobs et al. 1997).

Although we restricted our discussion to two dimensional flows, based on these observations we expect to see coexistence in similar competitive models in three dimensional open chaotic flows and possibly in two dimensional turbulence (Spall & Richards 2000) as well.

Other simplification in this model is that we neglected the inertia and the finite size of the individuals. Taking into account the inertia and finite size, the unstable manifolds along which the individuals move are different for species with different size. We show that this "physical niche differentiation" leads to the persistence of different species even in cases when the passively advected species cannot coexist (Benczik et al. submitted).

Finally I remark that in the absence of enzymes, replicating macromolecules at high concentrations are bound together effectively with hydrogen bonds (Zielinski & Orgel 1987; Sievers & von Kiedrowski 1994). This self-inhibition can lead to the so-called parabolic growth implying that competitive replicators coexist even in a well stirred environment (Szathmáry & Gladkih 1989). The concentrations required are, however, unrealistically high. The pure hydrodynamic effect I presented here shows that the coexistence is a consequence of the imperfect mixing dynamics of the flow, and the concentrations of replicators accumulated along the outflow curve need not reach unrealistically high values as needed for parabolic growth.

Open chaotic flows have the role of maintaining diversity in competing advected populations (e.g. phytoplankton), and also give a natural solution

for the problem of information integration in early evolutionary units. The issues presented in this section are, however, of larger generality. They show that novel effects and phenomena can arise if a population dynamics is subjected to an underlying chaotic spatial mixing.

2.2 Competitive exclusion in the ocean

We have studied the effect of the small scale structure of open chaotic flow in the previous section. However, structures are also present at very large scales in oceans. Large scale filamental structures can be observed in satellite pictures (see Fig 2.1, for example). At the same time, coherent structures, such as vortices can be observed in oceans. While vortices emerge and dissappear continuously, the vortex structure itself is present permanently because of the rotation of the Earth. In the following, we focus on the effect of vortex structures on the competitive exclusion of plankton species.

More precisely, we examine a scenario where horizontal mesoscale turbulence, characterized by the presence of coherent vortices, influences the fate of competitive plankton populations. The vortices generate dynamical transport barriers and allow for prolonged survival of competitive species in an otherwise homogeneous environment. Clearly, vortices alone cannot assure an infinitely long plankton coexistence, as the species trapped inside vortices will sooner or later come into contact with species outside, due to small-scale turbulent mixing and to the finite lifetime of the vortices themselves. However, thanks to the shielding offered by the vortex cores, the less-fit plankton species can survive for several months, until environmental conditions (related for example to the marching of the seasons) become more favorable. Mesoscale features can also help to explain the different (but somehow related) issue of plankton patchiness (e.g., Denman & Platt 1976; Steele 1978), as discussed by Flierl & Davis (1993), Smith *et al.* (1996), Abraham (1998), Spall & Richards (2000).

Long-lived coherent vortices do indeed permeate the world oceans, as revealed by both observation (Hooker & Brown 1994) and high-resolution numerical simulation (Chassignet 1992; Paiva *et al.* 1999). Vortices play an important role in the transport of material constituents and dynamical quantities across the ocean, and affect the overall distribution of eddy kinetic energy (Siegel *et al.* 2000). The flow model used here, known as quasi-geostrophic turbulence (Pedlosky 1987), is a simplified dynamical description of mesoscale ocean motions that is characterized by the spontaneous emergence of coherent vortices (McWilliams 1984, 1990; Babiano *et al.* 1987). Coherent vortices are spatially localized patterns in the vorticity field, with

a long lifetime (hundreds of rotation periods). Most of the energy and vorticity of the system is concentrated in these vortices, which extend their influence over large distances (Bracco *et al.* 1999).

It is known that coherent vortices affect the dynamics of advected tracers in several ways. Vortices act as barriers to material exchanges between their cores and the external background turbulence, and enhance transport of constituents trapped in their interior (Elhmaïdi *et al.* 1993; Provenzale 1999). This impermeability induces strong inhomogeneities in the tracer distributions over long time scales. In particular, ocean eddies have been shown to trap plankton communities in their cores for periods longer than one year (Ring Group 1981).

Below I show that the presence of coherent vortices can slow down the selection process to time scales that are long enough to allow for the survival of competitive phytoplankton species.

2.2.1 Simulated plankton dynamics

In the following, we adopt a mixed Eulerian-Lagrangian description of the turbulent dynamics and integrate the motion of plankton-carrying fluid elements in a flow representing the surface layer of the ocean. For simplicity, we consider only two passively advected plankton species that compete for a homogeneously distributed resource.

In our approach, vertical motions of the fluid elements are not allowed. Thus, the fluid patches considered here represent vertically-integrated sample portions of the surface mixed layer and the model dynamics describes large and mesoscale horizontal mixing by geostrophic turbulence.

The time integration of the model proceeds as follows. Each fluid element, labelled by j, is located at the position (X_j, Y_j) at time t. A generic fluid element contains two competitive phytoplankton populations, called A and B, that have concentrations $a_j(t)$ and $b_j(t)$ respectively. Note that both species can be present in the same fluid parcel.

The fluid elements are advected by a turbulent horizontal velocity field, $\mathbf{u} = (u, v)$, that is a function of space and time. The positions of the fluid elements evolve in time as

$$d\mathbf{X} = \mathbf{u}(\mathbf{X}, t)dt \tag{2.38}$$

where $d\mathbf{X} = (dX, dY)$ is the infinitesimal increment in the position of the fluid parcel and dt is an infinitesimal time increment. We keep a differential notation instead of the more standard time derivative because the velocity field can be a stochastic variable.

In the model, we make the simplifying assumption that the concentrations a_j and b_j can change only at specified time intervals (e.g., once a day due to the diurnal cycle), when the two species compete and their concentrations change due to the different reproduction and survival rates. To practically implement the competitive dynamics, at the selected time intervals we evaluate the local concentrations of the two species on a spatial Eulerian grid, as obtained by averaging the concentrations carried by all the fluid elements that are inside a given grid cell with size ϵ, where ϵ defines the length of small-scale homogenization. This leads to the definition of two averaged macroscopic concentration fields $a_\epsilon(x, y, t)$ and $b_\epsilon(x, y, t)$, where (x, y) are the coordinates of the grid points (i.e., geographical coordinates on the ocean surface). The concentrations after competition are then given by

$$a'_\epsilon = \frac{\alpha a_\epsilon}{\alpha a_\epsilon + \beta b_\epsilon} \qquad b'_\epsilon = \frac{\beta b_\epsilon}{\alpha a_\epsilon + \beta b_\epsilon} \tag{2.39}$$

where α and β are the multiplication rates. Clearly, the species with the largest multiplication rate selects out the other one. The new concentration in each grid cell is then assigned to all the fluid elements contained inside that cell, simulating diffusion and homogenization on the scale of one grid cell. Note also that the total concentration in each grid cell and for each fluid element is normalized such that $a + b = 1$ at any time (however, the results remain qualitatively the same if $a + b$ is normalized to another constant or to a slowly decaying function of time, representing e.g. mortality).

In the model considered here, the annual cycle of planktonic ecosystems is not taken into account. In nature, this cycle leads to the creation of a mixed layer at the end of winter, followed by a phytoplankton bloom at the beginning of spring. Then, during summer and fall, phytoplankton growth is limited by the availability of nutrients and inhomogeneities in the environment can dominate over bloom behavior. In the present approach, the role of turbulence is tested on time scales of at most $6 - 9$ months, corresponding to the period between two subsequent spring blooms.

Clearly, the model assumptions are very crude. The model, in particular, neglects sinking, incomplete vertical mixing, relative grazing and interactions between nutrient limitation and competition for light, even though those factors can have a major impact on the species compositions. On the other hand, the extreme simplification of this model allows for clearly elucidating the basic effects of horizontal mesoscale structures on phytoplankton coexistence.

2.2.2 The flow models

Geostrophic turbulence

The equation that describes barotropic turbulence in the quasi-geostrophic approximation (see Pedlosky 1987 for a complete derivation) is

$$\frac{D\omega}{Dt} = \frac{\partial \omega}{\partial t} + J[\psi, \omega] = D + F \tag{2.40}$$

where $\frac{D}{Dt}$ is the total advective derivative, $J[\psi, \omega] = \partial_x \psi \partial_y \omega - \partial_y \psi \partial_x \omega$ is the two-dimensional Jacobian operator, ψ is the streamfunction and $\omega = \nabla^2 \psi$ is relative vorticity. The velocity field $\mathbf{u} = (u, v)$ is given by $u = -\partial_y \psi$ and $v = \partial_x \psi$. The dissipative term D represents horizontal eddy viscosity and it provides a parameterization of both unresolved small-scale motions and large-scale friction (see below). The forcing F represents an energy input from large-scale motions.

Barotropic turbulence is characterized by a direct cascade of enstrophy (the integral of squared vorticity, Z) toward small scales and by an inverse cascade of kinetic energy from small to large scales (Kraichnan 1967; Batchelor 1969). In this flow, a random initial vorticity field spontaneously evolves into coherent vortices that carry most of the energy and vorticity of the flow and dominate the dynamics (McWilliams 1984, 1990). Figure 2.11. shows a picture of the vorticity field after vortex emergence.

In the following, forcing is imposed at a given wavenumber k_f, keeping the energy at this scale fixed in time. Thus, inverse energy cascade is observed for $k < k_f$ and direct enstrophy cascade for $k > k_f$. With this type of forcing, vortices have a size close to the forcing scale. The dissipative term is given by the sum of two terms, $D = D_v + D_f$. Here D_v is a hyperviscous term acting at small scales, $D_v = -\nu \nabla^8 \nabla^2 \psi$ where ν is the viscosity coefficient, and D_f is a friction term, proportional to ψ, which acts at the largest scale to dissipate the energy piled up by the inverse energy cascade. Forcing and dissipation are balanced so to obtain a statistically stationary turbulent flow. In this system, plankton-carrying fluid elements are advected by using equation (2.38).

Equation (2.40) is numerically integrated on a doubly periodic square domain with size $L = 2\pi$ by using a pseudo-spectral code with standard 2/3 dealiasing and 256^2 collocation points (see Canuto *et al.* 1987 for details on the numerics). The forcing wavenumber is fixed as $k_f = 10$, and dissipation and forcing are kept as small as possible in order to achieve a large Reynolds number. The time integration of the vorticity field is performed by a third order Adams-Bashford scheme. When the flow has reached statistical equilibrium between forcing and dissipation, 256^2 plankton-carrying fluid elements are uniformly released in the domain. The motion of the fluid elements is

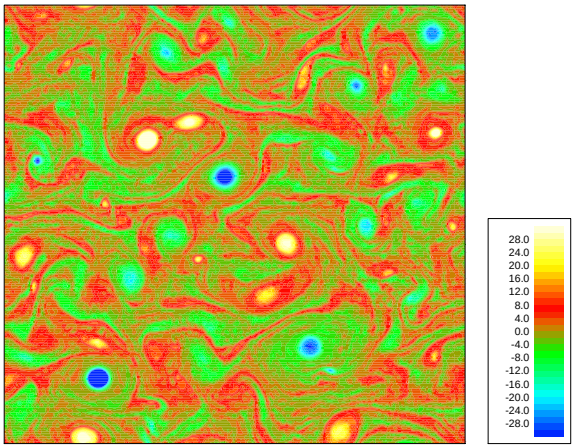

Figure 2.11: Vorticity distribution at the time when plankton-carrying fluid elements are released. The relative vorticity coded by different colors from blue to red.

integrated by using a third order Adams-Bashford time integration scheme and a third order spectral spline interpolator for a total time $T = 20$.

To obtain a physical estimate of the time and space scales of the model, we recall that the typical eddy-turnover time, T_e, in the ocean is ~ 8 days. In the present simulation, $T_e = Z^{-1/2} \sim 0.25$. Comparing the two values, we obtain that one adimensional time unit of the model corresponds to a physical time span of one month. In physical units, the total integration time is thus $T \sim 20$ months. The physical length scale can be determined by recalling that the typical forcing scale in the ocean is of the order of 50 km. Since $k_f = 10$ in the model, the physical size of the integration domain can be fixed as $L \sim 500$ km, and one grid spacing corresponds to about 2 km.

Random walk

Together with vortex-dominated, self-consistent geostrophic turbulence, we also consider two standard homogeneous stochastic models (see Griffa 1996 for a review) in order to have test cases of plankton dynamics in unstructured turbulence. The continuous limit of these models leads to various forms of standard reaction-diffusion dynamics.

The first stochastic model we consider is a classic 'random walk', and it

assumes that the tracer position is a Markov variable. The equation that describes the tracer motion can be written as

$$\begin{aligned} d\mathbf{X} &= \mathbf{u}dt \\ d\mathbf{u} &= (\sigma^2/T_L)^{1/2} d\mathbf{w}. \end{aligned} \tag{2.41}$$

Here $d\mathbf{X}$ is the total displacement of the particle during the time dt and $d\mathbf{u}$ is the velocity increment, σ^2 is the velocity variance, T_L the average Lagrangian integral time scale and $d\mathbf{w}$ is a random increment extracted from a normal distribution with $\langle d\mathbf{w} \rangle = 0$ and $\langle dw_i(t)\, dw_j(t') \rangle = 2\delta_{i,j}\, \delta(t - t')\, dt$, where the subscripts indicate vector components and $\langle \cdot \rangle$ indicates ensemble average.

The second model, usually referred to as an Ornstein-Uhlenbeck process, assumes that the particle position $\mathbf{X}$ and the turbulent velocity $\mathbf{u}$ are jointly Markovian. In this case, the advection equations become

$$\begin{aligned} d\mathbf{X} &= \mathbf{u}dt \\ d\mathbf{u} &= -\frac{1}{T_L}\mathbf{u}dt + (\sigma^2/T_L)^{1/2} d\mathbf{w}. \end{aligned} \tag{2.42}$$

where $\mathbf{u}$ is drawn from a Gaussian distribution with zero mean and variance σ. This stochastic process has been shown to provide an approximate description of the second order particle statistics in the upper ocean (Griffa 1996), although it does not capture the effects of vortex dynamics (Pasquero *et al.* 2000).

For consistency, we fix the values of σ^2 and T_L in the stochastic models equal to those obtained from the geostrophic turbulence simulation. In particular, the average Lagrangian integral time scale is defined as

$$T_L = \int_0^\infty R(\tau) d\tau \tag{2.43}$$

where $R(\tau)$ is the ensemble-averaged Lagrangian velocity autocorrelation, i.e.

$$R(\tau) = \lim_{T \to \infty} \frac{1}{\sigma^2} \int_0^T \langle \mathbf{u}(t) \cdot \mathbf{u}(t + \tau) dt \rangle. \tag{2.44}$$

where the average $\langle \cdot \rangle$ is taken over the ensemble of fluid elements advected by the barotropic turbulent field.

2.2.3 Results

In the following, we discuss the dynamics of the two competitive plankton populations A and B, advected by the different types of turbulent models described above.

The competitive dynamics start with all fluid elements in $0 < x < L/2$ occupied by species A (here, $a_\epsilon = 1$ and $b_\epsilon = 0$ at $t = 0$) and elements in $L/2 < x < L$ occupied by B-type entities (here, $a_\epsilon = 0$ and $b_\epsilon = 1$ at $t = 0$). We choose the species A to be the competitively inferior one, i.e., $\alpha/\beta < 1$.

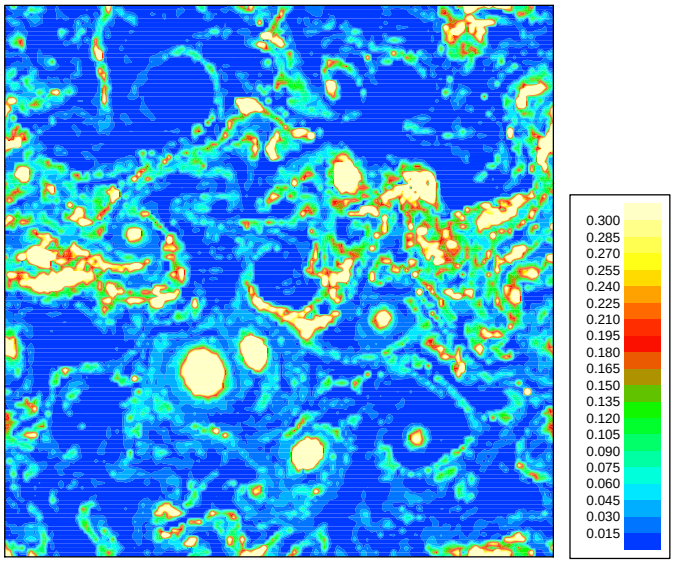

Figure 2.12: Distribution of $a_\epsilon(x, y, t)$ at time $t = 10 \sim 10$ months after release, as indicated by the grey scale. Yellow patches contain only species A, blue patches are dominated by species B.

Figure 2.12. shows the concentration field $a_\epsilon(x, y, t)$ at time $t = 10 \sim 10$ months for the case of geostrophic turbulence, with $\epsilon = 1$ grid spacings (physically, this corresponds to diffusive plankton homogenization on scales of about 2 km) and $\alpha/\beta = 0.9$. After several months, A-type entities are still concentrated inside the coherent vortices that were initially in $0 < x < L/2$ and in the vorticity filaments generated during vortex-vortex interactions. During this time, the vortices have moved around in the whole domain, but, due to the strong vorticity gradients present on their edge, they have acted as transport barriers protecting the A-type weaker plankton present in their cores from competition with the other species allowing a prolonged survival of the less-fit species.

By contrast, the less-fit species survives for a much shorter time when unstructured stochastic advection is considered. To provide a quantitative comparison of the different cases, in figure 2.13. we show the time evolution of the average concentration of A for different values of α, β and ϵ, for the

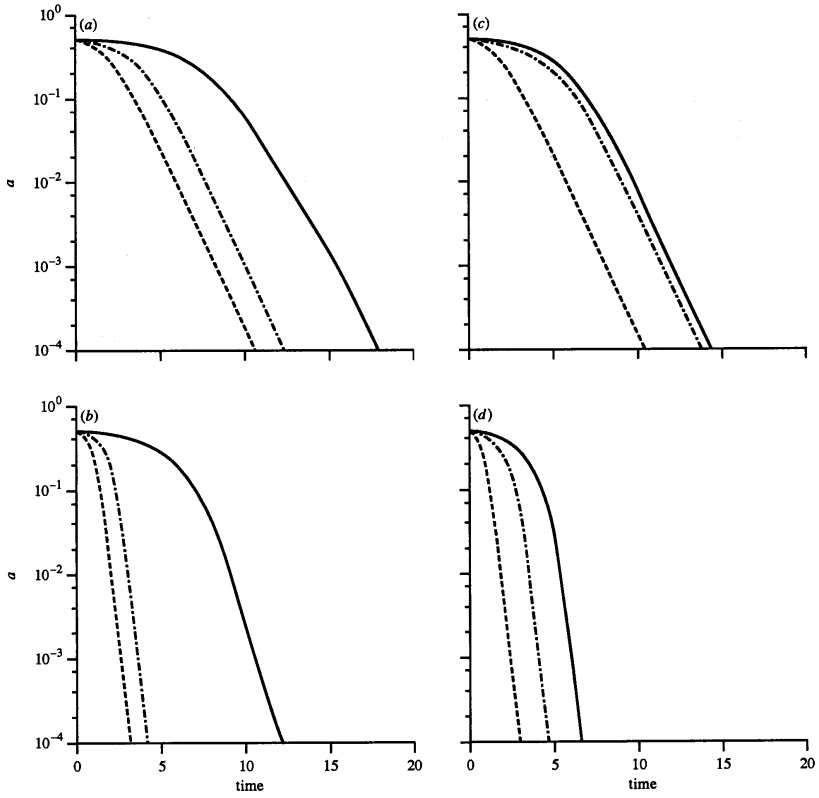

Figure 2.13: Time evolution of the average concentration of species A for advection by geostrophic turbulence, equation (2.40) (solid line), by the Ornstein-Uhlenbeck process, eq. (2.43) (dashed-dotted line), and by the Brownian random walk, eq. (2.42) (dotted line). The values of the parameters are $\alpha/\beta = 0.9$ and $\epsilon = 1$ grid spacings (panel a), $\alpha/\beta = 0.67$ and $\epsilon = 1$ grid spacings (panel b), $\alpha/\beta = 0.9$ and $\epsilon = 2$ grid spacings (panel c), and $\alpha/\beta = 0.67$ and $\epsilon = 2$ grid spacings (panel d).

three types of advection discussed above. In panel (a) and (b), ϵ is one grid spacing. The ratio α/β is 0.9 (a) and 0.67 (b). In panel (c) and (d), ϵ is set equal to two grid spacings, again with $\alpha/\beta = 0.9$ and 0.67. When tracers are advected by Brownian motion or by a Ornstein-Uhlenbeck process, the concentration of the species with the lower multiplication rate decreases rapidly, and the less-favored plankton population is soon eliminated. After just a few months, the average concentration of A in the turbulent mesoscale flow is already much larger than for random advection. At $t \sim 10$ months, for random dispersion with no coherent vortices the system is homogeneously occupied by B-type entities.

We performed several simulations, varying the homogenization range ϵ, the ratio α/β and the time interval between subsequent competition events, finding analogous results. For all values of α/β that we considered, the concentration of the population with the lower multiplication rate maintains significant level for a longer time when it is advected by geostrophic turbulence. The value of the homogenization range ϵ is more critical, as the survival of the less favored population is significantly shortened as ϵ grows beyond a few kilometers. All together, these results indicate that when small-scale horizontal plankton homogenization is confined below about 5 km and mesoscale advection is dominated by vortex dynamics, the less-fit species can survive over relatively long time scales (~ 10 months) inside the coherent vortices.

2.2.4 Discussion

In this work, we have studied the dynamics of different planktonic species that are in competition for the same resources, and we have explored the role of mesoscale vortices in the advecting flow. We have shown that coherent vortices in a turbulent environment can lead to strongly non-uniform spatial planktonic patterns and to prolonged survival of competitive species, preventing the less-fit species from being driven out completely during the most critical months. Since in real ecosystems the environmental conditions vary in space and time, a weaker competitor at a given location in one year can become the stronger one in the following year or in another place. Thus, competing phytoplankton, with the help of mesoscale vortices, can remain in nonequilibrium coexistence on very long time scales. On the contrary, horizontal dispersion by unstructured random walks with mixing-length step size with an homogeneous resource distribution is not able to sustain the great number of coexisting planktonic species observed in oceanic surface waters, leading to disappearance of the less-fit species on time scales that are presumably shorter than those associated with the varying environmental conditions. This provides further indication of the important dynamical role

that coherent vortices play in the ocean.

2.3 Cyclic competition hierarchy in chaotic flow

2.3.1 Introduction

One of the most prominent questions of ecology is to explain the mechanisms maintaining biodiversity. While there are several diversity enhancing mechanisms (Chesson 2000), finding the most important ones in a given community is a challenging task (Wilson 1990; Sommer 2002). In case of phytoplankton, for example, ecologists generally emphasize the intermediate level environmental disturbance or temporally variable conditions in promoting high diversity (Hutchinson 1961; Reynolds 1993; Sommer 2002), though recent works have pointed out that intrinsically generated complex dynamics (Husman & Weissing 1999; Huisman & Weissing 2001b) or, as I have shown above chaotic mixing of aquatic media (Károlyi et al. 2000; Scheuring et al. 2000, 2003) can also maintain high species diversity in these communities. Interestingly, plankton model systems show complex chaotic dynamics and high species diversity most frequently when there is no clear competition hierarchy, due to a cyclic relation between competitive abilities of some species (Schippers et al. 2001; Huisman et al. 2001). While the physiological mechanism of cyclic competitive relation is not clear in plankton systems, it is evidently detected among other taxa including different microorganisms (Buss & Jackson 1979; Paquin & Adams 1983; Kerr et al. 2002; Paine 1984; Sinervo & Lively 1996; Kirkup & Riley 2004).

Cyclic competition often appears as a result of toxin production by one of the species. Many species belonging to very distant taxa can synthesize and excrete allelopathic substances for their continuous warfare with other individuals. The best-known such example is bacteria synthesizing antibiotic molecules, but numerous terrestrial plants, yeast species, macrophytons, ciliates and phytoplankton also produce toxins that inhibit or kill other individuals around them (Chater & Losick 1997; Hallegraeff 1993; Scheffer 1998; Putnam & Tang 1986; Riley & Gordon 1999; Wium-Andersen et al. 1982). In the case of bacteria and yeast it is known that the so called "killer" types (which produce the allelopathic substance) may coexist with the "sensitive" (non-producer) strains or closely related species (Riley & Gordon 1992; Starmer et al. 1987) and in some cases a "resistant" strain is also detected (Riley & Gordon 1999; Paquin & Adams 1983).

The presence of killer, sensitive and resistant strains establishes a cyclic

competition hierarchy (Riley & Gordon 1999). The killer (K) strain of *Escherichia coli* bacteria contains a plasmid which encodes the toxic colicin and a protein defending the bacteria from the colicin. Sensitive cells (S) are inhibited or destroyed by the toxin, while the resistant strain (R) is protected by special cell surface proteins (Riley & Gordon 1999). However, the colicin receptor proteins are in conflict with nutrient uptake (Adams et al. 1979; Feldgarden & Riley 1999; Riley & Gordon 1999), therefore R cells replicate slower than S cells. Similarly, due to the metabolic cost of colicin production, K cells have a lower replication rate than R cells. Like in the rock-scissors-paper game, K can displace S, S can invade R and R wins over K, thus there is no obvious outcome of the competition when all three strains are present (Hofbauer & Sigmund 1998). Furthermore, the dispersion of cells also plays an important role in this process.

Experiments and numerical models have shown that in well mixed environments the sensitive-killer relationship is bistable (Chao & Levin 1981; Durrett & Levin 1997), i.e. the winner depends on the initial concentrations of the two strains. But, when the two strains are distributed in space, e.g. bacteria on the surface of agar, the killer has an overall competitive advantage (Chao & Levin 1981; Durrett & Levin 1997). Similar results are found in a more complex model where toxin producing and toxin sensitive phytoplankton species and two heterotrophic bacteria interact taking the toxin, inorganic material and detritus dynamics into account explicitely (Hulot & Huisman 2004). The invasion of the killer is well understood mathematically by the traveling wave solution of the nonlinear diffusion equations in these models. However, the killer-sensitive coexistence is possible in a metapopulation model where local stochastic extinctions and recolonizations from the occupied patches maintain a dynamical equilibrium (Durrett & Levin 1994; Czárán & Hoekstra 2003)

In three-species allelopathic systems with cyclic competition hierarchy, it was shown that coexistence of all species is possible in spatially distributed models with short range interaction (Tainaka 1994; Durrett & Levin 1997; Nakamaru & Iwasa 2000; Kerr et al. 2002), even when they can not coexist in the corresponding well mixed system. Similar results have been found for other three-species models with cyclic competition (Durrett & Levin 1998; Czárán et al. 2002). In these cellular automata type simulations performed on a two-dimensional lattice, the different species aggregate in patches that invade each other in a cyclic fashion. Note, that coexistence also disappears in a one-dimensional system, due to the difference in the invasion speeds of the various species, leading to front collisions (Nakamaru & Iwasa 2000).

The importance of mixing in cyclic competition has been confirmed experimentally by Kerr et al. (2002). They have shown that killer, resistant

and sensitive strains of *E. coli* can coexist when cultured on the surface of a plate, while in a continuously shaken flask two of the three strains are outcompeted and disappear.

The well mixed and static environments, however, are only two limiting situations. In general, there is a competition between the homogenization due transport processes and the population dynamics generating non-uniformities. In many cases, the mixing is not sufficiently strong to produce a spatially uniform distribution. For example, plankton populations can maintain strongly non-uniform patchy distribution in spite of mixing by ocean currents and mesoscale eddies (Abraham 1998; Arístegui et al. 1997). Also, dispersion of bacteria by viscosity dominated fluid flow at small scales in biofilms or small droplets, may not be efficient enough to achieve complete mixing. Furthermore, the strength of mixing is quite often non-uniform in space as partially isolated weakly mixed regions may exist within a fluid flow (vortices for example).

The typical effect of fluid flows is to stretch and fold fluid regions, that leads to chaotic dispersion of the fluid elements (Ottino et al. 1988). In this section we investigate the effect of chaotic dispersion on the coexistence of cyclic competitors living in aquatic media. We consider both spatially uniform and non-uniform chaotic mixing. Using an explicit model for the dispersion of the populations, allows us to access the intermediate range between the well mixed and static environments. The model used in the numerical simulations is described in Subsection 2.3.2 and the results are presented in Subsection 2.3.3 followed by discussion and conclusions in Subsection 2.3.4.

2.3.2 The model

For describing the interaction between killer, sensitive and resistant species with cyclic competition hierarchy, we use the same model as Kerr et al. (2002). The competitors are distributed on a rectangular lattice of unit length with periodic boundary conditions. Each of them may die or reproduce into adjacent empty sites according to stochastic update rules.

Lattice sites are chosen randomly for update. If the selected site is empty, it is filled by phenotype i ($i = K, R$ or S) with probability p_i, given by the proportion of that phenotype among the eight neighboring sites. When a non-empty site is selected, the occupant may die with a probability δ_i. The relationship between the death rates, $\delta_K > \delta_R > \delta_S^0$, reflects the metabolic costs of producing both toxin and antidote (K), only antidote (R), or neither of these (S). The death rates of K and R are fixed, while δ_S depends on the proportion of killers in the neighboring cells, $\delta_S = \delta_S^0 + \tau p_K$, where τ is a constant characterizing the toxicity of the substance produced by the killer.

We define the time unit such that the number of updates per unit time is equal to the total number of lattice sites, N^2. Thus, on average, each site is updated once per unit time.

In a well mixed environment, with no spatial correlations in the distributions, p_i can be approximated by the fraction of lattice sites occupied by each species, $f_i = N_i/N^2$ (Durrett & Levin 1997). In this mean field approximation, the evolution of the competing populations is described by the equations:

$$\begin{aligned} \dot{f}_K &= f_K(1 - f_K - f_R - f_S) - \delta_K f_K \\ \dot{f}_R &= f_R(1 - f_K - f_R - f_S) - \delta_R f_R \\ \dot{f}_S &= f_S(1 - f_K - f_R - f_S) - (\delta_S^0 + \tau f_K) f_S \end{aligned} \tag{2.45}$$

where the birth rate is proportional to the population of each species and to the fraction of empty lattice sites, and the last terms represent the death rates of each species. The nontrivial steady state solutions of this system are: *i.)* $f_K = f_R = 0$, $f_S = 1-\delta_S^0$; *ii.)* $f_K = f_S = 0$, $f_R = 1-\delta_R$; *iii.)* $f_R = f_S = 0$, $f_K = 1-\delta_K$; *iv.)* $f_R = 0$, $f_K = (\delta_K-\delta_S^0)/\tau$, $f_S = (1-\delta_K-(\delta_K-\delta_S^0)/\tau)$. With the assumptions about the death rates given above, it is easy to show that all of them are unstable, except the first one (see Appendix C.). Numerical simulations show that this is the only attractor of the system. Consequently, in a well mixed population only one of the competing species survives, in qualitative agreement with the experiments of Kerr et al. (2002). (However, in Kerr et al.'s (2002) experiment the winner was the R strain not the S predicted by the mean field model. This discrepancy will be discussed later.)

Microorganisms living in a fluid environment (bacteria, plankton etc.) are transported by fluid flows. Since the velocity field is typically non-uniform in space this leads to dispersion and mixing of patches occupied by the different species. The velocity field of a fluid can be obtained by solving the Navier-Stokes equation with appropriate boundary conditions and external forcing. However, we are interested in the generic effects of mixing on the biological competition, that are not sensitive to the details of the flow. Therefore we will model fluid mixing by a simple kinematic dispersion model. At small scales relevant for microorganisms, the dynamics of fluid flows is dominated by viscosity and the velocity field is a smooth function of space (as opposed to the irregular large scale turbulent flows). Mixing in this type of flows can be modelled by a unidirectional shear flow with a changing direction. In order to satisfy the periodic boundary conditions we choose a sinusoidal shear flow with periodically alternating direction along the x and y axis, respectively:

$$\begin{aligned} v_x = V_0 \sin(2\pi y + \phi), \;\; v_y = 0 \quad \text{for} \;\; nT < t < (2n+1)T/2 \\ v_x = 0, \;\; v_y = V_0 \sin(2\pi x + \phi), \quad \text{for} \;\; (2n+1)T/2 < t < (n+1)T \end{aligned} \tag{2.46}$$

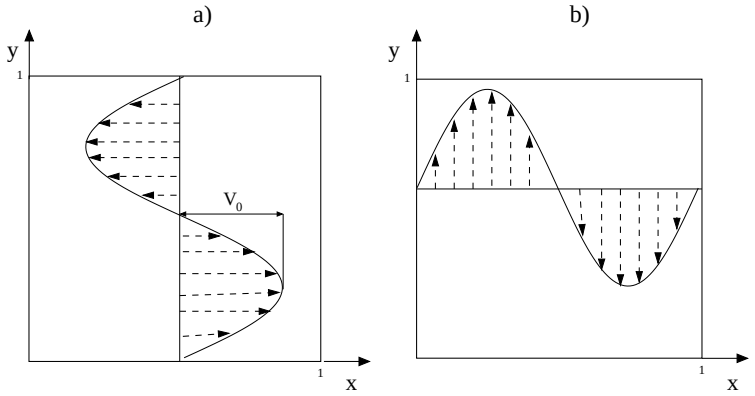

Figure 2.14: Velocity distribution in the sinusoidal shear flow. The velocity is parallel to the x (y) axis and its magnitude is function of the y (x) coordinate in the first (second) half of the time period, $\phi = 0$.

The spatial structure of the velocity field is illustrated in Fig. 2.14. This flow has often been used before as a generic model for chaotic mixing of fluids in a bounded domain (Varosi et al. 1990; Pierrehumbert 2000). Since the coordinates of the competitors sitting on a rectangular lattice are restricted to a discrete set, for simplicity, we apply the mixing step intermittently, at times separated by a half period of the flow, $T/2$. Thus, after updating $TN^2/2$ randomly selected points for biological activity, a mixing step follows. The new coordinates of each individual initially at x, y is first calculated as

$$\begin{aligned} x' = x + (V_0 T/2)\sin(2\pi y + \phi),\ y' = y \\ \text{when}\ \ t = (2n+1)T/2, \quad \text{or} \\ y' = y + (V_0 T/2)\sin(2\pi x + \phi),\ x' = x \\ \text{when}\ \ t = nT, \end{aligned} \tag{2.47}$$

then they are moved to the lattice sites closest to x', y'.

The above procedure defines a one-to-one mapping between the old and new positions, that leaves the populations of each species unchanged. The frequency of the mixing step is controlled by the parameter $\nu = 1/T$. This chaotic mixing stretches and folds different regions as a consequence of fast separation of close points in the direction of the so called unstable foliation and rapid convergence in a transverse direction, at each point of the domain (Giona et al. 1999). This is qualitatively different from the stochastic dispersion models used in previous cellular automata type simulations (Toffoli & Margolus 1987). Further, I note here that this flow is a *closed* chaotic flow, that is fluid parcels leaving the boarder of the domain enter into on the other side of it. (UTOLSO mondatot megnezni!)

We consider two qualitatively different mixing regimes. When the phase ϕ is a random variable, different in each mixing step, all trajectories produced by the repeated action of (2.47) are irregular, and cover the whole domain uniformly after a certain time. We will refer to this case as the *uniform mixing* regime. When ϕ is kept constant, however, there are transport barriers separating well mixed regions and islands where mixing is weak. This *non-uniform mixing* is a well known property of area preserving maps like (2.47), and also occurs in fluid flows, e.g. in the presence of strong vortices. Numerical results for both cases are presented in the following section.

2.3.3 Results

In order to study the effect of dispersion on the competition between the three species, we performed numerical simulations for different mixing rates (ν), while keeping the parameters of the population dynamics constant, $\delta_K = 1/3, \delta_R = 10/32, \delta_S^0 = 1/4, \tau = 3/4$ as in Kerr et al. (2002), with flow parameter $V_0 = 1.4/T$. The simulations have been repeated for different lattice sizes in the range from 200^2 to 4000^2. Initially, each lattice site is filled by one of the competitors chosen at random with equal probabilities. (Other initial conditions gave similar results.)

In the limit $\nu \to \infty$, very frequent mixing destroys the spatial correlations in the distributions of the phenotypes. Therefore, the mean field behavior described above is observed, i.e. killer, sensitive and resistant strains cannot coexist and after a certain time only the sensitives remain. Note, that strong mixing breaks the cyclic competition hierarchy by diluting the toxicity of the K strain, that can only maintain its competitive advantage over S locally, when there is a well defined front separating them. This is different from other models of cyclic competition that have marginally stable oscillatory solutions in the mean field approximation (Hofbauer & Sigmund 1998; Frean & Abraham 2001; Czárán et al. 2002).

In the absence of mixing ($\nu = 0$), patches occupied by different species emerge from the initially random distribution. This is analogous to the clustering observed by Young (2001), and by Hernandez & López (2004). in the birth and death process of a single species. Once the patches are formed, the competition is restricted to the permanently moving boundaries separating the species, so that each patch is simultaneously invaded at certain parts of its borderline while it expands elsewhere. In a finite population, there are irregular fluctuations in the proportion of the lattice occupied by different species (f_i), but these fluctuations became smaller as the size of the lattice (N) is increased. The time-averaged populations of the species are different, in general, and depend on the parameters of the population dynamics. In

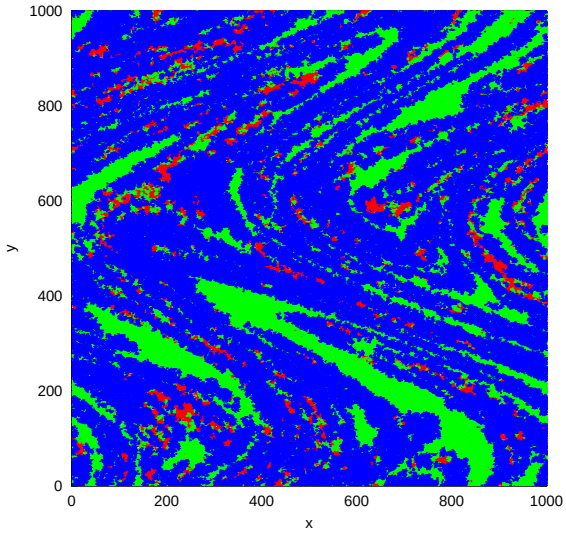

Figure 2.15: Distribution of killer (red), resistant (green) and sensitive (blue) species for $\nu = 0.025$ (ϕ random) on a 1000^2 lattice in the stationary regime.

our case, $\bar{f}_K \approx 0.24$, $\bar{f}_R \approx 0.26$, $\bar{f}_S \approx 0.16$.

Uniform mixing

To achieve uniform mixing, ϕ is chosen to be a random variable, uniformly distributed in $[0, 2\pi]$. When the mixing frequency (ν) is low, the three species still coexist, similarly to the case with no mixing. The effect of mixing, however, is clearly visible in the spatial structure formed by patches stretched into elongated stripes (Fig. 2.15). This type of filamental pattern is characteristic to chaotic mixing (Ottino et al. 1988), for example, when dye is mixed in a laminar fluid flow. An interesting consequence of mixing, is that the proportion of different species in the population oscillates in time (Fig. 2.16). Each species invades sequentially most of the domain, while its competitors are present only in a few small patches. The period of the oscillations is much longer than the time interval between the mixing steps, indicating that this is not an artifact of the mixing protocol. Rather, the dispersion synchronizes the inherently present fluctuations in the regional composition of the population, producing coherent oscillations. Similar synchronization induced by chaotic mixing has also been observed in oscillatory chemical reactions (Neufeld et al. 2003).

We found that the period and the amplitude of the oscillations of f_i is not affected by the size of the lattice (N), however, the amplitude clearly increases with the mixing frequency, as shown in Fig. 2.16b. For strong dispersion, the

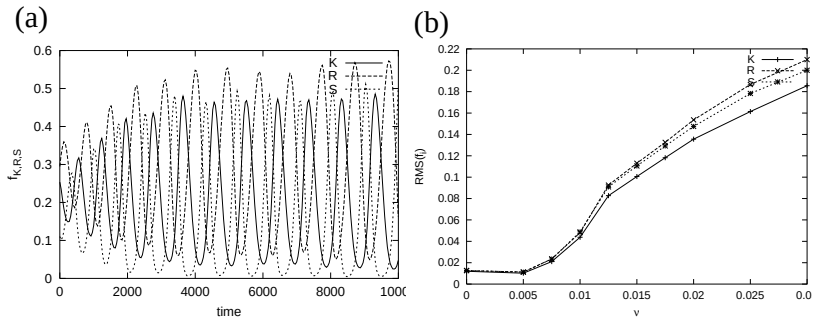

Figure 2.16: The proportion of lattice sites occupied by different species as a function of time (a) ($\nu = 0.025$, ϕ is random and $N = 1000$). In figure (b) the standard deviation of the populations from the mean is shown as a function of mixing rate.

number of individuals of a certain species can be very low at the minima and as a result it may go extinct. This automatically leads to the disappearance of one of the two remaining species leaving a single survivor. Obviously, larger lattice with larger population can tolerate stronger oscillations without extinction. Therefore, the critical dispersion rate, ν_c, that marks the limit of coexistence, increases with the size of the lattice (Fig. 2.17). However, the critical stirring rate appears to have a finite asymptotic value $\nu_c(N \to \infty) \to \nu_c^* \approx 0.043$ for large N, showing that for dispersion rates higher than ν_c^* extinction is unavoidable, regardless how large is the total population.

This is because, the surviving populations at the minima became smaller and smaller after each cycle.

When, the mixing rate is larger than the critical value ν_c^*, the winner of the competition depends on the mixing rate, and can be either of the three strains. Just above the critical value, the first species that disappears is the sensitive one, followed by the killer, that is outcompeted by the resistant due to its lower death rate. This is, however, not a generic feature of this problem, but depends on the parameters of the population dynamics. Naturally, the species with the lowest average population is the most sensitive to fluctuations. Simulations performed with other values of the parameters confirm that, in general, the species with the lowest average population is the first one to dissappear as the amplitude of the oscillations increases. When the strength of mixing is increased even further ($\nu \gtrapprox 1.0$) the population dynamics is described by the mean field model and the winner is the sensitive species.

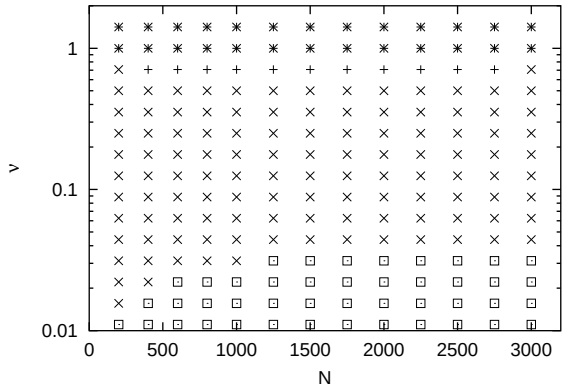

Figure 2.17: The final outcome of species competition for different mixing rates and lattice sizes. The symbols represent the winner: stars - S, crosses - K, x's - R and boxes - coexistence.

Non-uniform mixing

The same set of numerical experiments have been repeated with non-uniform mixing ($\phi = 0$). Also in this case, the three species coexist when the dispersion is not too strong. The spatial structure reflects the different mixing properties within the domain: larger islands isolated from the strongly mixed central region are clearly visible in Fig. 2.18. An important difference, however, is that coexistence persists to much higher mixing rates, $\nu_c \approx 6.0$, than in the case of uniform mixing. At high ν the central region is at any time dominated by one or temporarily two species, while others manage to survive in a few small partially isolated patches around the borderline of the well mixed region. Later, they invade the central region from there, as soon as it becomes mostly populated by their inferior competitor. Within the islands mixing is restricted to concentric layers. Here circular bands of different species propagate slowly inward or outwards.

For very strong mixing $\nu \gtrapprox 6.0$, the coexistence breaks down and only one competitor survives. However, for $6 \lessapprox \nu \lessapprox 7$ long time coexistence of killer and sensitive strains can also be observed for some initial conditions (Fig. 2.19). This transient metastable state may persist for thousands of generations, that is practically detected as coexistence on ecological time scales (Hastings 2004). In this case, killer cells aggregate in the slowly mixed islands from where individuals continuously disperse into the well mixed region. Here, strong mixing dilutes the toxin, therefore sensitive cells dominate. Within the weakly mixed islands killers maintain a compact structure, that prevents invasion by sensitive cells along the borderline (Fig. 2.20).

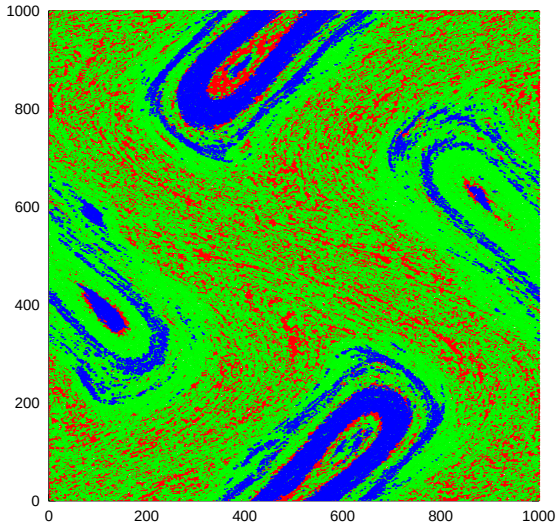

Figure 2.18: Spatial structure in the case of non-uniform mixing ($\phi = 0, \nu = 0.667, N = 1000$)

Eventually, the killers' density in the central region becomes sufficient for completely displacing the sensitive cells from the populations.

2.3.4 Discussion

We have shown, that chaotic mixing induces regular oscillations in the populations of competing phenotypes. This breaks their coexistence when the mixing rate is increased beyond a certain threshold. We also found similar mixing induced oscillations in the standard model of the rock-scissors-paper game (Frean & Abraham 2001), suggesting that this is a robust feature of population models with cyclic invasion. Oscillations of this type have also been observed recently in cyclic competition on complex networks by Szabó et al. (2004). We believe, that the long range interaction introduced in these network models is analogous to the effect of chaotic mixing, that can bring together initially distant individuals allowing them to interact.

In the absence of mixing, the boundaries separating different phenotypes, intersect in points surrounded by patches of all three competitors, where they can circle around cyclically. Such points are therefore important for sustaining the coexistence in systems with cyclic competition hierarchy. The chaotic mixing stretches the patchy distribution into stripes with locally parallel boundaries aligned with the unstable foliation, following the direction of fastest divergence of the mixing trajectories. The laminated structure with-

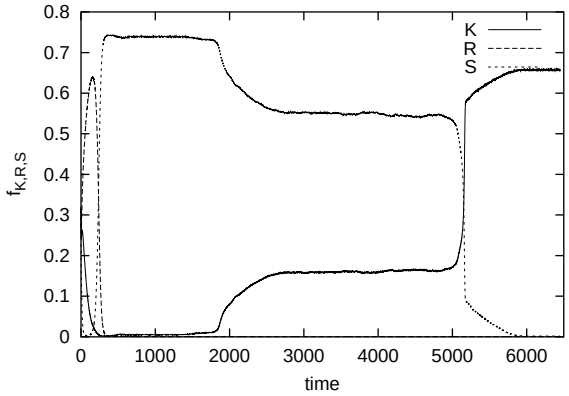

Figure 2.19: Long time transient coexistence of killer (K, solid line) and sensitive (S, dotted line) species for $\nu = 6.5$ ($\phi = 0$) on a 1000^2 lattice.

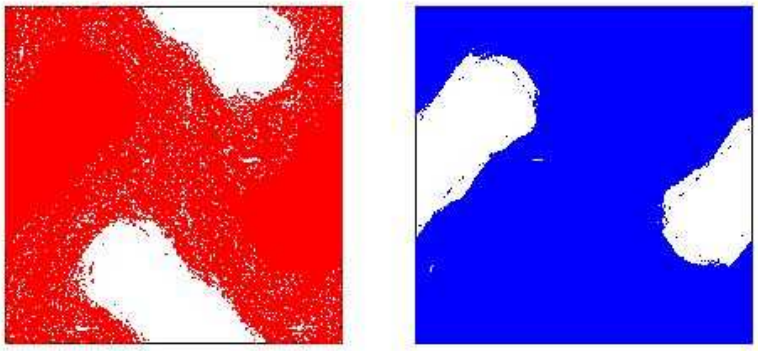

Figure 2.20: Spatial distribution of killer and sensitive cells at long time transient coexistence. Parameters and color codes are the same as in the previous figure.

out intersecting boundaries is analogous to a one-dimensional distribution, and does not allow cyclic invasion.

The motion of the boundaries is affected by both dispersion and invasion. Thus, coexistence, depends on the competition between these two processes. Weak mixing only distorts the spatial structure, without significantly changing its topology. When invasion is much slower than the characteristic speed of dispersion, the spatial structure will have no boundary intersections, inhibiting coexistence.

An estimate for the limit of coexistence (ν_c^*) can be obtained by assuming that at the transition, the two effects have similar magnitudes. To verify this, we measured the invasion speed of each species numerically and obtained: $v_{S\to R} \approx 0.078, v_{R\to K} \approx 0.04, v_{K\to S} \approx 0.056$. The characteristic speed of dispersion can be estimated as $v_D \sim \nu L$, where $L = 1$ is the length of the domain. (In real systems, the characteristic dispersion speed could be estimated, for example, as the root-mean-square velocity of the flow.) At the critical stirring rate, $v_D \approx L\nu_c^* = 0.043$ is indeed comparable to the invasion speeds given above.

The transition to the mean field behavior appears at higher mixing rates, when the characteristic time of dispersion $T = 1/\nu$ becomes shorter than the typical time of birth and death processes, that in our case was chosen as the time unit. Thus, the mean field approximation is expected to be valid when $\nu > 1$, in agreement with the simulations (see Fig. 2.17). Note, that around the transition region $\nu \approx 1.0$ any of the three species can be the winner in a relatively small range of the mixing rate. Furthermore, in this range there is also some sensitivity on the random initial conditions. We believe, that the experiments by Kerr et al. (2002). could correspond to this somewhat weaker than perfect mixing, that may explain the difference between the experimental results and the mean field model. An alternative explanation could be, that if the transfer into the fresh medium took place at a transient low concentration of one of the species (S), the small size of the transferred sample population may have caused the extinction of the species in minority.

Another conclusion resulting from the numerical experiments, is that the critical dispersion rate (ν_c) is much higher in the case of non-uniform mixing. Clearly, non-uniform dispersion favors coexistence by providing the species in minority with temporary refuge within small partially isolated islands, so it can avoid extinction even when large parts of the domain are almost uniformly mixed. Hence, partially isolated refuges could play a role in maintaining ecological diversity in aquatic ecosystems. This effect leads to long term metastable coexsitence of killer and sensitive strains.

In order to compare the effect of chaotic mixing with more standard dispersion models, we performed a set of simulations in which the mixing step

was replaced by a local dispersion protocol based on exchanging occupants of lattice sites with one of their randomly selected neighbors. This diffusive type dispersion could be interpreted as a random Brownian motion of swimming microorganisms. Typical time dependence of the total populations of the three species and a snapshot of the spatial distribution are shown in Fig. 2.21. We find that the effect of diffusive dispersion is rather different from the

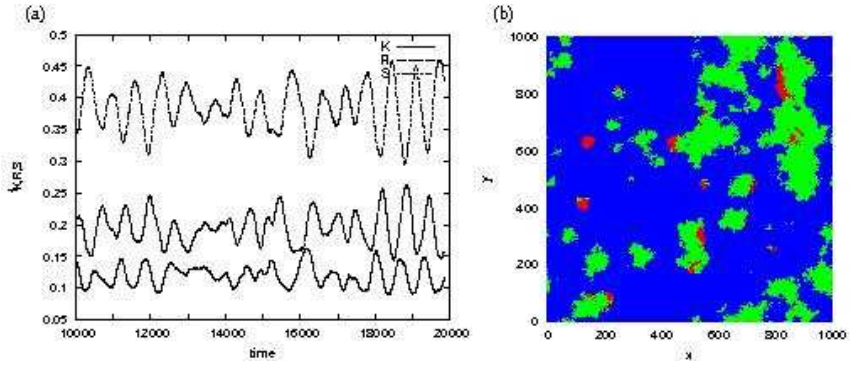

Figure 2.21: Time dependence of the populations of the three species (a) and their spatial distribution (b) for the local dispersion model on a lattice $N = 1000$. The number of dispersion steps per unit time is $2N^2$. Color code is the same as before.

chaotic mixing. While chaotic mixing preserves the sharp boundaries between different species, local dispersion makes the these interfaces more diffuse. This decreases the effective toxicity of the killer strain. As the strength of local dispersion is increased the time-averaged population of the killers decreases, leading to extinction at very strong dispersion, similarly to the case of very strong chaotic mixing ($\nu > 1$). So the strains remain in coexistence at weak mixing and the sensitive strain wins the competition at strong mixing. However, in contrast to the chaotic mixing model the local dispersion does not produce regular oscillations and extinction due to oscillations, characteristic to weak or intermediate chaotic mixing. This suggests, that weak (or slow) mixing can only produce collective oscillatory behavior in the presence of a spatially coherent transport mechanism.

In summary, our results show, that mixing has important effects on the cyclic competition in aquatic media. By changing the strength or character of mixing a rich variety of behaviors can be observed. The existence of various mixing conditions (e. g. non-uniform mixing) may be a contributing factor in preserving species diversity. Mixing can interfere with biological competition and this could be used in controlling the evolution of microorganism populations, e.g. in bioreactors.

Chapter 3

Populations as discrete state dynamical systems

The continuous and discrete state descriptions. Analytical vs. CA models.

3.1 Discrete and continuous state population models in a noisy world

3.1.1 Introduction

Mathematical models of populations use either continuous or discrete time as an independent variable. The former is applied when the size of the population changes very often. These models lead to differential equations. The latter approach is most commonly adopted in the cases when the size of the population changes suddenly and periodically (e.g. annual plants, insects). This model applies iterated (return) maps of the type $\mathbf{N_{t+1}} = \mathbf{F}(\mathbf{N_t})$, where $\mathbf{N_t}$ is a general density vector at time t describes either a structured population or even the community of interaction populations and $\mathbf{F}$ is a nonlinear operator. This chapter is dedicated to this latter case. We investigate whether and under which conditions the $\mathbf{N}$ size of the population can be modeled by continuous (real-valued) variables instead of integers. (Since most populations contain individuals, models can be transformed so that the population size – the habitat area times the population density –, is an integer value.) At first sight this discrepancy appears to be irrelevant, nevertheless, it can cause large deviation between the actual statistical behavior of biological populations and that predicted by the corresponding models, especially if the underlying dynamics is chaotic. This type of dynamical be-

Table 3.1: Classification of discrete time population models of $\mathbf{N_{t+1}} = \mathbf{F}(\mathbf{N_t})$

Properties of F	**Properties of $\mathbf{N_t}$**	
	Continuous (C), $\mathbf{N_t}$ is real	*Discrete* (D), $\mathbf{N_t}$ is integer
Deterministic (D) models, **F** is deterministic	DC models	DD models
Stochastic (S) models, **F** is a stochastic process	SC models	SD models
Noisy (N) models, **F** is a combination of a deterministic part and a random noise	NC models	ND models

havior implies stretching, so as time is iterated, arbitrarily small differences between the models are blown up to finite size. No matter how closely a continuous model approximates a discrete system, after a (small) finite number of steps the models diverge and even the statistics may differ radically (Domokos & Szász 2003). For further reference we define a classification for discrete time population models based on their mathematical approach, this is summarized in Table 3.1.

Among continuous (C) models the deterministic ones (DC) are by far the simplest. This is probably a reason why they are widespread, e.g. in logistic, Ricker or Beverton-Holt models. The noisy versions (NC) are successfully used for population data series analysis (Turchin & Taylor 1992; Ellner et al. 1998; Stenseth et al. 1998) and in studying extinction risk in varying environments (Morales 1999; Ripa & Heino 1999). The simplicity is not true for discrete models; deterministic (DD) versions can be rather sophisticated (as we discuss this below). Discrete stochastic (SD) models are very adequate to describe real populations but less tractable mathematically (e.g. Renshaw 1991)). (We are not aware of the application of SC models.) The relatively less complicated ND models, however, are still close to reality: the most populations do consist of integer number of individuals and random fluctuations do exist. In spite of their suitability, ND models are almost totally absent in the literature (e.g. Begon et al. 1986; Gurney & Nisbet 1998). There is a rather recent interest in DD and ND models : the appearance of 'lattice effects' caused by the discreteness of the population (Henson et al. 2001; Domokos & Scheuring 2002). Our goal is to study the conditions under which ND models can be substituted by simpler DC or NC models, or, alternatively, the conditions under which ND models cannot be replaced. Below we consistently refer to two models as being similar if the probability density functions describing the size of the population are sufficiently close. Nevertheless, it is clear that two models, even with identical statistics, can predict different time series: the statistical measure cannot tell the difference between two time series if (i) they have totally different patterns, (ii) but happen to spend the same amount of time in the same parts of the phase space. This latter difference is, however, of

secondary importance in case of sufficiently long time series and will not be discussed here. In case of short time series the last mentioned difference can be relevant, and the tools developed above can capture this subtle difference, as we will point out in section 3.1.4.

One may think naively that deterministic discrete (DD) systems can be approximated by their continuous (DC) counterparts if the population size is sufficiently large, while discrete effects are important in small populations. This is certainly the case as long as the proposed continuous system behaves regularly. However, if the continuous dynamics is chaotic, it displays aperiodic, random-like behavior, which and this feature can *never* appear in a deterministic discrete system defined on a closed interval, due to its finite number of states. In such cases the convergence between discrete and continuous models cannot be established by increasing the population size N (c.f. Domokos & Szász 2003). It is argued that it is imperative to consider the naturally existing *random noise* in the original discrete system, since only such noisy, discrete models can converge to their continuous counterparts (ND $\rightarrow$ DC convergence). We will show that this convergence can be drastically improved if we add the same amount of noise to the continuous model (ND $\rightarrow$ NC convergence). The magnitude of the noise and the dynamical characteristics of continuous models play a key role: if the noise is too small and the DC model is chaotic, then discrete and continuous models will never display similar behavior, while NC and ND models behave similarly at regular dynamics. For sufficiently large noise, independently of the dynamical behavior, ND and NC appear almost identical from the statistical point of view. We describe a "grey zone" for the magnitude of the noise where the similarity is only partial. Adequate continuous models can be only applied to chaotic systems if the *noise* is outside the "grey zone", otherwise they have to be treated with caution, or alternatively, the discrete model has to be used.

Interestingly, questions with rather similar mathematical content, though with completely different background arise when the efficiency of computer simulations on continuous dynamical systems is investigated. As pointed out first by Stanislaw Ulam (Ulam 1960), due to the unavoidable discreteness of the computer simulation (finite arithmetic precision), often not even the statistical properties of the modeled continuous dynamical system can be captured. Ever since, this question has been systematically investigated by the mathematical community and several fundamental results are at hand (Kifer 1997; Liverani 2001; Domokos & Szász 2003). One of the main messages of these investigations is that the perturbed discrete system with appropriately added random noise behaves similarly to the unperturbed (purely deterministic) continuous one. (Using the notations of Table 1, Ulam's prob-

lem concerns the ND → DC relationship and transition.) However, environmental and demographic noise cannot be *prescribed*, it is dictated by the given ecological system. As we will show in Section 3 under general conditions ND and DC models behave similarly only for very small range of demographic and environmental noise. Since we are interested in the application of continuous models for wide intervals of noise, we investigate the ND→ NC transition under the assumption that the noise is equal in both systems. To the best of our knowledge, there are no rigorous mathematical convergence results for this problem, however, our simulations show that for sufficiently large noises (noise outside the *grey zone*) the ND→ NC substitution is legitimate. Moreover, the rigorous results concerning Ulam's problem make this more general statement plausible.

As a fundamental tool of our study we will define the distance between two models in Subsection 3.1.2 in such a way that two models will be close if they behave similarly in the statistical sense. In Subsection 3.1.3 we measure the distance between ND, NC and DC models of the Ricker map for different dynamical behavior, population sizes and a wide range of demographic noise. In Subsection 3.1.4 we study whether the dynamical description of the experimental *Tribolium castaneum* data series (Costantino et al. 1997; Cushing et al. 2003) requires the application of an ND model, or the NC description is adequate. (We will study this question from another point of view in Subsection 3.2.) I draw conclusions and discuss some related issues in Subsection 3.1.5.

3.1.2 Method for measuring the difference between the model systems

Let us consider the following simple population dynamical model:

$$N_{t+1} = N_t f(\mathbf{q}, N_t) \tag{3.1}$$

where N_t is the number of individuals at time t; $f(\mathbf{q}, N_t)$ is the realized per capita rate of population change depending on the population size and the demographic parameter $\mathbf{q}$. We stress here that N generally denotes the population density, but multiplying the density with the habitat size transfer N into the number of individuals. The state of the population is calculated in discrete time steps, while N_t can assume any positive real value, i.e. this is a DC model widely used in the literature with many different realizations of $f(\mathbf{q}, N_t)$ (see e.g. Begon et al. 1986; Cohen 1995). Despite their simplicity, these models can be very rich in dynamical behavior. Depending on the function $f(\mathbf{q}, N_t)$ and its parameters, models can tend to a fixed point,

oscillate periodically, quasi-periodically or can fluctuate chaotically as well (May 1976; Cohen 1995). One possible DD model corresponding to Eq. (3.1) is constructed simply by the integerization of the right hand side of Eq. (3.1)

$$N_{t+1} = int\left[N_t f(\mathbf{q}, N_t)\right] \tag{3.2}$$

where $int[x]$ denotes the integer part of x.

Since different types of stochastic processes (environmental, demographic) make noise inherent in every population, Eqs. (3.1) or (3.2) can be modified to describe this stochasticity. If Nt has a Poisson distribution because of demographic variability, then $\sqrt{N_t}$ has approximately a normal distribution with a constant variance (Rao 1973; Dennis et al. 2001). Consequently the demographic stochasticity modifies Eq. (3.1) to

$$N_{t+1} = \left(\sqrt{N_t f(\mathbf{q}, N_t)} + \varepsilon_t\right)^2 \tag{3.3}$$

and Eq. (3.2) to

$$N_{t+1} = int\left[\left(\sqrt{N_t f(\mathbf{q}, N_t)} + \varepsilon_t\right)^2\right]. \tag{3.4}$$

Here ε_t is a normally distributed uncorrelated random variable with mean zero and variance σ^2. If stochasticity originates from environmental variablity then logarithmic transformation of N_t leads to a standardized noise structure (Dennis & Taper 1994; Dennis et al. 2001), so it modifies Eq. (3.1) to

$$N_{t+1} = N_t f(\mathbf{q}, N_t) e^{\varepsilon_t} \tag{3.5}$$

and Eq. (3.2) to

$$N_{t+1} = int\left[N_t f(\mathbf{q}, N_t) e^{\varepsilon_t}\right] \tag{3.6}$$

Eqs. (3.3) and (3.6) are NC systems with different types of noise, while Eqs. (3.4) and (3.6) are their ND counterparts, respectively.

One realization of Eq. (3.4) is the ND version of the so-called Ricker model will be discussed in the next section. Figure 3.1 illustrates the dynamical behavior of the discrete and continuous Ricker models with and without noise. The first two rows show the behavior of the DD and DC models (with zero noise), while the third and fourth rows illustrate the ND and NC models with identical, moderate noise levels. Time series (shown in the left column: Fig. 3.1 a,c,e, g) display the behavior of the system to some extent, however frequency distribution of the different population sizes (right column: Fig. 3.1 b,d,f,h) are often much more informative. In particular, if the system is

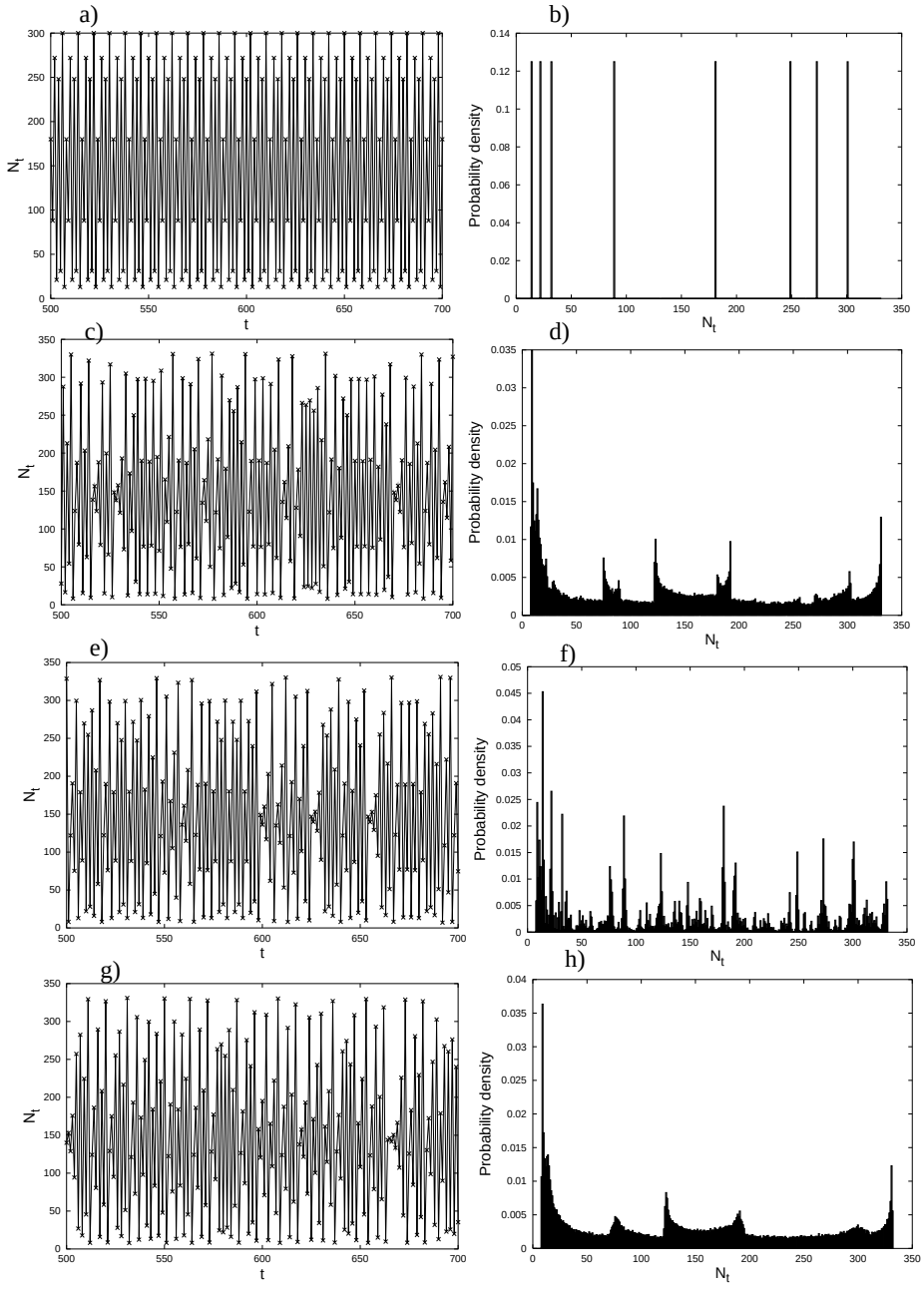

Figure 3.1: Time series (left column) and probability density distributions (right column) of different versions of the Ricker model. (The DC model is defined as $f(\mathbf{q}, N_t) = bexp(-cN_t/K)$, $b = 18$, $c = 1$, K= 50. Corresponding DD, NC and ND models are derived via equations 3.3-3.6. More details in section 3). At the selected control parameter b the DC model is chaotic. (a, b): Time series and probability density distribution of the DD model. The system is purely periodic with period 8. (c, d): Time series and probability density distribution of the DC model. (e, f): Time series and probability density distribution of the ND model with σ=0.16. (g, h) Time series and probability density distribution of the NC model at $\sigma = 0.16$.

chaotic and (or) noisy, the frequency of different states can be hardly seen based solely on time series (Fig. 3.1 d,f,h). It can be observed that already at this rather low noise level, Fig. 3.1 f and h appear to be more similar to each other than the deterministic densities in Fig. 3.1 b and d. Since we are interested in quantitative comparison, we define the difference between two models m_1, m_2 based on their differences in frequency distributions in the following way: Let us consider the two models, and we also consider the associated discretized frequency distributions denoted by $p_1(X) > 0$ and $p_2(X) > 0$, where $X(= 1, 2, ...n)$ is the integer value of x (if x is itself an integer then $x = X$). We define the distance as

$$d\left[m_1, m_2\right] = \sqrt{\frac{\sum(p_1(X) - p_2(X))^2}{\sum p_1(X)^2 + \sum p_2(X)^2}} \tag{3.7}$$

where summation is carried out for all X values where $p_1(X)+p2(X) > 0$. We apply the discrete frequency distributions because we want to handle both discrete (D) and continuous (C) models and one can assign integers to real numbers in a natural way by rounding, however, the inverse is not true. The distance d will assume only positive values between 0 and 1. The former extreme appears if the two density functions are identical, the latter if they are completely disjoint in the sense that $p_1(X)p_2(X) = 0$ for all values of X. The distance $d[.]$ in eq.(7) is the discretized version of the $\mathcal{L}^2$ norm (Korn & Korn 1968).

If $p_1(X)$ and $p_2(X)$ are very similar with high peaks which are slightly offset in X, then $d[m_1, m_2]$ will be large, although intuitively one would think that $d[m_1, m_2]$ should be small. To render this discrepancy we applied slightly larger intervals for the densities which "smears out" the singular peaks and regarded the *minimal* distance $\delta[m_1, m_2]$ among slightly shifted densities (i.e. we considered *"coarse grained"* models M_1, M_2 with densities

$$q_1(Y) = \sum_{i=1}^{c_1} p_1(c_1(Y-1)+i), q_2(Y) = \sum_{i=1}^{c_1} p_2(c_1(Y-1)+i+c_2), \tag{3.8}$$

where $Y = 1, 2, ...int\left[n/c_1\right]$ and set $\delta[m_1, m_2] = min_{c_2}\left\{d[M_1, M_2]\right\}$ with $3 \leq c1, c2 \leq 7$ being integers). The distance $\delta[m_1, m_2]$ is similar to the Levy distance, also permitting small shifts in the independent variable (Levy 1937). The above defined distance will measure the difference between the density functions in case of sufficiently long data series. In case of relatively short series (where the number of data points is smaller than the number of possible states) the suggested distance will, to some extent, measure the more subtle difference between the actual time series: it compares the domains

of phase space visited by the two (short) data series (cf. Section 3.1.4, Fig. 3.4). Naturally, the statistically indistinguishable time series may differ by several reason:

(a) The two series may visit the domains of phase space with equal frequency, however, at different times.

(b) The two series may visit the same domain at the same time, however show different patterns.

Difference of type **(b)** will never be detected by our method. However, difference of type **(a)** can be detected if the time series is short.

3.1.3 Differences between ND, DC and ND, NC versions of the Ricker model

We use the well known Ricker equation (Ricker 1954) and its adequately modified counterparts to illustrate the relations between different types of models described in Table 3.1. The Ricker model is defined by

$$N_{t+1} = bN_t exp\left(-\frac{cN_t}{K}\right) \tag{3.9}$$

where N_t is the number of individuals at time t, b is the per capita birth rate, K refers to the habitat size and c measures the strength of intraspecific competition at unit density of individuals. Since, depending on the birth rate b, the model tends to a fixed point ($0 < b < 7.4$), fluctuates periodically ($7.4 < b < 16.9$) or chaotically ($16.9 < b$), it is an ideal system to compare the different models defined in the previous section.

The traditional Ricker equation is a DC model, but according to (3.3) or (3.5) and (3.4) or (3.6) we can generate the corresponding NC and ND versions. Since (according to the simulations) the basic conclusions are independent of the source of stochasticity, henceforth we investigate only the case of demographic noise, i.e. we replace $f(\mathbf{q}, N_t)$ with $bexp(-cN_t/K)$ in Eqs. (3.3) and (3.4).

We measured the distances $\delta[ND, DC]$ and $\delta[ND, NC]$ numerically for the Ricker model at different noise levels, population sizes and dynamical behaviour; Fig. 3.2 summarises our results. The magnitude of the noise can be measured based on two different philosophies. Either we are interested in the *input noise*, i.e. the level of stochasticity of the input parameter measured by the control parameter σ (standard deviation): in Section 3.1.5 we will discuss this approach. Physically, the input noise is represented either

by demographical or environmental stochasticity. The other alternative is to measure the *output noise* by averaging the absolute value of the difference between the noisy and the noise-less maps; this approach is adopted in this section. The output noise is represented by the stochastic fluctuation of the size of the population. It is not surprising that the two approaches differ radically: the input noise is transformed by a (possibly strongly) nonlinear map into the output noise, so not even the statistical properties can be expected to be similar. The approach based on input noise admits a better comparison of the biological and environmental stochasticity affecting on the population size, the *output noise* approach is more adequate if we are interested in the *effect* of noise on populations.

We can distinguish four characteristic types of behavior, which are plotted schematically in Fig. 3.3. and analyzed below. The common feature of all four types in Fig. 3.3 is that one can clearly separate 3 zones: **(A)** the *'clear zone'* where noise does not play an essential role, **(B)** the *'grey zone'* where transition occurs and **(C)** the *'noisy zone'* where noise dominates the original dynamics.

Type I. (Fig. 3.2 a and c) ND–DC comparison in case of regular dynamical behavior (fixed point or periodic oscillation). In the clear zone they appear to be similar ($\delta[.]$ is small) because discretization does no play a crucial role for regular behavior. Both in the grey zone and in the noisy zone the deterministic continuous model remains identical since it does not contain any noise, however, in the discrete system noise starts to dominate the behavior so the distance between the two models grows rapidly close to the maximum ($\delta[.] = 1$).

Type II. (Fig. 3.2 b and d) ND – NC comparison in case of regular dynamical behavior. As in case of Type I, in the clear zone the distance is very small. In the noisy zone the distance is small as well, however, for a completely different reason: both systems are 'far' from their original version, they appear similar because the noise is dominant. Since in the clear zone and the noisy zone the models are close for different reasons, it is not surprising that in the grey zone the distance grows temporarily.

Type III. (Fig. 3.2 e) ND – DC comparison in case of chaotic dynamics. In the clear zone they appear to be far apart, this is due to the reasons discussed in section 1. As noise increases in the grey zone, the statistics get relatively close when the noise's magnitude is of order 1, this is in fair qualitative accordance with the results concerning Ulam's problem (cf. Domokos & Szász 2003). Later on, the distance increases again

close to maximum and in the noisy zone the two models are far apart. The latter is plausible if we consider that the statistics of the discrete model is dominated by the noise while the continuous model's density function is independent of the noise structure.

Type IV. (Fig. 3.2 f) ND – NC comparison in case of chaotic dynamics. In the clear zone the models are apart for the same reason as in case of Type III. However, after a relatively slow transition in the grey zone (see the logscale of x axes), the models appear to be close in the noisy zone – this is a similar effect to Type II: noise dominates both models.

This summary shows that DC models are not very adequate, neither for regular, nor for chaotic systems (Type I. and Type III. plots). On the other hand, NC models proved to be a better choice: in case of regular (periodic) dynamics the distance $\delta[ND, NC]$ is small even in the grey zone, as represented in Type II. In case of chaotic dynamics NC models are adequate if we are in the noisy zone (Type IV.), i.e. the biological noise is sufficiently large. For populations with small noise only the ND model can offer adequate description.

The grey zone of Type IV is not negligible (approximately two orders of magnitude) and certain biological systems may fall into this range. We can observe that the noise causes initially *small departure* from the periodic attractors in the above-defined sense, i.e. the trajectory remains close to the original attractor. This indicates that in the grey zone of Type IV. (ND–NC, chaotic) behavior the original, periodic behavior of the discrete system is still perceptible - this is called 'lattice effect' by (Henson et al. 2001).

3.1.4 ND and NC models of chaotic *Tribolium castaneum* data series

One of the main conclusions deduced from Figs. 3.2 and 3.3 is that ND and NC models behave similarly, except if the dynamics is chaotic and the demographic (and/or environmental) noise is not strong enough (cf. Fig. 3.2 f, and Type IV in Fig. 3.3.). The natural question to ask is whether (and under which circumstances) we can apply NC models, i.e. whether (and under which circumstances) noise can conceal the discreteness of populations in a natural system. If the answer is negative, we have to apply the less comfortable ND models. To answer this question, a comprehensive database on a huge number of different populations would be needed. This database would contain (among others) complex chaotic-like time series, the corresponding, verified population dynamical models, as well as the demographic and environmental noise levels. Unfortunately, to the best of our knowledge, there is

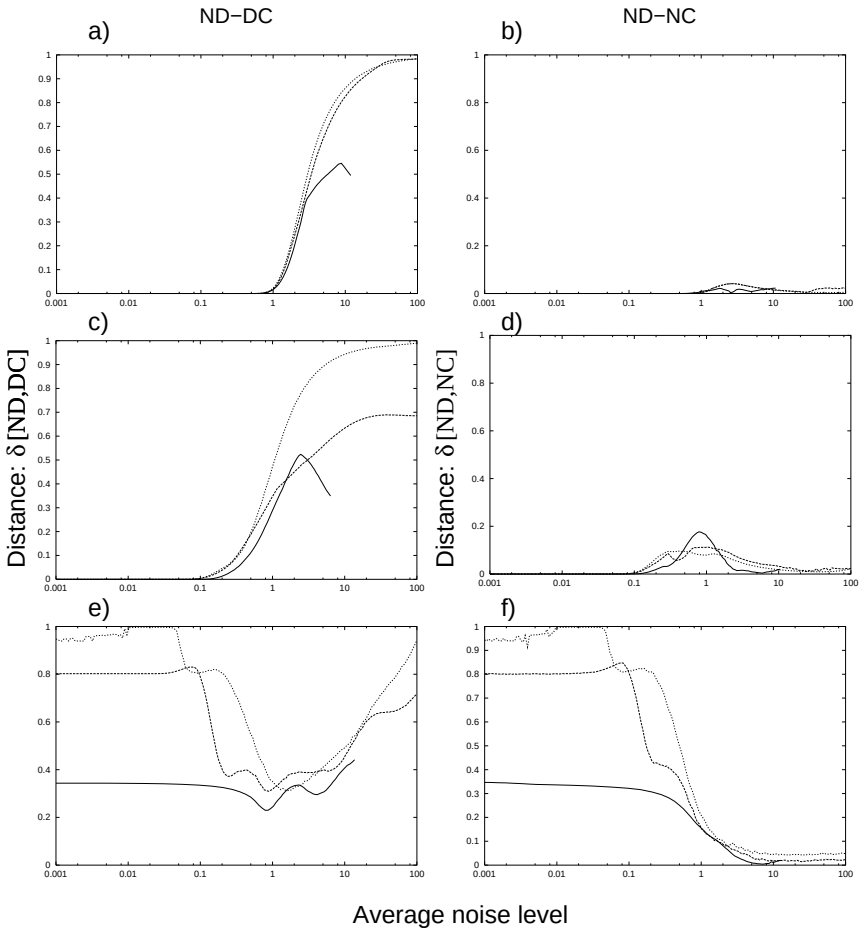

Figure 3.2: The differences between models as function of demographic noise. Distances are computed at different carrying capacities, $K = 5$ (solid line), $K = 50$ (dashed line) $K = 500$ (dotted line). (a, b) The classical DC model converges to a fixed point ($b = 4.5$, $c = 1$). (c, d) The DC model behaves periodically with period 2 ($b = 12.2$, $c = 1$). (e, f) The DC model is chaotic (b= 18, c=1). The compared time series contained 2×10^5 data points. Average effective noise level was computed as the average of the difference between the noisy and deterministic maps along the time trajectory of the noisy maps at different values of σ in the $[10^{-5}, 10]$ interval. (At K=5 only $\sigma < 6$ could be considered, otherwise the model produced very frequently physically irrelevant, negative population values).

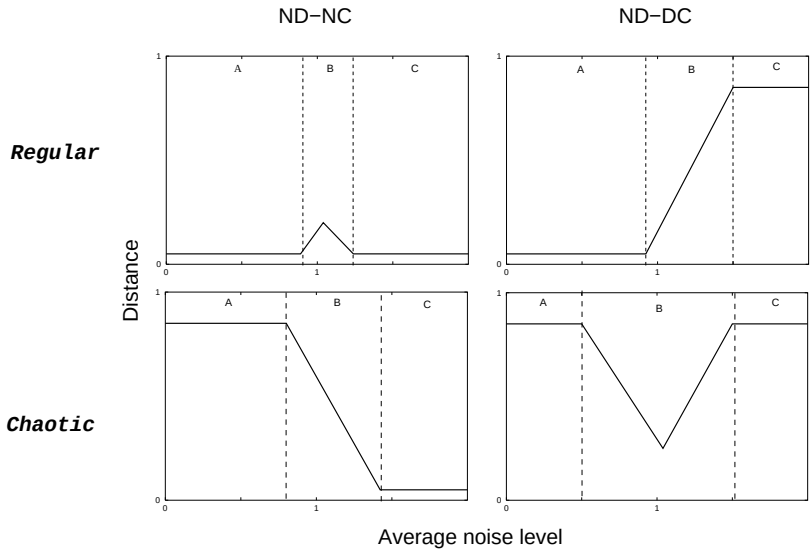

Figure 3.3: Schematic, qualitative behavior of the distance as function of the average effective noise. Type I: ND–DC distance for regular dynamics. Type II: ND–NC distance for regular dynamics. Type III: ND–DC distance for chaotic dynamics. Type IV: ND–NC distance for chaotic dynamics. Observe clear **(A)**, grey **(B)** and noisy **(C)** zones for all Types.

no such database at hand. We are only aware of the experiments and mathematical analysis made on flour beetle *Tribolium castaneum* (Costantino et al. 1997; Cushing et al. 2001; Dennis et al. 2001; Cushing et al. 2003), which can serve as the only database where the comparison of ND and NC models is possible. In the cited study the authors report on maintaining the beetle population for years in the lab. They have not only shown that the so called LPA model gives a precise description of the population dynamics, they also verified experimentally the forecasted chaotic dynamics at different manipulated demographic parameters (Costantino et al. 1997; Cushing et al. 2001; Dennis et al. 2001; Cushing et al. 2003). All the parameters and the level of demographic stochasticity of the LPA model is estimated in a comprehensive statistical study (Dennis et al. 2001). Below we briefly discuss the cited study and use our results to decide on the applicability of NC and ND models.

The LPA model of flour beetle has taken account its larva (L) pupa (P) and adult (A) stages. Since the noise is mainly caused by the demographic stochasticity in this lab experiment (Dennis et al. 2001), the standardized noise can be added to the square root transformed equations of the deterministic model (see eq. (3)). Thus the NC version of the LPA model is a

noisy difference equation system:

$$L_{t+1} = \left(\sqrt{bA_t exp\left(-\frac{c_{ea}}{V}A_t - \frac{c_{el}}{V}L_t\right)} + \varepsilon_{1t}\right)^2, \quad (3.10)$$

$$P_{t+1} = \left(\sqrt{(1-\mu_l)L_t} + \varepsilon_{2t}\right)^2, \quad (3.11)$$

$$A_{t+1} = P_t exp\left(-\frac{c_{pa}}{V}A_t\right) + (1-\mu_a)A_t \quad (3.12)$$

where L_t, P_t and A_t are the number of feeding larvae, nonfeeding larvae and adult individuals, respectively at time t. The LPA model assumes that the main interactions among the life-stages is the cannibalism, so the exponentials represent the fractions of individuals surviving cannibalism within one unit of time (as in the Ricker model). The parameters c_{ea}/V, c_{el}/V and c_{pa}/V measure the strength of cannibalistic interactions. V is proportional to the habitat size. The parameter b is the average number of larvae recruited by an adult per unit time. The fractions μ_l and μ_a are the larval and adult mortality rates per unit time, respectively. The terms ε_{1t}, ε_{2t} are random normal variables with mean zero and and variances σ_1 and σ_2. (Naturally, there is a random term ε_{3t} in the third equation as well in the general case and there are covariances among the different random variables, but in this experiment ε_{3t} and covariance entries of the variance-covariance matrix are practically zero). A discretized version (ND model) of the above system is

$$L_{t+1} = int\left[\left(\sqrt{bA_t exp\left(-\frac{c_{ea}}{V}A_t - \frac{c_{el}}{V}L_t\right)} + \varepsilon_{1t}\right)^2\right], \quad (3.13)$$

$$P_{t+1} = int\left[\left(\sqrt{(1-\mu_l)L_t} + \varepsilon_{2t}\right)^2\right], \quad (3.14)$$

$$A_{t+1} = int\left[P_t exp\left(-\frac{c_{pa}}{V}A_t\right)\right] + int\left[(1-\mu_a)A_t\right]. \quad (3.15)$$

(Alternative discretization algorithms and the robustness of the model against the discretization will be studied in Section3.2.) Studying this noisy, discretized model system at the parameter sets fitted to the chaotic data series, (Henson et al. 2001) concluded that there are intermittent patterns in the time series which resemble the 6-cycle characteristic in the DD model (σ_1=σ_2=0), while other parts of the series resemble the chaotic attractor of the DC model. The authors compared visually the ND time series with an experimental series, and they argued that due to the noise, real population dynamics occasionally resemble the DD model, at different time periods the DC model (Henson et al. 2003). They called this phenomenon 'lattice effect'. Using the terminology of our study the question is whether their data

falls somewhere into the "grey zone" as Henson et al. (2001) observation might suggest, or their conclusion is premature. Beside the already considered effects we will need to pay attention to the length of the available experimental data series in order to answer the above question. With the help of the introduced distance function we could compute $\delta[NC, ND]$ of the LPA model, so we could compare the models quantitatively at the given noise level. For simplicity, $\delta[NC, ND]$ is measured for L, P, and A variables independently (in a more complex approach one would measure the distance between the joint distributions of L, P, A). To reveal the effect of noise, we computed $\delta[NC, ND]$ at different $\alpha\sigma_1$, $\alpha\sigma_2$ variances, where α was varied in the $(10^{-5}, 10)$ interval, and $\sigma_1 = 2.332$, $\sigma_2 = 0.2374$ was estimated from the data series (Dennis et al. 2001; Henson et al. 2001). It is remarkable that the plots for $\delta[NC, ND]$ of L, P, and A (Fig. 3.4 a-c.) follow the Type IV pattern which was experienced in the chaotic Ricker model (Fig. 3.2 f, Fig. 3.3 d), except that the distance at low noise level is relatively small due to the coincident peaks in both (continuous and discrete) models. In Fig. 3.4 arrows indicate the noise level of the cited study; we can observe that the point is at the left end of the noisy zone, i.e. $\delta[NC, ND]$ is close to zero. Consequently (and in contrast to the Hensons' conclusion) for the given parameters, NC and ND models behave statistically very similarly.

However, there are only some hundred data points in the experiment, much smaller than the number of data points used beforehand in the computation of $\delta[ND, NC]$. Due to the small number of experimental data points the difference of NC and ND models remains meaningful even at higher noise levels since the different models generate different short transient time series (Fig 3.2 d-f). With other words, in case of short data series the number of possible states of the population is larger (or, at least, of the same order) than the length of the time series, thus the measured time series are not related to the invariant statistics. They are rather related to the short term temporal behavior of the investigated systems. As we pointed out in section 3.1.2, the defined distance can be applied both for long and short data series. In the latter case the distance measures the more subtle difference between the time series: it compares the domains of phase space visited by the two (short) data series.

3.1.5 Discussion

In this section I presented a systematic study of noisy discrete and continuous models in population dynamics. The main goal of our investigation was to find criteria for the application of simple continuous models. We defined the *distance* between two models based on their statistical properties

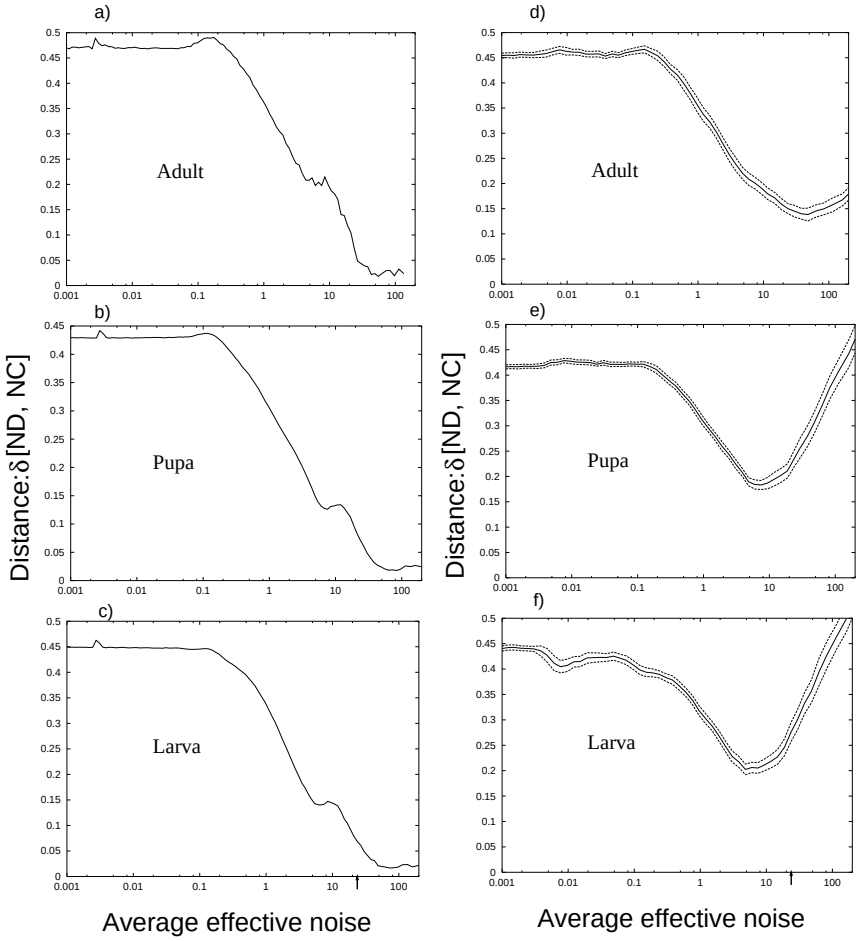

Figure 3.4: Distance between the ND and NC versions of LPA model of *T. castaneum* at different average effective noise and different length of time series. Arrows indicate the estimated noise level from the data series ($\alpha = 1$). The parameters of the model: b= 10.67, μ_l = 0.1955, μ_a= 0.96, c_{el}=0.01647, c_{la}=0.01313, c_{pa}= 0.35, σ_1=2.332, σ_2=0.2374. The magnitude of the noise was varied by multiplying σ-s with a parameter α (see the text), the average effective noise were measured as in Fig. 3.2. The left column (a-c) depicts $\delta[ND, NC]$ when time series is very long (2×10^5), the right column (d-f) when $\delta[ND, NC]$ is measured from time series is short (2×10^2). Dashed lines below and above the solid line indicate the variance of the average $\delta[ND, NC]$ function.

and measured the distances (as a function of the noise magnitude) between noisy and deterministic, discrete and continuous versions of the well-known Ricker map. The computations revealed four types of characteristic behavior, summarized in Fig. 3.3. The computations on the LPA model revealed that the described four types are meaningful beyond the Ricker model; we believe that they give an adequate qualitative picture for a wide range of dynamical models. Based on the four types our practical conclusions can be summarized as follows:

(1) Deterministic continuous models can represent the dynamical behavior of real (discrete, noisy) populations only for rather limited ranges of noise, so, in general, their application can not be recommended.

(2) In case of *regular* dynamical behavior (fixed point, periodic oscillations) there is no need to consider the discrete character of the population, simple, *noisy* continuous models are adequate for *all levels of noise*.

(3) In case of *chaotic* dynamical behavior the noisy continuous models are adequate only if the noise is sufficiently large. If the noise is small, the discrete dynamics with added noise has to be studied directly.

The last two points focus on the statistical similarity of the models, that is the case when time series are much larger than the possible population states. If this is not true our tool for measuring the distance can be still applied. In such cases the statistical comparison is practically meaningless, our tool compares the domains of phase space visited by the two (short) data series.

(4) Our computations indicate that the *short term behavior* of chaotic, discrete, noisy systems cannot be well approximated by continuous models, except for very small, special intervals of the noise amplitude.

In the third observation we referred to 'sufficiently large' and 'small' noise. It is very difficult to give a general estimate on what we call sufficiently large, however, based on our numerical results and the mathematical theory related to Ulam's problem, we believe that the biological noise can be called 'sufficiently large' if the actual random fluctuations are on average larger than the actual *derivative of the map* (Domokos & Szász 2003). Observe that this is not related to the size of the population. However, since the absolute value of output noise level increases with population size independently of the source of stochasticity (see Eqs. (3.3)-(3.6)) it can be expected that for large populations the biological noise is sufficiently large, while for small populations, especially with high derivatives (high birth rate), the noise is relatively small and discrete effects have to be considered. This effect can be illustrated if we

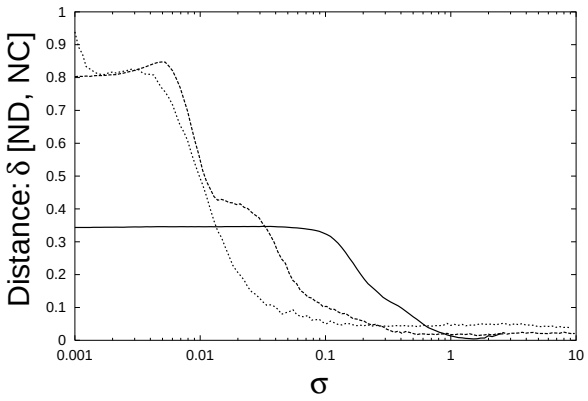

Figure 3.5: Distance between ND and NC versions of Ricker models at different noise level when the DC model is chaotic (b= 18, c=1). K= 5 (solid line), K = 50 (dashed line) K = 500 (dotted line).

re-draw Fig. 3.2 f in such a way that the distances $\delta[ND, NC]$ are plotted as functions of the noise parameter σ (Fig. 3.5). The parameter σ measures the level of stochasticity (input noise), but its effect of the dynamics depends on the population size (cf. Eqs. (3.3)-(3.6)). In Fig. 3.5 we can observe how the effect of σ depends on the size of the population: smaller populations display "lattice effects" (large distance from the continuous dynamics) for higher values of σ. Since our analysis of the *T. castaneum* data series showed that at the given population size the dynamics is *just above* the grey zone, we expect that for substantially smaller population sizes lattice effect will be very apparent.

As we illustrated on the LPA model, our study not only provides general recipes, but it also admits the systematic study of individual models by the application of the distance measurements. The *Tribolium castaneum* data series has another lesson: the noise level is high enough to keep the dynamics in the "noisy zone" (Fig. 3.3) even in this small laboratory population living under controlled environmental conditions. So, even for this chaotic system the NC model appears to be adequate. On the other hand, despite the statistical similarity of NC and ND versions of LPA model in this case, the real short time series of the models can be rather different. So here the biologically more adequate ND model is suggested. We showed that for non-chaotic systems NC models are always applicable if time series are long enough.

We may conclude that NC models generally describe population dynamics more precisely than the used DC models, and knowing that chaos (or more precisely dynamic systems which are noise-amplifying) is rather rare in field

populations (Berryman & Milstein 1989; Turchin & Taylor 1992; Godfray & Grenfell 1993; Ellner & Turchin 1995; Scheuring 2001), the application of more complicated ND models is necessary if the time series is too short compared to the possible population states, that is, in some cases when the population behaves chaotically.

3.2 Sturdy cycles in the chaotic *Tribolium castaneum* data series

3.2.1 Introduction

Ever since the classical paper by (May 1976) appeared, there has been considerable interest in the investigation of chaotic population dynamics. Recent results both in ecology (Henson et al. 2001, 2003; Domokos $ Scheuring 2002,2004; King et al. 2004) and in mathematics (Domokos & Szász 2003) indicate that due to the extreme sensitivity of chaotic systems, there might be striking differences between predictions based on discrete models applying integers versus continuous models applying continuous variables for population densities (see the previous Section).

Continuous models are widespread, however, their validity in case of chaotic dynamics was first questioned in (Henson et al. 2001). Continuous models of chaotic population dynamics predict typically aperiodic, random-like fluctuations of population densities. Discrete models, due to the finite number of states, contain always a finite number of finite cycles which can be regarded as stable, in the sense that they are reliably reproduced in each computation. Apparently, neither the purely deterministic discrete nor the deterministic continuous model offers a full and satisfactory description of the experimental data. (Henson et al. 2001; Henson et al. 2003) observed that experimental data of the *T. castaneum* contained some nearly-periodic patterns, similar to some of the cycles contained in the *discretized* version of their continuous population dynamical model. This model, named as LPA, is a three dimensional nonlinear map describing the dynamics of the flour beetle in the larvae (L), pupae (P) and adult (A) stages. The authors observed that by adding random noise to the discrete LPA model its predictive power was radically increased, the time series became more similar to experimental data.

These observations prompted a brief discussion on the mathematical background (Domokos & Scheuring 2002; King et al. 2002) and later a systematic analysis in (Domokos & Scheuring 2004) of discrete (D) and continuous (C) population models, both their deterministic (DD,DC) and noisy

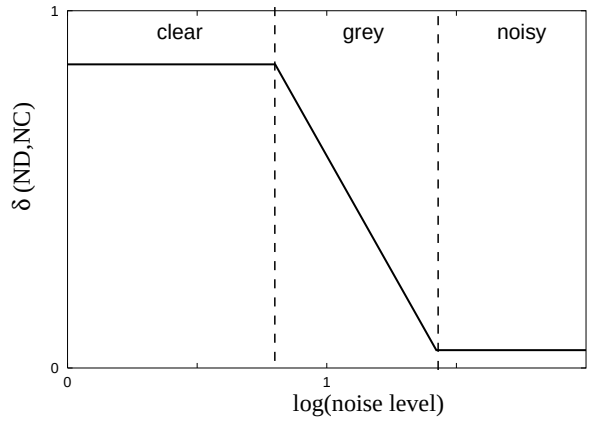

Figure 3.6: Schematic plot of $\delta(ND, NC)$, showing the statistical distance between the noisy, continuous and the noisy, discrete model as a function of the noise parameter. Observe the "clear", "grey" and "noisy" zones.

(ND,NC) versions. One key observation in (Domokos & Scheuring 2002; Domokos & Scheuring 2004) is that the noise amplitude σ can be regarded as a *transition parameter* (or "homotopy parameter") between discrete models and their continuous counterparts (see the previous Section). This heuristic idea is based on rigorous mathematical results on expanding maps, cf. (Kifer 1997; Domokos & Szász 2003). After defining a suitable distance $\delta(X, Y)$ between two noisy models $X(\sigma)$ and $Y(\sigma)$ (based on the difference between the statistical behavior associated with them), (Domokos & Scheuring 2004) describes how the $\delta(X(\sigma), Y(\sigma)) = \delta(\sigma)$ function behaves typically between different type (DD,ND,DC,NC) models. From our current point of view, the most interesting relationship is $\delta(ND, NC)$, displayed as a schematic plot in Fig. 3.6 in case of chaotic dynamics. The investigations in the previous Section (Domokos & Scheuring 2004) (partly illustrated in Fig. 3.6) revealed the following conclusions:

1. Since individuals are discrete entities, the model closest to the physical population is generally a discrete model with a *certain* amount of noise originating from the demographic and environmental stochasticity (i.e. a suitable ND model). While it is very hard to estimate the noise parameter σ(originating from biological and environmental fluctuations), we believe that real populations are generally in the "noisy zone".

2. If σ is very small ("clear zone") and the system is chaotic, then the difference between the prediction of the noisy discrete (ND) and noisy continuous (NC) models is large, so NC models are not applicable in

this range.

3. If σ is very large ("noisy zone"), then the statistical behavior predicted by NC and ND models practically coincide, so NC models can be applied in this range.

4. For a relatively large, intermediate range of σ ("grey zone") neither of the above simple rules can be applied.

We compared this theoretical predictions with experimental data series for the *T. castaneum* and computed data from he LPA model cf. (Henson et al. 2001) in the previous Section, and we show that the experimentally observed population is on the *border* of the noisy and the grey zone (Domokos & Scheuring 2004). In recent papers (Henson et al. 2003; King et al. 2004) the authors study the time series associated with the discrete and continuous LPA model and compare them with the experimental data. In the time series from the experiments they identify periodic patterns which correspond partly to cycles of the discrete model, partly to an unstable, quasi-periodic attractor in the continuous model. The same patterns are detected in the time series produced by the noisy discrete (ND) model. Their conclusion is that "..it is the transient but recurrent cyclic patterns generated by chaotic attractors and their discrete state analogies, woven together by stochasticity, that distinguish chaos as manifested in noisy, discrete state population systems.."(King et al. 2004). This conclusion implies that both the continuous and the discrete models are needed to understand the behavior of a real population.

Although these conclusions are certainly interesting, some questions remain open. The most important ones are associated with the applied aspects, i.e. how to find a proper model with reliable predictions for a given population? Assuming that an adequate continuous model is available, the following natural questions may be asked:

(a) How to find the proper discrete model, i.e. how to choose between several possible rounding algorithms?

(b) How to identify those cycles in the discrete model which will persist as nearly-periodic patterns in the presence of noise?

(c) How to identify the nearly periodic patterns in experimental or model-predicted time series?

In this Section we address these issues. In particular, Subsection 3.2.2 describes the behavior of cycles in deterministic discrete (DD) models. Based

on simple examples we will show that discrete cycles may or may not be sturdy with respect of small perturbations of the model parameters and different choices of the rounding algorithm (questions (a, b). From the point of view of applications the sturdy DD cycles are important, because these are the ones which we expect to see as recurrent nearly-identical patterns in noisy discrete (ND) models, in particular if the noise level is in the grey zone. Subsection 3.2.3 describes a systematic statistical approach to the identification of nearly-periodic patterns (question (c)) in noisy, discrete systems which can be either ND models or experimental data sets. Subsection 3.2.4 is devoted to the discussion of the results on the LPA models and on experimental data, obtained by the aforementioned statistical method. On one hand, these findings confirm some of the observations in (Henson et al. 2003; King et al. 2004), however, they also offer new clues.

We will point out that whenever "mixing" of discrete and continuous model occurs, it can be observed on the border of the grey and noisy zones. We discuss and summarize our results in Subsection 3.2.5.

3.2.2 Cycles in deterministic discrete (DD) models

Discretization algorithms

We assume that the continuous model is given by an iterated map of the form

$$N_{i+1} = f(N_i), \tag{3.16}$$

where N_i denotes the number of individuals (size of the population). Such models describe population dynamics in discrete time, however, the size of the population (N_i) can be any real number. When dealing with deterministic discrete (DD) models, only integer values of the population size N_i are admitted (which will be denoted by X_i), so f needs to be discretized and this can be performed in various ways. The function $int(N)$ will describe the largest integer that is smaller than N. Throughout this section we will refer to the following discretization strategies:

1. *Floor* model: $X_{i+1} = floor(f(X_i)) = int(f(X_i))$.

2. *Ceiling* model: $X_{i+1} = ceiling(f(X_i)) = int(f(X_i)) + 1$.

3. *Round* model: $X_{i+1} = floor(f(X_i))$ if $f(X_i) - int(f(X_i)) < 0.5$, otherwise $X_{i+1} = ceiling(f(X_i))$.

One could also use a probabilistic discretization algorithm where the probability p_1 of rounding down is given by $p_1 = (N - int(N))$ (so the probability of rounding up is of course $p_2 = (1 - N + int(N))$ and $p_1 + p_2 = 1$). Although this latter method appears to be rather natural, it is rarely applied. Discretized models produced by this algorithm would fall even without added environmental noise into the "noisy, discrete" (ND) category, defined in (Domokos & Scheuring 2004). In pervious works on discrete population dynamics (Henson et al. 2001; Henson et al. 2003; Domokos & Scheuring 2002; King et al. 2004; Domokos & Scheuring 2004) the *Floor* (as in the previous section) and *Round* models have been investigated.

Dynamics of the discrete map: sturdy and fragile cycles

After one of the listed three discretizations has been performed, the model is discrete and deterministic, i.e., it has a finite number of different states, each corresponding to possible (integer) values of the population's size. The dynamical behavior of such a finite state model may be best visualized via an oriented graph, the vertices of which correspond to the different population sizes, the oriented edges describe the action of the discrete map. Each vertex has exactly one outgoing edge (defined by the map) and zero or more incoming edges. Such a finite, oriented graph has necessarily a finite number of cycles. (One, trivial example is a tree graph with a single root, edges oriented towards the root. Such a graph has one cycle of length one.) The structure of the graph (i.e. number and length of cycles and paths leading into the cycles) is characteristic for the dynamical behavior of the modeled population. For example, the above mentioned tree graph describes a population that will have constant size after a finite number of time-steps, regardless of the initial (starting) size.

We will investigate the simple example of the well-known logistic map

$$N_{i+1} = f_{logistic}(N_i) = \frac{\mu}{N} N_i (N - N_i) \tag{3.17}$$

and its discretized *floor*, *ceiling*, and *round* versions. Our goal is to show how the structure of the graph (and thus the global dynamics) depends on the maximal size N of the population (carrying capacity of the environment), the discretization strategy and the control parameter μ. The map (3.17) is known to be chaotic for a range of the control parameter μ, in particular, for $\mu = 4$ the statistical behavior is characterized by a unique, absolutely continuous probability density function and no stable periodic orbit exists. One would expect that as N is increased, the statistical density associated with the deterministic discrete model converges to the continuous function. However, this is not the case. As we pointed out before the discrete model always

possesses a finite number of (stable) cycles. For discretized ergodic maps, little is known about the length and distribution of these cycles which appear in rather irregular patterns as N is varied. Random map models predict a cycle length of $\approx \sqrt{N}$ (Domokos 1990; Domokos 2005; Lanford 1998) which, in turn, implies the presence of very few ($\approx \log N$) cycles. Although these rules seem to be correct on average for discrete maps, large irregular fluctuations can be observed. Since the statistical behavior of the discrete map is mainly determined by the cycles, it is hard to predict anything definite.

Although there is no mathematical evidence at hand, one can observe that some of these cycles appear to be rather sturdy, while others are extremely fragile with respect to variations of the control parameter and rounding algorithm. On the other hand, changing the population maximum N almost always leads to a radical transformation of the cycle pattern. Fig. 3.7 shows the complete graph associated with different versions of the logistic map (3.17). The columns correspond to different values of the control parameter μ, the rows show different discretization strategies. The first three rows correspond to $N = 22$, the last row to $N = 21$. As we can observe, the 3-cycle $\approx [4] \to [13] \to [21]$ and the fixed point at [0] proves to be sturdy with respect to variation of μ and the discretization strategy, other cycles appear only locally. The same pattern can be clearly observed for much larger values of N and for more complicated, higher dimensional maps as well; some cycles are sturdy, others are rather fragile. These concepts could be made more precise by introducing suitable norms both for the parameters and the discrete trajectory, however, rigorous analysis is beyond the scope of the recent study (but see the last chapter).

It is well understood mathematically (Domokos & Szász 2003; Kifer 1997) that certain random perturbations added to the deterministic discrete map not only destroy the just described exotic cyclic structure but also restore the original invariant density function. From the point of view of biology the crucial question is whether the existing environmental and biological noise have this property or not. The answer is not binary, since as the noise level is increased, cycles dissolve gradually, We called this transition as "grey zone " earlier (Domokos & Scheuring 2004). One of our key observations here is that the cycles which survive the disturbing effect of noise are the very same cycles which appear as "sturdy" in the deterministic discrete model, so these cycles are of prime importance for biological applications.

Later in this section we will investigate the so-called LPA model associated with the *Tribolium castaneum* data series. In that case, because of the high number of possible states ($\approx 300^3$) the illustration of the full discrete graph is impossible, however, exactly the same qualitative behavior will be demonstrated. The data series associated with the noisy, biological system

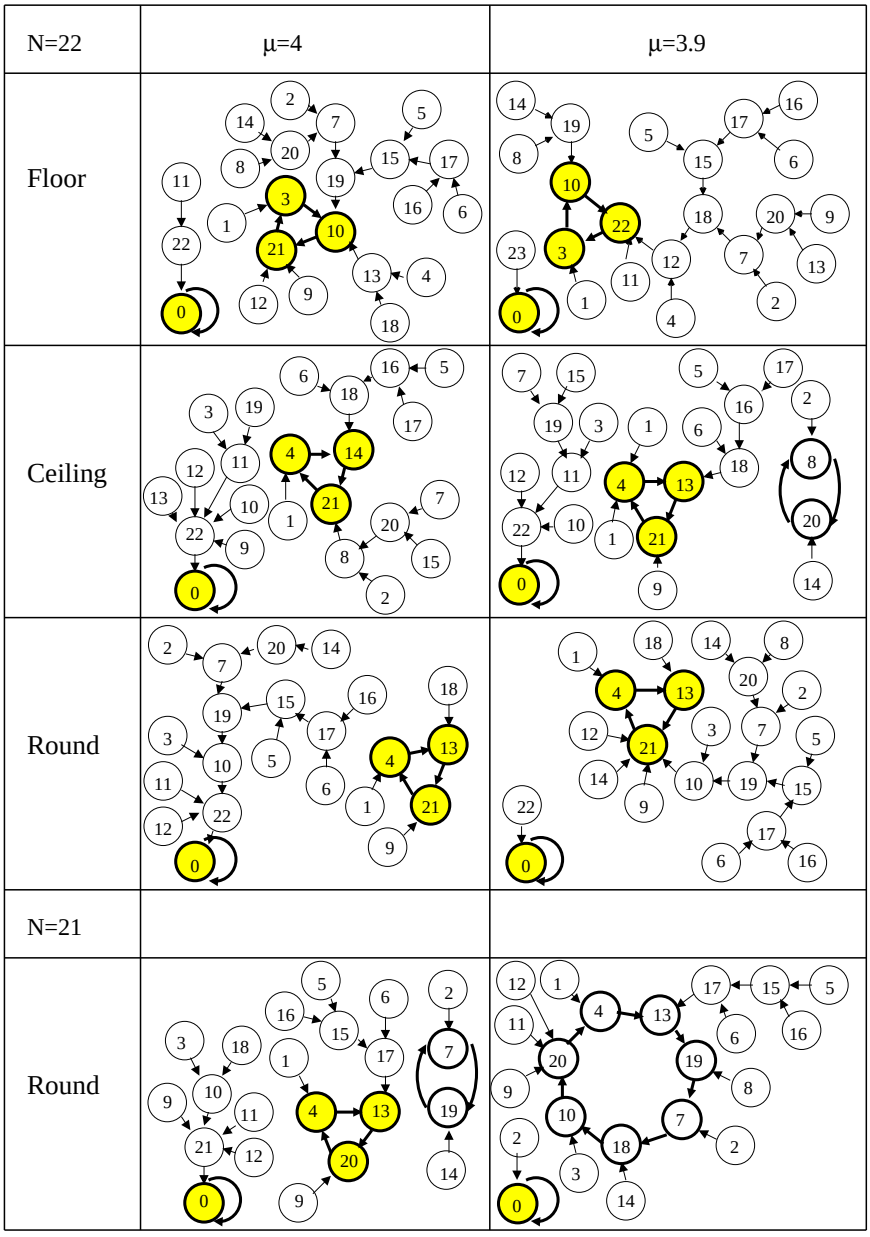

Figure 3.7: The complete graph appearing in the floor-, ceiling and round-discretization of the logistic map at $N = 22$ and $N = 21$. Observe sturdy (grey and bold) and fragile cycles (bold).

will carry the fingerprints of the sturdy cycles identified in the deterministic discrete map in the form of nearly-periodic patterns. Our next, immediate goal is to introduce the statistical tools needed to identify such fingerprints.

3.2.3 A systematic approach to detecting nearly-periodic patterns

It is a common task in many different fields to seek intermittently periodic patterns, trends or anomalies in data series. Applications include in stock data, alarms of telecommunications and event logs of computer networks (Han et al. 1998; Han et al. 1999; Ozden et al. 1998). The general aim is to find characteristic patterns with unknown periods by an effective algorithm in these huge data series (Han et al. 1999; Ma & Hellerstein 2001).

Although we are also looking for nearly-periodic patterns, the emphasis is completely different. Our main question is, whether there exist patterns in a given data series (produced either by experiments or by numerical simulation of the model with added noise) which are *significantly similar* to one of the periodic cycles present in the associated deterministic DD model. Thus, in contrast to the aforementioned applications, we are looking for *a priori given* sample patterns, and the numerical efficiency of analysis is not a central issue because the biological time series are relatively short.

To measure similarity, we define the distance $D\left(\mathbf{X}^{(p)}(t), \mathbf{S}^{(p)}\right)$ between the p-length sequence of d-dimensional data vectors $\mathbf{X}^{(p)}(t) = \{\mathbf{x}(t), \mathbf{x}(t+1), ... \mathbf{x}(t+p-1)\}$ and the sample sequence $\left\{\mathbf{S}^{(p)}\right\} = \{\mathbf{s}(0), \mathbf{s}(1), ...\mathbf{s}(p-1)\}$ with period p (that is $\mathbf{s}(p) = \mathbf{s}(0)$), as

$$D\left(\mathbf{X}^{(p)}(t), \mathbf{S}^{(p)}\right) = \sum_{j=1}^{d} \left(\frac{1}{p} \frac{2\left|\sqrt{\sum_{i=0}^{p-1}\left[x_j(i+t) - s_j(i)\right]^2}\right|}{\left|\sqrt{\sum_{i=0}^{p-1}\left[x_j(i+t)\right]^2}\right| + \left|\sqrt{\sum_{i=0}^{p-1}\left[s_j(i)\right]^2}\right|} \right), \tag{3.18}$$

where $x_j(i+t)$ and $s_j(i)$ are the j-th coordinate of the data and sample vectors in the d-dimensional space. The expression in the big parenthesis measures the relative Euclidean distance of sequences $\{x_j(i+t)\}_{i=0}^{p-1}$ and $\{s_j(i)\}_{i=0}^{p-1}$ in the j-th subspace. (The absolute Euclidean distance of the sequences is divided by the period p of the sample. It is also divided by the average obtained from the total lengths of data and the total lengths of the sample sequences in the j-th subspace.) The total distance of $\mathbf{X}^{(p)}(t)$ and $\mathbf{S}^{(p)}$ is the sum of these subspace distances. A related distance function was defined for similar analysis earlier (King et al. 2004), however application of relative distance provides direct comparison between the different pieces of sequences.

The distance $D\left(\mathbf{X}^{(p)}(t), \mathbf{S}^{(p)}\right)$ can be computed for every $t = 1, 2, ...T - p + 1$, where T is the length of the data series. A sequence $\mathbf{X}^{(p)}(t^*)$ is said to be ε-similar to $\mathbf{S}^{(p)}$ at t^* if $D\left(\mathbf{X}^{(p)}(t^*), \mathbf{S}^{(p)}\right) < \varepsilon$, where ε is set to be a small positive number. The sum of events where the data sequence is ε-similar to the sample is denoted by $N^{(p)}(\varepsilon)$. As we have seen in the previous section, different cyclic patterns can be found in the same DD model, so the above mentioned procedure has to repeated for all $\mathbf{S}^{(p_l)}$ sample sequences with period p_l, emerging in the studied DD-model. Consequently, it might occur that a piece of data sequence is assigned to more than one sample sequence, that is, $\mathbf{X}^{(p_i)}(t_1)$ is ε-similar to $\mathbf{S}^{(p_i)}$, and $\mathbf{X}^{(p_j)}(t_2)$ is ε-similar to $\mathbf{S}^{(p_j)}$, and $\mathbf{X}^{(p_i)}(t_1) \bigcap \mathbf{X}^{(p_j)}(t_2) \neq 0$. Then the assignment is skipped which is valid only at the higher ε level. For example, assuming $\mathbf{X}^{(p_i)}(t_1) \bigcap \mathbf{X}^{(p_j)}(t_2) \neq 0$ and $\varepsilon > D\left(\mathbf{X}^{(p_i)}(t_1), \mathbf{S}^{(p_i)}\right) > D\left(\mathbf{X}^{(p_j)}(t_2), \mathbf{S}^{(p_j)}\right)$, then $\mathbf{X}^{(p_j)}(t_2)$ is ε-similar to $\mathbf{S}^{(p_j)}$, but $\mathbf{X}^{(p_i)}(t_1)$ is not considered to be ε-similar to $\mathbf{S}^{(p_i)}$. (Naturally, the same procedure is applied if $\mathbf{S}^{(p_i)} \equiv \mathbf{S}^{(p_j)}$.) After excluding these overlaps there will be $N_{\cap}^{(p_l)}(\varepsilon)$ number of ε-similar sequences in the data series for every $\mathbf{S}^{(p_l)}$. In this analysis, at any ε level, one data point is assigned either to one (and only one) sample sequence or to no sample sequence at all.

To determine whether the presence of ε-similar patterns are significant in the T-length sequence, we use a standard randomization test (Manly 1991). We produce $K - 1$ random permutations of the original data sequence, and compute $N_{\cap,per}^{(p_l)}(\varepsilon)$ again for every permuted case. If $N_{\cap,per}^{(p_l)}(\varepsilon) < N_{\cap}^{(p_l)}(\varepsilon)$ for every $K - 1$ permutated sequence, then the ε-similar patterns are considered to be significantly present in the original sequence at $1/K$ significance level, in the opposite case the result is said to be non-significant at this level. We set henceforth $K = 999$, i.e., the significance level is 0.001. (Because of the small statistical strength of the randomization tests we use a rather low significance level.)

3.2.4 Nearly-periodic patterns in the noisy LPA models and the *T. castaneum* data series

The LPA models

There exist only a very limited number of field and experimental data series in ecology which are of sufficiently high quality to check theoretical hypothesis about the existence sturdy nearly-periodic patterns present in Nature. The *T. castaneum* data series from the experiments of Costantino et his co-workers (Costantino et al. 1997; King et al. 2004) are certainly among these few, making theoretical predictions and experimental data comparable. They grew twenty-four cultures of flour beetles for more than 8 years

in a controlled environment. Knowing the life-history of this species they suggested a deterministic map for the dynamics of the beetle *Tribolium* (Costantino et al. 1997), which was introduced already in the previous section. For the popularity, however we introduce this system again in a detailed manner. The continuous state version of the model is

$$\begin{aligned} L_t &= bA_{t-1}exp\left(-\frac{c_{ea}}{V}A_{t-1}-\frac{c_{el}}{V}L_{t-1}\right), \\ P_t &= (1-\mu_l)L_{t-1}, \\ A_t &= P_{t-1}exp\left(-\frac{c_{pa}}{V}A_{t-1}\right)+(1-\mu_a)A_{t-1}, \end{aligned} \tag{3.19}$$

where L_t denotes the number of larvae, P_t denotes the number of pupae and A_t denotes the number of adults at time t. The unit of time is two weeks to fit the model to the experiment, b is the average number of larvae recruited per adult per unit time. Eggs are eaten by adults and larvae while pupae are eaten by adults at the same time, so exponentials represent the fractions of individuals surviving this cannibalism within the unit time with coefficients c_{ea}/V, c_{el}/V and c_{pa}/V, respectively. V denotes the size of habitat, the unit of which is 20g flour, the amount of medium used in the laboratory experiments. This DC (deterministic-continuous) version of the LPA model describes successfully a wide variety of nonlinear phenomena, including chaos observed in laboratory data series (Costantino et al. 1997; Cushing et al. 2001). However, there are weaknesses of this model: the noise present in all populations is neglected. Thus, rather some NC-LPA models including environmental (Costantino et al. 1997) and/or demographic noise (Dennis et al. 2001) have to be studied. Even more elaborate ND-LPA models take the role of discreteness of variables L, P and A into account as well (Henson et al. 2001, 2003; King et al. 2004; Domokos & Scheuring 2004). Assuming that the main source of stochasticity is demographic noise, the generally used ND-LPA equations are

$$\begin{aligned} L_t &= discr\left[\left(\sqrt{bA_{t-1}exp\left(-\frac{c_{ea}}{V}A_{t-1}-\frac{c_{el}}{V}L_{t-1}\right)}+\varepsilon_{1t}\right)^2\right], \\ P_t &= discr\left[(\sqrt{(1-\mu_l)L_{t-1}}+\varepsilon_{2t})^2\right], \\ A_t &= discr\left[P_{t-1}exp\left(-\frac{c_{pa}}{V}A_{t-1}\right)\right]+discr\left[(1-\mu_a)A_{t-1}\right], \end{aligned} \tag{3.20}$$

where $discr[.]$ denotes an operation creating integer values on the right side of the map. This could be any of the three alternative algorithms described in subsection 3.2.2, however because of direct manipulation of adult numbers

in the experiment the round operation is the most adequate in the last equation. The symbols ε_{1t}, ε_{2t} denote normal random variables with mean zero and variance-covariance matrix Θ (Henson et al. 2001; Henson et al. 2003; King et al. 2004).

The adult mortality rate (μ_a) is experimentally set to be 0.96. The parameter c_{pa} was manipulated to be 0.00, 0.05, 0.10, 0.25, 0.35, 0.50, 1.00 in the different treatments. It is important to note that μ_a and c_{pa} are set by adding or removing adults in the experimental protocol (Costantino et al. 1997), thus any of the described discretization methods can be only regarded as valid as far as it agrees with the experimental procedures. The other parameters were estimated from the first 80 weeks of data: b=10.45, μ_l=0.2000, c_{ea}=0.1310 and c_{el}=0.01731 (Dennis et al. 2001). The variance Θ_{11} andΘ_{22} of ε_{1t} and ε_{2t} was estimated as 2.332 and 0.2374 respectively and $\Theta_{12} = \Theta_{21} \approx 0$ (Dennis et al. 2001). The experiments were initiated with 250 L-stage, 5 P-stage and 100 A-stage individuals, and the numbers of L, P and A stage animals were counted biweekly. This experiment resulted in three data series containing more than two hundred points for every treatment. It was demonstrated that the data series behaves chaotically under the c_{pa}=0.35 treatment in concordance with the dynamics of the DC-LPA model (Costantino et al. 1997; Dennis et al. 2001). Thus, our analysis utilize data series under this treatment, as other related studies have done earlier (Henson et al. 2003; King et al. 2004). The only difference is that we analyzed all the three time series, while earlier works used only one replicate at this treatment.

Qualitatively different cycles in different DD-LPA models

In this subsection we will provide a complete list of all qualitatively different cycles appearing in the deterministic, discretized LPA modes. As we mentioned beforehand, two of the different $discr[.]$ operators listed in Subsection 3.2.2 have been applied previously: the $floor[.]$ and the $round[.]$ (Henson et al. 2003; King et al. 2004). Unless the experimental protocol is exactly known there are no strong biological or mathematical reasons to apply one or the other discretization procedure and, as pointed out in Subsection 3.2.2, other methods can be defined as well. As we pointed out in Subsection 3.2.2, the applicability of models depend on the robustness of the emerging cycles against the structural and parameter perturbations.

Below we will list all co-existing cycles belonging to two different DD-LPA models (Floor and Round, differing in the discretization algorithm) and we will identify the sturdy ones. The Floor-LPA has three different 6-cycles, one 3-cycle (which will be denoted by 3a) and one 1-cycle at the given parameter

values. Two among the three 6-cycles are very similar to each other, so we can consider them as one type (6a), the third will be referred to as 6b. The Round-LPA contains six different 6-cycles, one 8-cycle and one 3-cycle, the latter will be denoted by 3b. Similarly to the Floor-LPA model, the six different 6-cycles form two groups. Five cycles are very similar not only to each other, but also to the 6a type of the Floor model, so we denote them by the same symbol. The sixth cycle is extremely close to the 6b type of the Floor model, so we denote it by the same symbol. So we have one 1-cycle (unstable fixed point), one 3-cycle (3a) and two qualitatively different 6-cycles (6a and 6b) in the Floor-LPA and one 3-cycle, two 6-cycles (6a and 6b) and one 8-cycle in the round-LPA model (Fig. 3.8). We remark that the 6b-cycle is very similar to the duplicated 3b-cycle of the Round-LPA model. This reduces the number of effectively different cycles in the two discretization models to 6: the 1-cycle, the 3a and 3b-cycles, the 6a and 6b-cycles and the 8-cycle. Similar classification is used by King et al. (2004), here we only refined it by compartmentalizing the 3b-cycle and 6b-cycles into different classes, and we classified the floor model in a similar way.

In Fig. 3.8 we can observe that the 1-cycle, the 3a-cycle and the 8-cycle are fragile, since their presence depends on the discretization procedure. The remaining three cycles (3b,6a, 6b) are present in both (Floor and Round) models, so they appear to be sturdy. (Although 3b only appears in the Round model, it is extremely close to the first 3 elements of the sturdy 6b, so it can also be regarded as sturdy.) To check further the sturdiness of the latter three cycles we varied the estimated dynamical parameters $(b, \mu_l, c_{ea}/V, c_{el}/V)$ by ten percent and identified the cycles after these perturbations. We observed minor (or none) modifications in the sturdy 3b,6a and 6b cycles. For example, perturbation of c_{ea}/V change the $\mathbf{C_i} = \{L_i, P_i, A_i\}_{i=1}^{6}$ values of 6a, 6b and 3b-cycles such that $c_{ea}/V\mathbf{C_i} \approx$ constant, while perturbing c_{el}/V does not change these cycles. In contrast, the remaining fragile cycles disappear and others appear abruptly in the perturbed system.

Although the DC-LPA model is chaotic at c_{pa}=0.35, it has an Arnold tongue with a 11-cycle at the estimated parameters (Cushing et al. 2001; King et al. 2004). Consequently, nearly-periodic patterns of length 11 are present in finite regions of the time series of the DC-LPA model (Fig. 3.9). We expect similar patterns in the noisy NC-LPA model, for moderate noise levels. This pattern is not exhibited in the DD-LPA models, however as the noise level increases, we enter the grey zone and the ND-LPA model becomes more and more similar to NC-LPA model (cf. Fig. 3.4, 3.6, for more details see the previous section (Domokos & Scheuring 2004)), thus the emergence of the 11-cycle in ND-LPA models can be also expected at some noise level in the grey zone. (The noise should be sufficiently large to make the discrete

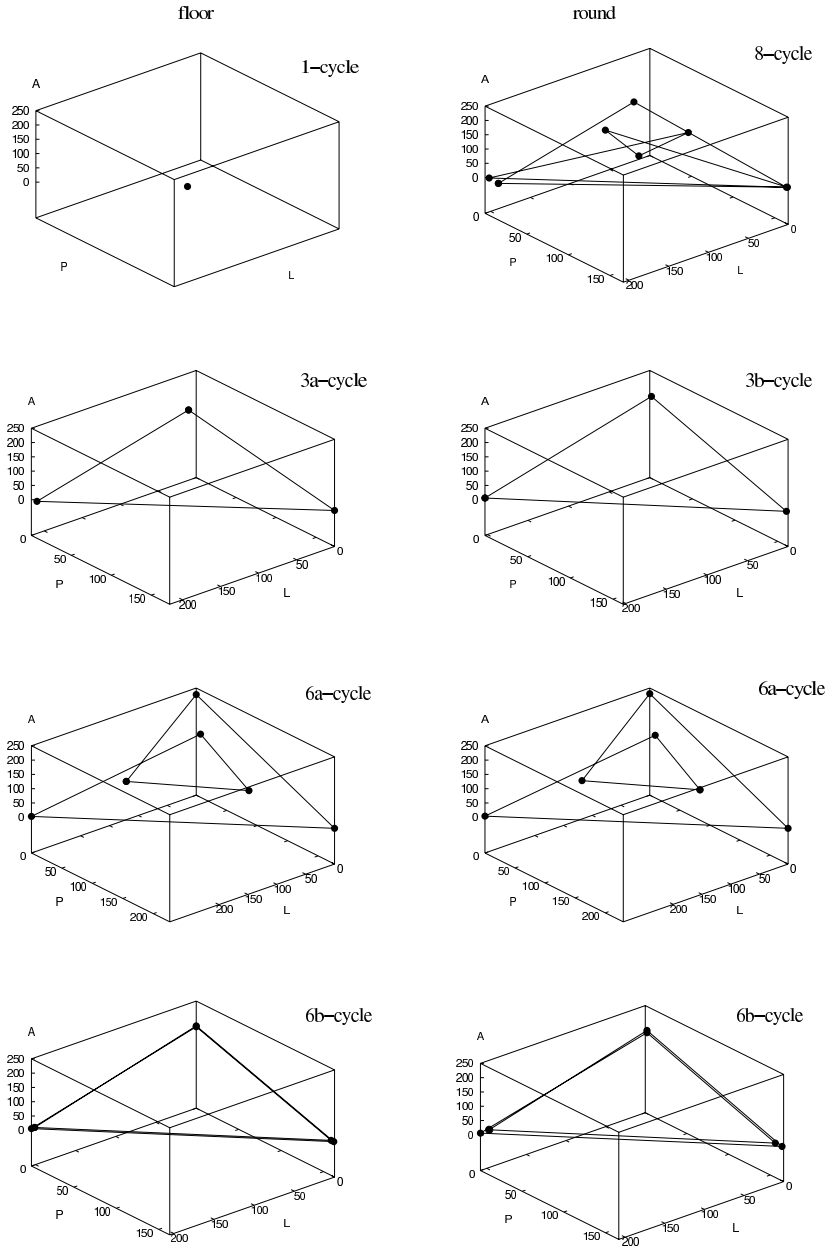

Figure 3.8: Cycles appearing in the Floor- and in the Round-LPA models at model parameters defined in the main text.

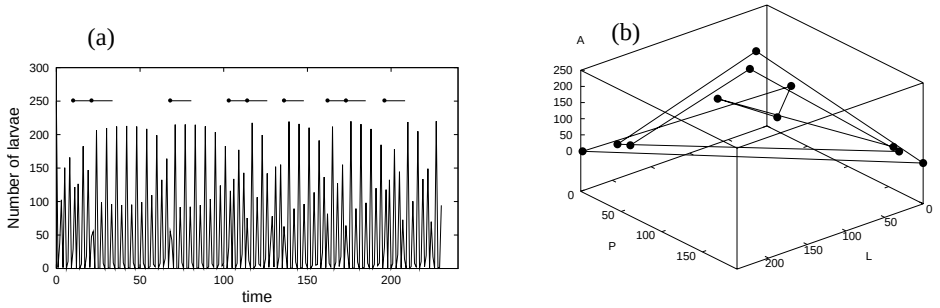

Figure 3.9: 11-cycle patterns in the data generated by the DC-LPA model. **(a)** The number of larvae as function of time. The points and intervals indicate positions in the data where the 11-cycle is detected according to the distance function (3.18) at ε=0.125. **(b)** The 11-cycle of eq. (3.20) in the L, P, A space at parameters defined in the text.

model appear similar to the continuous, however, sufficiently small to leave the 11-patterns partially intact.) As a consequence, together with the 6 cycles appearing in the DD models we also have to look for the 11-cycle of the DC model in the studied data series. Besides the experimental data, we generated data series from the model equations (3), using the estimated parameters.

Identification of nearly-periodic patterns in experimental and simulated data series

In this subsection we will apply the statistical technique of Subsection 3.2.3 to identify nearly-periodic patterns belonging to the cycles listed in subsection 3.2.4.

According to the method introduced in Subsection 3.2.3, we measured the number $N_{\cap}^{(p_l)}(\varepsilon)$ of hits for nearly-periodic patterns in the real and simulated data series for all the 7 qualitatively different cycles (6 of them present in the deterministic Floor-LPA and Round-LPA models plus the 11-cycle of the NC-LPA).

Figure 3.10 depicts the number $N_{\cap}(\varepsilon)$ of non-overlapping segments of sequences similar to one of the 7 sample cycles as functions of the similarity level ε. Significant appearance of the observed patterns is denoted by a plus mark in the center. The 1-cycle of the floor-model was never observed. It can be seen from Figure 3.10 that none of the 7 cycles appear *exactly* in the data series, the best fitting patterns are at ≈ 0.05 relative distance from the exact cycles. The fragile cycles either do not appear at all, or rather sparsely,

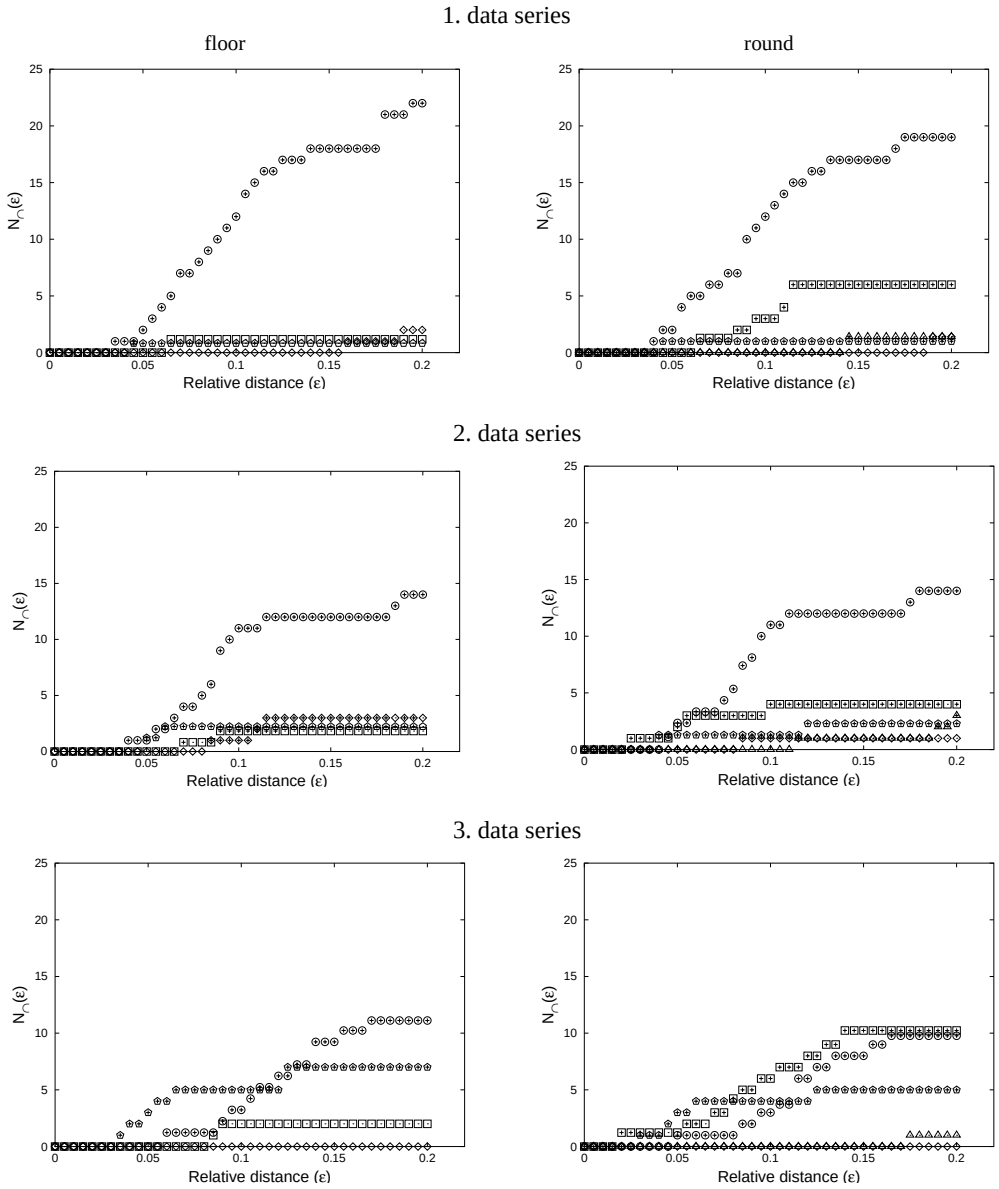

Figure 3.10: The number $N_{\cap}(\varepsilon)$ of non-overlapping intervals similar to one of the cycles of the Floor- (left column) and the Round-model (right column) as functions of similarity level ε. Circles denote the 6a-cycle, squares the 3a- or 3b-cycle respectively, diamond is the mark of 11-cycle, pentagons denote the 6b-cycle and triangles mean the 8-cycle in the round model. Significant appearance of the patterns is denoted by the plus mark. Some marks are shifted along the y axis for the better visualization

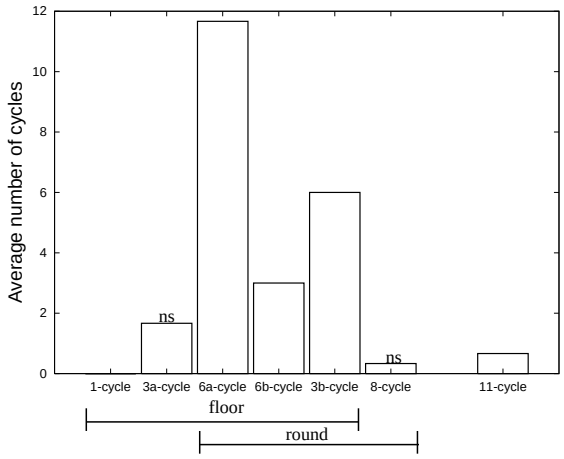

Figure 3.11: The number of cyclic patterns averaged on the three data series at $\varepsilon = 0.125$. Non-significant results are denoted by ns on the top of the bars.

such as the 3a-cycle in the Floor and the 8-cycle of the Round models. These cycles are generally present in a non-significant manner in the experimental data (except the 3a-cycle in the second data series at some ε level) (Fig. 3.10., 3.11).

The first and the second data series behave very similarly: the 6a-cycle like patterns dominate the data followed by low numbers of the other cycles. There are less 6a-cycles and more 6b-cycles in the third data series. Since the 6b-cycle is very similar to two subsequent 3b-cycles (Fig. 3.8), it is clear that the 3b-cycle like patterns can appear in the same region in the Round-model analysis where the 6b-cycle is detected in the floor model. Since longer cycles are destroyed by noise more effectively, the 3b-cycle patterns can be found with smaller distances at the same region of the sequence where the similar 6b-cycle would be detected only at higher ε level. This is the reason why the 3b-cycle is more pronounced in the Round-model analysis than in the Floor-model one. It is interesting to observe that the 11-cycle pattern is present only in the second data series in a significant manner. We remark that earlier analysis (Henson et al. 2003; King et al. 2004) applied only this second data series.

Naturally, there is no a priori given level for the similarity measure ε. Too low ε excludes all correspondence, while too high ε level indicates poor correspondence between the data and sample sequence. However, the number of hits saturates at about 0.1-0.13 for all data series (Fig. 3.10), which suggests to choose for practical purposes ε from this interval.

We generated data series by the noisy floor-LPA and round-LPA models at different noise levels, while the other parameters took the estimated values. Omitting the initial transients we recorded 213 time-steps. (In order to analyze longer time series we included the initial transient in the experimental data. Since the transient is short (about ten time steps) to include or omit the transition causes only small difference in the analysis.) The same pattern-detecting analysis was applied as before. If noise was set to be weak (i.e., the model was in the "clear zone"), then the 6a-cycle dominates the series (Fig. 3.12., $\alpha = 0.1$). The other cycles emerge in the "grey zone", similarly as we observed in the experimental data (Fig. 3.12, $\alpha = 0.4, 1$). Few patterns, (typically the 11-cycle) are detected in the "noisy zone" only at high levels of epsilon (Fig. 3.12., $\alpha = 3$).

3.2.5 Discussion

Since experimental and field population data are generally missing or too weak to confirm a given model with its details, population dynamical equations are based often on somewhat arbitrary assumptions. One strong counter-example is the *T. castaneum*, where the family of LPA models of population dynamics have been widely tested by experimental data (Costantino et al. 1997; Dennis et al. 2001; Henson et al. 2001). An interesting question in this field is whether the deterministic or noisy continuous-models (DC, NC) or the their corresponding discrete-state (DD, ND) counterparts provide better fit to the population data (Section 3.1) (Henson et al. 2001; Domokos & Scheuring 2004). Ambiguity in the discretization procedure makes the situation more complex.

We investigated two types of DD models, the Floor-LPA, and the Round-LPA, which have been applied earlier as well. Recent studies argue that if population is chaotic then characteristics of DC- and DD-LPA-models emerge in mixed manner in the data: there are patterns in the data similar to both the 11-cycle of the DC and to the cycles of the DD model. Consequently, for the mathematical description of the dynamics both type of models have to be considered (Henson et al. 2003; King et al. 2004).

We re-analyzed the experimental data with a different method. We looked for disjoint intervals being similar to one of the cyclic patterns present in the Floor-LPA, Round-LPA and the DC-LPA models. We checked the significance of the results at different similarity levels. The same analysis has been carried out on the data generated by the noisy Floor-LPA and Round-LPA models at different noise levels.

Since real population dynamical processes are built up by complex stochastic steps (Dennis et al. 2001), any discretized, noisy LPA model is rough and

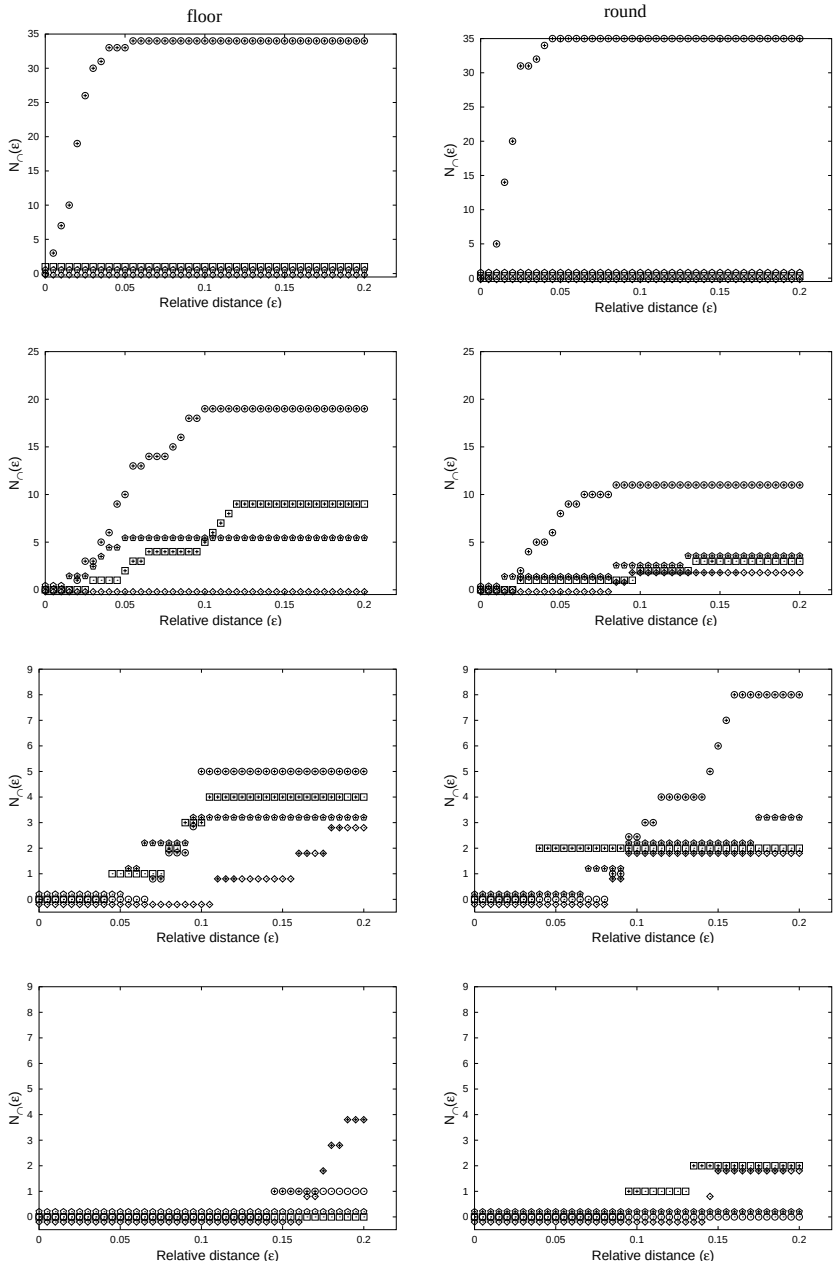

Figure 3.12: Model generated data series. The number of non-overlapping intervals similar to one of the cycles ($N_{\cap}(\varepsilon)$) of the floor- (left column) and the round-LPA model (right column) in function of similarity level (ε). The noise level is varied by multiplying the estimated Θ values with $\alpha > 0$ (α=0.1, 0.4, 1, 3 increasing from top to down). Initial conditions were L_0=250, P_0=5 and A_0=100 as in the experiment. Circles denote the 6a-cycle, square= 3-cycle (3a in the floor and 3b in the round model), diamond is the mark of 11-cycle, pentagons denote the 6b-cycle. The 1-cycle in the floor- and 8-cycle in the round-model were never detected. Values are shifted along the y axis a bit for the better visualization.

contains more-or less arbitrary approximations. For example, how to discretize the continuous LPA is such an arbitrary step. If small structural and parameter changes cause only small differences in the behavior of these models, they can be considered as equivalently good and robust approximations of the real processes. This is the case when the dynamics of DC models (DC-LPA in our case) is regular. However, if the DC model is chaotic, then the DD models are structurally unstable: any small perturbation in the structure and parameters of the model can generate new and annihilate existing cycles (Domokos & Scheuring 2002; Domokos & Szász 2003). However, there are "sturdy" cycles in the DD models as well, which resist small perturbations. We pointed out that in the statistical analysis for nearly-periodic patterns these sturdy cycles of the Floor- and Round-LPA models dominate the results, nearly-periodic patterns corresponding to fragile cycles are identified very rarely. Moreover, the fragile cycles are found only in a non-significant manner (Fig. 3.11). This result corroborates the hypothesis that because of inner stochasticity of dynamical processes only the sturdy cycles can be significantly present in real population time series.

The 11-cycle of the DC-LPA was found in a much less pronounced manner in our analysis than an earlier study has suggested (King et al. 2004). There are three reasons of this discrepancy: first, and most importantly King et al. (2004) seek the cyclic patterns in a "non-disjoint" manner in their analysis, that is, some intervals are frequently assigned to more than one cycle (see e.g. their Fig. 2., 5.,6.), while we introduced here a "disjoint" method. (There is rationality in both analyses: Since the cycles, or part of them, are very similar to each other it is probable that a segment of data lies close to more than one cycle. The "non-disjoint" method solves this problem by assigning a pattern to different cycles. The "disjoint" method is based on the numerical observation that time series are composed by the noisy but disjoint periodic orbits in the grey zone, so it concentrates on finding them.) Second, they use only one fixed (and relatively high) similarity level, so the fact that the 11-cycle is fitted only at higher similarity level than any sturdy cycles of the DD models cannot be explicitly realized in their analysis. (A careful study of the figures reveals this fact.) Third, they studied only the second data series, where we also found the 11-cycle to be present significantly, but according to our method, the 11-cycle was not present in a significant manner in the other two data series. So, our results hardly support the view that characteristics of DD and DC models *typically* appear hand-in-hand in real data, however they apparently confirm this as a real possibility. This possibility is, in fact, realized in the current problem: the 11-cycle is the consequence of Arnold-tongue being present of DC-LPA model nearby the determined parameters (Cushing et al. 2001). Frequency

locking, and consequently Arnold-tongues emerge typically in systems where two (or more) oscillators are coupled nonlinearly, and the ratio of oscillator's frequencies are rational numbers (Ott 2002). We do not know whether population dynamical models generally satisfy these conditions, nevertheless there exist other population dynamical models where Arnold tongues are present (Greenman & Benton 2004). External periodic environmental forcing can cause the presence of Arnold tongues as well (King & Schaffer 1999). The cycles present in the tongue (like 11-cycle in the LPA model) determine the basic frequency of the attractor close to the Arnold tongue even when the system is chaotic (King & Schaffer 1999; Cushing et al. 2001). So, as it was shown earlier and also in this analysis, this periodicity can be detected even in noisy systems. This cycle is unstable, but it is "much less" unstable than any other periodic orbit. However, in other chaotic systems (e.g. the logistic map, $\mu = 4$) there is no such strong periodicity. The infinite number of unstable periodic orbits have almost the same weight in creating the time series. These unstable orbits can be detected by an algorithm similar to the one described here (Lathrop & Kostelich 1989; Dhamala et al. 2000), however, because these cycles are unstable in a "similar strength", the probability to detect a periodic orbit depends on its length, and decreases exponentially with the noise and with the length of the cycle (Dhamala et al. 2000).

It is highly probable that demographic and environmental noises are inherently high in every real population, thus it seems unlikely that the unstable cycles of DC systems (especially if they are long) could be detected in field data series. Furthermore, we concluded that even the characteristics of Arnold-tongues can be important merely at specific noise levels. If a small noise keeps the NC system in the "clear" zone, the data series will be practically periodic with periods determined by the applied DD model and the initial conditions (Fig 3.12, $\alpha = 0.1$). The time series produce the richest in patterns in the "grey" zone (Fig 3.12, $\alpha = 0.4, 1$), including some 11-cycles on the border of the "grey" and "noisy" zone (α=1). Patterns, similar to the periodic orbits are practically not detected in the "noisy" zone (Fig 3.12, $\alpha = 3$). We have shown in the previous section that this dynamical system is on the border "grey" and "noisy" zone in this experiment (Domokos & Scheuring 2004). This implies a peculiar situation where the sturdy cycles of the DD systems can *still* be detected and the 11-cycle of the DC system can *already* be observed. Since environmental noise is suppressed meaningfully in this (and every other) experimental situation, we suspect that sturdy cycles of the corresponding DD and DC systems could not be detected significantly in chaotic field population data sets, even if they are longer than this experimental data.

The direct consequence of this conclusion is that the NC model provides

generally a good approximation of real population dynamics (as we stressed earlier (Section 3.1) (Domokos & Scheuring 2004)), however the *sturdy* periodic cycles of the DD model will be present in the form of nearly-periodic patterns in populations with low noise levels. The latter is realized either in laboratory experiments or under special circumstances in Nature.

Chapter 4

Summary and outlook

4.1 Competition in aquatic ecosystems

Although the aquatic medium might seem to be an unstructured and homogeneous habitat for the phytoplankton at first sight, actually it is a highly structured and typically inhomogeneous for all of the passively advected species, like phytoplankton. Water, as every real (viscous) fluid shows numerous nontrivial nonlinear phenomena, many of them not entirelly understood (see e.g. Ott 2002).

To describe phytoplankton dynamics in the moving water, we concentrated on the characteristics of mixing and stirring since these processes determine the density distribution of phytoplankton. Since the characteristics of mixing in fluids depend on the control parameters (e.g. Reynolds number, etc.) many different situations can be studied, and since physical circumstances are so diverse in oceans and freshwaters, almost all possible situations must be studied. On the other hand, competitors form complex hierarchical networks in real ecosystems; networks are built up by two elementary structures: transitive hierarchy (e.g. if B beats A and C beats B, then C beats A), and cyclic hierarchy (e.g. B beats A, C beats B, but A beats C).

Thus, we have studied the dynamics of transitive and cyclical hierarchy either in open and closed chaotic flows (with and without coherent structures) or in turbulent flows to map the possible effects of interaction of population and hydrodynamics in competitive situations. Naturally our mapping is not complete, there are biologically interesting situations which are under study or not studied yet (Table 4.1), and there are numerous open biological questions related to the studied cases as well.

As Table 4.1 indicates, the present work has dealt with four different

Table 4.1: Classification of competition studies in moving fluid. Flow is either chaotic or turbulent, open or closed. *) Closed flow seems to be interesting only if there are coherent structures in the flow like in Section 2.2 and partly in Section 2.3. In cases where mixing destroys structures effectively (and thus leads to a well-mixed situation), seems to be not interesting, mainly when competition hierarchy is transitive.

Flow		Competition hierarchy	
		Transitive	*Cyclic*
Chaotic	open	Section 2.1	not studied
	closed	not studied*	Section 2.3
Turbulent	open	under study	not studied
	closed	Section 2.2*	not studied

situations. I summarize our main results following their order of presentation:

1. Section 2.1: Motivated by the numerical simulations we derived a mathematical description for passively advected competing species living in open chaotic flow. We have given the probabilities of species to be on the boundary of filaments on a general functional form (see 2.19). We have shown that competitors remain in coexistence if these probabilities increase in a sublinear manner with the ratio of partial stripe widths ($\alpha < 1$). I note here that this nontrivial exponent means a special *advantage of rarity* principle similar to the parabolic replication present at non-enzymatic replication of macromolecules (Sievers & von Kiedrowski 1994; Szathmáry & Gladkih 1989). This result is confirmed by our numerical simulations. We studied competition of two species in detail, but our study can be extended to more complex networks of competing species.

2. Section 2.2: We have shown that coherent structures in mesoscale turbulence increase the time of exclusion for competing phytoplankton species with order of magnitudes. Thus, the typical timescale of complete exclusion of competitively inferior species is longer than the period of the vegetation cycle. Consequently, this inhomogeneous mixing can have a keystone effect on maintaining species diversity.

3. Section 2.3: We have shown that chaotic mixing leads to coherent oscillations in communities with cyclical competition hierarchy. In cases when mixing is non-uniform, that is large coherent structures are present, competitors remain in coexistence even at intense mixing

rate. We have found that non-uniform mixing can maintain metastable coexistence of killer and sensitive strains for a very long time.

Table 4.1 informs us about the possible future directions in this field. I already mentioned that the inertia of particles was neglected in the presented works. It has, however, been considered recently, where we show numerically that taking inertia into account increases the parameter ranges where species can coexist in the von Kármán vortex street. If inertia is considered in open chaotic flow, then different species with different size and inertia accumulate along slightly different unstable manifolds. Thus, this physical separation leads to decreased competition among different species. Consequently, the inertia might positively effect the coexistence of phytoplankton in other types of flows. While mixing in labs are typically closed, the problem of cyclic competition hierarchy in open chaotic flows can be interesting in natural ecosystems where circulation time is longer than a year. So, it would be important to repeat these studies in open chaotic flows as well.

It is known that if the Reynolds number is greater than about 400, then the flow becomes turbulent in the wake of the cylinder in the von Kármán vortex street. Turbulent flow could be studied in a simple way by adding some chaotic noise term to the periodic velocity field present in chaotic flow. Although this model does not consider the vortex hierarchy present in every exposed turbulent flow, this is a reasonable model of weak turbulence (Zakharov et al. 1992). We are working on this project as well (see Table 4.1).

Finally, I mention that the "paradox of enrichment", that is the decreasing dynamical stability of predator-prey systems with increasing carrying capacity of prey (Gurney & Nisbet 1998) in model ecosystems can shed new light upon the problem of considering the predator (zooplankton) and prey (phytoplankton) living in open chaotic flows. Since zooplankton and phytoplankton are different in size, they move on different fractal sets in open chaotic flows, so they can interact only along the intersections of these fractal sets. Thus, it seems to be probable that mainly the geometry of phase space, and not the food availability for prey, determines the dynamics. This and similar problems are challenges for future research.

4.2 Populations and discrete state dynamics

Since populations are generally composed of discrete entities (individuals), population dynamics is a field of science where discrete-state dynamical models are extremely adequate. However, because of tradition and comfort, an-

alytical models are generally considered as continuous state dynamical systems. Naturally, discrete-state models are also being used for describing population dynamics. These are the so-called stochastic models and cellular automata (see e.g. Gurney & Nisbet 1998). Stochastic models concentrate on the discreteness and randomness of the processes and are (in theory) capable of estimating not only the dynamics of mean values but also computing higher moments of distributions and extinction probabilities. The problem with stochastic models is that they become intractably complex even in the simplest cases.

Besides stochasticity and discreteness, cellular automata take the topological relations into account as well. Th latter has an outstanding importance for example, in cases when individuals disperse slowly and interact only with their neighbors. (I note here that all of the numerical works presented in Chapter 2. are special cellular automata.) While cellular automata describe the elementary interactions among the individuals, very often it is impossible to derive the dynamics of the population from this elementary microdynamics. There are only approximations (mean field, pair correlation etc.) which generally reproduce the dynamics simulated in cellular automata rather weakly (see e.g. Czárán 1997). Since differential and difference equations are more tractable than the above mentioned discrete state models, they have a dominating role in the ecological literature. Adding stochastic terms to the deterministic equations, considering spatial relations by partial differential equations or by coupled map lattices make these analytical models able to handle those characteristics which are inherently studied by stochastic or cellular automata models. (Naturally, these models are less tractable than the non-spatial deterministic ones, like ordinary differential equations for example.)

Discreteness is the only characteristic which is generally neglected in these analytical models. Chapter 3. concentrated on this issue in our present work. We studied noisy maps (difference equation systems perturbed with stochastic terms) and were interested in the general difference between the statistical behavior of discrete and continuous state models as a function of the noise level. We studied these phenomena for maps with various dynamic behaviour. With the help of our new statistical methods and our new findings on the dynamics of discrete-state maps we re-analyzed the *Tribolium castaneum* data series. Our most important results are the following:

1. Section 3.1: The noisy discrete-state (ND) and noisy continuous-state models (NC) are statistically very similar if the deterministic skeleton of the continuous model (DC) behaves regularly. Consequently, neglecting discretization does not result in a meaningful error. However, if the DC

model is chaotic then three zones can be identified as the noise level is varied: if the noise is weak (clear zone) then NC and ND models behave differently, i.e. the distance between them is large. By increasing the noise level, the distance between NC and ND tends to decrease radically in a certain interval of the noise. This is the so-called grey zone where cycles, which are present in the discrete model, disappear continuously as the noise increases. At high noise level (beyond the grey zone), noise dominates the dynamics (noisy zone), thus the two models behave in a practically identical manner (see Fig. 3.3). Using this method for the LPA model at parameters estimated from a chaotic data series of *Tribolium castaneum* (Henson et al. 2001), we pointed out that this lab population is on the border of grey and noisy zones (see Fig. 3.4). Consequently, only very accurate methods could extract the cycles from these data series. Section 3.2 focuses on this task.

2. Section 3.2: We pointed out that concerning the structural stability of discrete state maps (perturbation in the control parameters and in discretization methods) we can distinguish between sturdy and fragile cycles. (Sturdy ones are robust against these perturbations while fragile ones are not.) We determined the qualitatively different sturdy and fragile cycles appearing in the discretized LPA model at the parameter set which fits the experiment. We introduced a new statistical method to detect cycles in noisy discrete-state maps. With the help of this method, we have shown that only the sturdy cycles are present significantly in the *Tribolium castaneum* data series. So, based on a cycles' structural stability one can predict its stability against noise.

An important open question is to identify the characteristics of a cycle which determine its "sturdyness" in a discrete-state map. According to our preliminary work (in cooperation with Gábor Domokos), the answer is not simple. However, it seems to be clear that those cycles which contain at least one point on the map where the derivative of the corresponding continuous-state map is close to zero, are sturdy. (This result is not completely surprising since the Lyapunov exponent is $-\infty$ of those cycles that contain at least one point where the derivative of the continuous-state map is zero, so these cycles are extremally stable, named superstable.) However, the stability of other sturdy cycles cannot be explained in this way.

Ecological systems are inherently noisy. Mainly because of this noisiness and lack of reliable, long data series, it is a really hard task to identify chaotic behavior in field data, that is to decide whether the deterministic skeleton of the noisy dynamics is chaotic, or not (Ellner & Turchin 1995; Ellner et al. 1998; Dennis et al. 2003; Ellner & Turchin 2005). I emphasize

here, however, that because of the skeleton is a discrete state dynamical system (although this fact is generally neglected) factors other than noise cannot induce chaos in real populations. As we have shown above, the interaction of discrete state skeleton and the noise can create unexpected dynamical behavior. Consequently I suspect that further studies may reveal a rich variety of peculiar dynamics of populations as a consequence of interaction of noise and the discrete state skeleton dynamics.

Acknowledgemets

First of all I thank my colleagues Annalisa Bracco, Gábor Domokos, György Károlyi, Áron Péntek, Antonello Provenzale, Zoltán Toroczkai and Tamás Tél for the cooperation. Thanks to late Pál Juhász-Nagy, Eörs Szathmáry and Tamás Tél from whom I learnt the much as scientist. Special thanks are due to my family and all of my collaborators at the Department of Plant Taxonomy and Ecology to keep ideal circumstances for the creative work. The author was supported by grants OTKA T047233, T049692 and holds the Széchenyi István Research Grant of the Hungarian Academy of Sciences.

Appendix A. Coexistence analysis of competing species: fixed points and their stabilities

It is simple and instructive to study the time-continuous dynamics of the widths ε_i, $i = 1, 2$ in and around steady states. Assuming, as before, $c =$ const., we find from (2.28)

$$\lambda\varepsilon_i^* = cv_i p_i \left(\varepsilon_1^*/\varepsilon_2^*\right). \tag{4.1}$$

The weighted sum of the fixed points widths (4.1) gives

$$\varepsilon_1^* v_2 + \varepsilon_2^* v_1 = \frac{cv_1 v_2}{\lambda}. \tag{4.2}$$

For the stability analysis we shall use the explicit form (2.19) for the function g. Thus (4.1) translates into:

$$\lambda\varepsilon_1^* = cv_1 \frac{\varepsilon_1^{*\alpha}}{\varepsilon_1^{*\alpha} + \omega\varepsilon_2^{*\alpha}} \tag{4.3}$$

$$\lambda\varepsilon_2^* = cv_2 \frac{\omega\varepsilon_2^{*\alpha}}{\varepsilon_1^{*\alpha} + \omega\varepsilon_2^{*\alpha}} \tag{4.4}$$

Formula (4.2) shows that one species always survives. Without loss of generality, we can choose this to be species B_2, and everything remains valid with the indices 1 and 2 switched. It is worth defining:

$$z^* \equiv \varepsilon_1^*/\varepsilon_2^*. \tag{4.5}$$

Since ε_2^* is not zero, the ratio of the fixed point equations (4.3,4.4) yields:

$$z^{*1-\alpha} = \frac{v_1}{v_2\omega} \quad \text{or} \quad z^* = 0 \tag{4.6}$$

The first equality describes the $z^* \neq 0$ *coexistence* fixed point while the second describes the *non-coexistence* fixed point.

Equations (2.28) of the continuous case written out explicitly are as follows:

$$\frac{d\varepsilon_1}{dt} = -\lambda\varepsilon_1 + cv_1\frac{\varepsilon_1^\alpha}{\varepsilon_1^\alpha + \omega\varepsilon_2^\alpha} \tag{4.7}$$

$$\frac{d\varepsilon_2}{dt} = -\lambda\varepsilon_2 + cv_2\frac{\omega\varepsilon_2^\alpha}{\varepsilon_1^\alpha + \omega\varepsilon_2^\alpha} \tag{4.8}$$

The linear stability of a fixed point ($\varepsilon_1^* > 0, \varepsilon_2^* > 0$) will be given by the eigenvalues of the stability matrix $\mathbf{E}$, calculated from (4.7-4.8) as follows (here we also used (4.3-4.4):

$$\mathbf{E} = \lambda \begin{pmatrix} -1 + \frac{\alpha\lambda}{cv_2}\varepsilon_2^* & -\frac{\alpha\lambda}{cv_2}\varepsilon_1^* \\ -\frac{\alpha\lambda}{cv_1}\varepsilon_2^* & -1 + \frac{\alpha\lambda}{cv_1}\varepsilon_1^* \end{pmatrix}$$

The eigenvalues of $\mathbf{E}$ are easily calculated:

$$\Lambda_+ = -\lambda(1-\alpha), \quad \Lambda_- = -\lambda. \tag{4.9}$$

One eigenvalue of the width dynamics is always the negative of the chaotic advection's positive Lyapunov exponent. As long as the parameter α is less than unity, the other eigenvalue is also negative.

We find that for $0 < \alpha < 1$ *coexistence is stable*, for $\alpha > 1$ it becomes unstable, that is one of the species dies out depending on the initial values.

The case $\alpha = 1$ is special. It follows from (4.6) that for $\alpha = 1$, and $\omega \neq v_1/v_2$, the non-coexistence point is the only fixed point, and it is stable. (If $\omega > v_1/v_2$ then $(\varepsilon_1^* > 0, \varepsilon_2^* = 0)$ is stable, if $\omega < v_1/v_2$ then $(\varepsilon_1^* = 0, \varepsilon_2^* > 0)$ is stable fixed point.) Having $\alpha = 1$ with $\omega = v_1/v_2$ implies that all points fulfilling (4.2) are fixed points of marginal stability. Thus, stable coexistence is found in the

$$0 < \alpha < 1 \tag{4.10}$$

regime.

The stability conditions are the same for discrete-time dynamics, as well.

Appendix B. Numerical determination of the probability p_1

We observe that by dividing the rearranged (2.26) for $i = 1$ by that with $i = 2$, one obtains

$$\frac{\sigma_1 p_1^{(n)}}{\sigma_2 p_2^{(n)}} = M^{(n)}, \tag{4.11}$$

where

$$M^{(n)} = \frac{e^{\lambda} N_1^{(n+1)} [N^{(n+1)}]^{\beta} - N_1^{(n)} [N^{(n)}]^{\beta}}{e^{\lambda} N_2^{(n+1)} [N^{(n+1)}]^{\beta} - N_2^{(n)} [N^{(n)}]^{\beta}}. \tag{4.12}$$

From this, $p_1 = 1 - p_2$ is easily found as

$$p_1^{(n)} = \frac{M^{(n)}}{M^{(n)} + \frac{\sigma_1}{\sigma_2}}, \tag{4.13}$$

This relation provides us with a method for measuring how the probability $p_1(z) \equiv g(z)$ depends on the ratio $z \equiv N_1/N_2$ at any instant of time. We use this observation to extract the form of the g function from numerical results.

In fixed points $N_i^{(n+1)} = N_i^{(n)} = N_i^*$, the fixed point value of $M^{(n)}$ is $M^* = N_1^*/N_2^* \equiv z^*$. From (4.13) it follows that

$$g(z^*) = \frac{z^*}{z^* + \frac{\sigma_1}{\sigma_2}} \equiv h(z^*), \tag{4.14}$$

This implies that the fixed point z^* must be the common point of the graphs of $g(z)$ and $h(z)$ for any $\alpha \neq 1$, where $h(z)$ happens to be the function g belonging to $\alpha = 1$ and $\omega = \sigma_1/\sigma_2$.

Appendix C. The stability of fixed points in the killer-resistant-sensitive system

We determine the local asymptotic stability of fixed points of system 2.46. The Jacobian matrix of system 2.46 is the following:

$$\begin{pmatrix} e^* - f^* - \delta_K & -f_K^* & -f_S^* \\ -f_R^* & e^* - f_R^* - \delta_R & -f_R^* \\ -f_S^*(1+\tau) & -f_S^* & e^* - \tau f_K^* - f_S^* - \delta_{S_0} \end{pmatrix},$$

where f_K^*, f_R^*, and f_S^* denote the frequencies of killer, resistant and sensitive strains, $e^* = 1 - f_K^* - f_R^* - f_S^*$ means the fraction of empty sites in the fixed points. Eigenvalues λ_1, λ_2 and λ_3 of the Jacobian can be calculated in the nontrivial fixed points:

1. If $f_K^* = f_R^* = 0$, $f_S^* = 1 - \delta_S^0$, then $\lambda_1 = \delta_{S_0} - \delta_K$, $\lambda_2 = \delta_{S_0} - \delta_K - \delta_R$, $\delta_3 = \delta_{S_0} - 1$. Since $1 > \delta_K > \delta_R > \delta_{S_0}$ all eigenvalues are negative, thus the fixed point is stable.

2. If $f_K = f_S = 0$, $f_R = 1 - \delta_R$, then $\lambda_1 = \delta_R - \delta_K < 0$, $\lambda_2 = \delta_R - 1 < 0$ and $\lambda_3 = \delta_R - \delta_{S_0} > 0$. Since δ_3 is positive, the fixed point is locally asymptotically unstable.

3. If $f_R = f_S = 0$, $f_K = 1 - \delta_K$, then $\lambda_1 = \delta_K - 1 < 0$, $\lambda_2 = \delta_K - \delta_R > 0$ and $\lambda_3 = \delta_K - \delta_{S_0} - \tau(1 - \delta_K)$. Again we have a positive eigenvalue, thus the fixed point is unstable.

4. If $f_R = 0$, $f_K = (\delta_K - \delta_S^0)/\tau$, $f_S = (1 - \delta_K - (\delta_K - \delta_S^0)/\tau)$, then $\lambda_1 = \delta_K - \delta_R > 0$,$\lambda_{2,3} = \frac{A \pm \sqrt{A^2 - 4(1+\tau)B^2}}{2}$, where $A = \delta_K - 1$, $B = \delta_K + \frac{\delta_K - \delta_{S_0}}{\tau} - 1$. While it is easy to show that $Re\{\lambda_{2,3}\} < 0$, this fixed point is unstable because $\lambda_1 > 0$.

Bibliography

[Abraham 1998] Abraham, E.R. 1998. The generation of plankton patchiness by turbulent stirring. *Nature* **391**, 577–580.

[Adams et al. 1979] Adams, J., Kinney, T. Thompson, S., Rubin, L. & Helling, R. B. 1979. Frequency-dependent selection for plasmid-containing cells of *Escherichia coli*. *Genetics* **91**, 627–637.

[Aref 1994] Aref, H. (Ed.) 1994. Special issue on Chaotic Advection. *Chaos, Solitons, Fractals* **4**, No. 6.

[Arístegui et al. 1997] Arístegui, J. Tett, P., Hernández-Guerra, A., Basterretxea, G., Montero, M.F., Wild, K., Sangrá, P., Hernández-León, S., Cantón, M., García-Braun, J.A., Pacheco, M. & Barton, E.D. 1997. The influence of island-generated eddies on chlorophyll distribution: A study of mesoscale variation around Gran Canaria. *Deep-See Research I* **44**, 71–96.

[Armstrong & McGehee 1980] Armstrong, R. A. & McGehee, R. 1980. Competitive exclusion *Am. Nat.* **115**, 151-170.

[Arnold 1963] Arnold, V. I. Proof of A. N. Kolmogorov's theorem on the preservation of quasiperiodic motions under small perturbations of the Hamiltonian. *Russian Mathematical Surveys* **18**, 9–36.

[Atkinson & Shorroks 1981] Atkinson, W. D. & Shorroks, B. 1981. Competition on a divided and ephemeral resource: a simulation model. *J. of Animal Ecology* **50**, 461-471.

[Babiano et al. 1987] Babiano, A., Basdevant, C., Legras, B. & Sadourny, R. 1987. Vorticity and passive-scalar dynamics in two-dimensional turbulence *J. Fluid Mech.* **183**, 379-397.

[Bartha et al. 1997] Bartha, S.; Czárán, T. & Scheuring, I. 1997. Spatiotemporal scales of non-equilibrium community dynamics: a methodological challenge. *N. Z. J. of Ecol.* **21**, 199–206.

[Barton et al. 1998] Barton, E. D., Arístegui, J., Tett, P., Cantón, M. García-Braun, J., Hernández-Leon, S., Nykjaer, L., et al. 1998. The transition zone of the Canary Current upwelling region. *Prog. Oceanography* **41**, 455–504.

[Batchelor 1969] Batchelor, G. K. 1969. Computation of the energy spectrum in homogeneous two-dimensional turbulence *Phys. Fluids Suppl.* **12**, II-233-239.

[Becks et al. 2005] Becks, L., Hilker, F. M., Malchow, H., Jürgens & Arndt, H. 2005. Experimental demonstration of chaos in a microbial food web. *Nature* **435**, 1226–1229.

[Bees et al. 1998] Bees, M. A., Mezic, I., & McGlade, J. 1998. *Mathematics and Computers in Simulation* **44**, 527-544.

[Begon et al. 1986] Begon, M., Harper, J. L. & Townsend, C. R. 1986. *Ecology: Individuals, Populations and Communities* Blackwell, Oxford, UK.

[Benczik et al. submitted] Benczik I.J. Károlyi, G., Scheuring, I. & Tél T. Coexistence of inertial competitors in chaotic flows. *Phys. Rev. E* submitted

[Berryman & Milstein 1989] Berryman, A. A. and Milstein, J. A. 1989. Are ecological systems chaotic - and if not why not? *Trends. Evol. Ecol.* **4**, 26–28.

[Birkhoff 1913] Birkhoff, G. D. 1913. Proof of Poincaré's geometric theorem. *Transactions of the American Mathematical Society* **14**, 14–22.

[Boerlijst & Hogeweg 1991] Boerlijst, M.C. & Hogeweg, P. 1991. Spiral wave structures in prebiotic evolution: hypercycles stable against parasites" *Physica D* **48**, 17–28.

[Bracco et al. 2000] Bracco, A., LaCasce, J., Pasquero, C. & Provenzale, A. 2000. The velocity distribution of barotropic turbulence *Phys. Fluids* **12**, 2478–2488.

[Britton 1989] Britton, N. F. 1989. Aggregation and the competitive exclusion principle *J. Theor. Biol.* **136**, 57-66.

[Buss & Jackson 1979] Buss, L.W. & Jackson, J.B.C. 1979. Competitive networks: nontransitive competitive relationships in cryptic coral reef environments. *Am. Nat.* **113**, 223–234.

[Canuto 1987] Canuto, C., Hussaini, M.Y., Quarteroni, A. & Zang, T.A. 1987. *Spectral Methods in Fluid Dynamics,* Berlin: Springer-Verlag.

[Chao & Levin 1981] Chao, L. & Levin, B.R. 1981. Structured habitats and the evolution of anticompetitor toxins in bacteria. *Proc. Natl. Acad. Sci. USA* **78**, 6324–6328.

[Chassignet 1992] Chassignet, E. 1992. Rings in numerical models of ocean general circulation: a statistical study *J. Geophys. Res.* **97 C**, 9479-9492.

[Chater & Losick 1997] Chater, K.F. & Losick, R. 1997. Mycelial life style of *Streptomyces coelicolor* A3(2) and its relatives. In: Shapiro, J.A., Dworkin, M.: *Bacteria as Multicellular Organisms*, pp. 149–182. Oxford UP.

[Chesson 2000] Chesson, P. 2000. Mechanism of maintenance of species diversity. *Annu. Rev. Ecol. Syst.* **31**, 343–366.

[Clodong & Blasius 2004] Clodong, S. & Blasius B. 2004. Chaos in a periodically forced chemostat with algal mortality. *Proc. Roy. Soc. B.* **271**, 1617–1624.

[Cohen 1995] Cohen J. E. 1995. Unexpected dominance of high frequencies in chaotic nonlinear population models. *Nature* **378**, 610-612.

[Collins & Glenn 1997] Collins, S. L. & Glenn, S. M. 1997. Intermediate disturbance and its relationship to within - and between-patch dynamics. *N. Z. J. of Ecol.* **21**, 103–110.

[Connell 1978] Connell, J.H. 1978. Diversity in tropical rain forests and coral reefs. *Science* **199**, 1302–1310.

[Costantino et al. 1997] Costantino, R.F., Desharnais, R.A., Cushing, J.M., Dennis, B. 1997. Chaotic dynamics in an insect population. *Science* **275**, 389–391.

[Cushing et al. 2001] Cushing, J. M., Henson, S. M., Desharnais, R. A., Dennis, B., Costantino, R. F. & King, A. A. 2001. A chaotic attractor in ecology:theory and experimental data. *Chaos, Solitons and Fractals* **12**, 219–234.

[Cushing et al. 2003] Cushing, J.M., Costantino, R.F., Dennis, B., Desharnais, R.A. & Henson, SM. 2003. *Chaos in ecology* Academic press, Amsterdam.

[Czárán 1997] Czárán T. 1997. *Spatiotemporal models of population and community dynamics.* Chapman & Hall, London.

[Czárán & Szathmáry 2000] Czárán, T. & Szathmáry, E. 2000. In: Dieckmann, U.; Law, R. & Metz, J.A.J. (Eds): *The Geometry of Ecological Interactions: Simplifying Spatial Complexity.* Cambridge Univ. Press, Cambridge.

[Czárán & Hoekstra 2003] Czárán, T.L. & Hoekstra, R.F. 2003. Killer-sensitive coexistence in metapopulations of microorganisms. *Proc. Roy. Soc. Ser. B* **270**, 1373–1378.

[Czárán et al. 2002] Czárán, T.L., Hoekstra, R.F. & Pagie L. 2002. Chemical warfare between microbes promotes biodiversity. *Proc. Natl. Acad. Sci. USA* **99**, 786–790.

[Denman & Platt 1976] Denman, K.L., & Platt, T. 1976. The variance spectrum of phytoplankton in the turbulent ocean *J. Mar. Res.* **34**, 593-601.

[Dennis & Taper 1994] Dennis, B. & Taper, M. L. 1994. Density dependence in time series observations of natural populations: estimation and testing. *Ecol. Monogr.* **64**, 205-224.

[Dennis et al. 2001] Dennis, B., Desharnais, R. A., Cushing, J. M., Henson, S. M. & Costantino, R. F. 2001. Estimating chaos and complex dynamics in an insect population. *Ecol. Monogr.* **71**, 277–303.

[Dennis et al. 2003] Dennis, B., Desharnais, R. A., Cushing, J. M., Henson, S. M. & Costantino, R. F. 2003. Can noise induce chaos? *Oikos* **102**, 329–339.

[Dhamala et al. 2000] Dhamala, M.,Lai, Y.-C., Kostelich, E. J. 2000. Detecting unstable periodic orbits from transient chaotic time series. *Phys. Rev. E.* **61**, 6485–6489.

[Domokos 1990] Domokos, G. 1990. Digital modelling of chaotic motion. *Studia Sci. Math. Hung.* **25**, 323–341.

[Domokos 2005] Domokos, G. 2005. Coarse-grained observation of discretized maps. *Int. J. Bifurcation and Chaos* **15**, 861–870.

[Domokos & Scheuring 2002] Domokos, G. & Scheuring, I. 2002. Random perturbation effects in chaotic population dynamics. *Science* **297**, 2163a

[Domokos & Szász 2003] Domokos, G. & Szász, D. 2003. Ulam's scheme revisited: digital modeling of chaotic attractors via micro-perturbations. *Disc. Cont. Dyn. Syst.* **9**, 859–876.

[Domokos & Scheuring 2004] Domokos, G. & Scheuring, I. 2004. Discrete and continuous state population models in a noisy world. *J. of Theor. Biol.* **227**, 535–545.

[Durrett & Levin 1994] Durrett, R. & Levin, S. 1994. The importance of being discrete (and spatial) *Theor. Popul. Biol.* **46**, 363-394.

[Durrett & Levin 1997] Durrett, R. & Levin, S. 1997. Allelopathy in spatially distributed populations. *J. of Theor. Biol.* **185**, 165–171.

[Durrett & Levin 1998] Durrett, R. & Levin, S. 1998. Spatial aspects of interspacific competition. *Theor. Popul. Biol.* **53**, 30–43.

[Eigen 1971] Eigen, M. 1971: Self-organization of matter and the evolution of macro-molecules. *Naturwissenschaften* **58**, 465–523.

[Eigen & Schuster 1979] Eigen, M. & Schuster, P. 1979. *The Hypercycle.* Springer, Berlin.

[Elhmaïdi et al. 1993] Elhmaïdi, D., Provenzale, A. & Babiano, A. 1993. Elementary topology of two-dimensional turbulence from a Lagrangian viewpoint and single-particle dispersion *J. Fluid Mech.* **257**, 533-558.

[Ellner & Turchin 1995] Ellner, S. & Turchin P. 1995. Chaos in a noisy world: new methods and evidence from time series analysis. *Am. Nat.* **145**, 343–375.

[Ellner et al. 1998] Ellner, S. P., Bailey, B. A., Bobashev, A. R., Gallant, B. T., Grenfell, D. W. & Nyschka D. W. 1998. Noise and nonlinearity in measles epidemics: combining mevhanistic and statistical approaches to population modeling. *Am. Nat.* **151**, 426–440.

[Ellner & Turchin 2005] Ellner, S. P. & Turchin P. 2005. When can noise induce chaos and why does it matter: a critique *Oikos* **111**, 620–631.

[Elton & Nicholson 1942] Elton, C. S., and Nicholson, M. 1942. The ten-year cycle of lynx in Canada. *J. Anim Ecol* **11,** 215–244

[Epstein 1995] Epstein, I. R. 1995. The consequence of imperfect mixing in autocatalytic chemical and biological systems. *Nature* **374**, 321–327.

[Feldgarden & Riley 1999] Feldgarden, M. & Riley, M.A. 1999. The phenotypic and fitness effects of colicin resistance in *Escherichia coli* K-12. *Evolution* **53**, 1019–1027.

[Flierl & Davis 1993] Flierl, G. F. & Davis, C. S. 1993. Biological effects of Gulf Stream meandering *J. Mar. Res.* **51**, 529-560.

[Frean & Abraham 2001] Frean, M. & Abraham, E.R. 2001. Rock-scissors-paper and the survival of the weakest. *Proc. Roy. Soc. Lond. B* **268**, 1323–1327.

[Fussmann et al. 2000] Fussmann, G. F., Ellner, S. P., Shertzer, K. W. and Hairston, N. G. 2000. Crossing the Hopf bifurcation in a live predator-prey system. *Science* **290**, 1358–1360.

[Gaedeke & Sommer 1986] Gaedeke, U. & Sommer, U. 1986. The influence of the frequency of periodic disturbances on the maintenance of phytoplankton diversity. *Oecologia* **71**, 98–102.

[Gause & Witt 1935] Gause, G.F. & Witt, A.A. 1935. Behavior of mixed populations and the problem of natural selections. *Am. Nat.* **69**, 596–609.

[Giona et al. 1999] Giona, M., Adrover, A., Muzzio, F.J., Cerbelli, S. & Alvarez, M.M. 1999. The geometry of mixing in time-periodic chaotic flows. *Physica D* **132**, 298–324.

[Godfray & Grenfell 1993] Godfray, H. C. J. & Grenfell, B. T. 1993. The continuing quest for chaos. *TREE* **8**, 43-44.

[Greenman & Benton 2004] Greenman, J. V. & Benton, T. G. 2004. Large amplification in stage-structured models: Arnol'd tongues revisited. *Math. Biol.* **48**, 647–671

[Griffa 1996] Griffa, A. 1996. Applications of stochastic particle models to oceanographic problems In *Stochastic Modelling in Physical Oceanography*, R.J. Adler, P. Muller and R.B. Rozovskii eds., Birkhauser, Boston.

[Gurney & Nisbet 1998] Gurney, W.S.C. & Nisbet, R.M. 1998. *Ecological Dynamics*. Oxford Univ. Press, Oxford.

[Hallegraeff 1993] Hallegraeff, G. M. 1993. A review of harmful algae blooms and the apparent global increase. *Phycologia* **32**, 79–99.

[Han et al. 1998] Han, J., Gong, W. & Yin, Y. 1998. Mining segment-wise periodic patterns in time-related database. In: *Int. Conf. on Knowledge Discovery and Data Mining* AAAI Press, Menlo Park. p. 214–218

[Han et al. 1999] Han, J., Dong, G. & Yin, Y. 1999. Efficient mining of partially periodic patterns in time series database. In *Int. Conf. Data Engineering* 106–115.

[Hardin 1960] Hardin, G. 1960. The competitive exclusion principle. *Science* **131**, 1292–1298.

[Hassel et al. 1994] Hassell, M. P., Comins, H. N. & May, R. M. 1994. Species coexistence and self-organizing spatial dynamics *Nature* **370**, 290–292.

[Hastings & Powell 1991] Hastings, A. & Powell, T. 1991. Chaos in three-species food chain. *Ecology* **72,** 896–903

[Hastings 2004] Hastings, A. 2004. Transients: the key to long-term ecological understanding? *Trends. Ecol. Evol.* **19**, 39–45.

[Henson et al. 2001] Henson, S. H., Costantino, R. F.,Cushing, J. M.,Deshernais R. A.,Dennis, B. & King, A. A. 2001. Lattice effect observed in chaotic dynamics of experimental populations. *Science* **294**, 602–605.

[Henson et al. 2003] Henson, S. H., King, A. A., Costantino, R. F., Cushing, J. M., Dennis, B. & Deshernais R. A. 2003. Explaining and predicting patterns in stochastic population systems. *Proc. Roy. Soc. Ser. B.* **270**, 1549–1553.

[Hernández-Garcia & López 2004] Hernández-Garcia, E & López, C. 2004. Clustering, advection and patterns in model of population dynamics with neighborhood-dependent rates. *Phys. Rev. E*, **70**, 016216(1-11).

[Hofbauer & Sigmund 1998] Hofbauer, J. & Sigmund, K. 1998. *Evolutionary games and replicator dynamics.* Cambridge University Press.

[Holm 1992] Holm, N.G. 1992. Marine hydrothermal systems and the origin of life. *Origins Life Evol. Biosphere* **22**, 5.

[Hsu et al. 1988] Hsu, G.H.; Ott, E & Grebogi, C. 1988. *Phys. Lett. A* **127**, 199.

[Husman & Weissing 1999] Huisman, J. & Weissing, F. J. 1999 Biodiversity of plankton by species oscillations and chaos *Nature* **402**, 407-410.

[Huisman et al. 1999] Huisman, J., van Oostveen, P. & Weissing, F. J. 1999. Species dynamics in phytoplankton blooms: Incomplete mixing and competition for light *Am. Nat.* **154**, 46-68.

[Huisman et al. 2001] Huisman, J., Johansson, A.M., Folmer, E.O. & Weissing, F.J. 2001. Toward a solution of the plankton paradox: the importance of physiology and life history. *Ecology Letters* **4**, 408–411.

[Huisman & Weissing 2001b] Huisman, J. & Weissing, F.J. 2001. Fundamental unpredictability in multispecies competition. *Am. Nat.* **157**, 488–494.

[Hulot & Huisman 2004] Hulot, F. D. & Huisman, J. 2004. Allelopathic interactions between phytoplankton species: The roles of heterotrophic bacteria and mixing intensity. *Limnol. Oceanogr.* **49**, 1424–1434.

[Huston 1979] Huston, M.A. 1979. General hypothesis of species diversity. *Am. Nat.* **113**, 81–101.

[Hutchinson 1961] Hutchinson, G.E. 1961. The paradox of plankton. *Am. Nat.* **95**, 137–147.

[Ives & May 1985] Ives, A. R. & May, R. M. 1985. Competition within and between species in a patchy environments: relations between microscopic and macroscopic models *J. Theor. Biol.* **115**, 65-92.

[Iwasa et al. 1998] Iwasa, Y., Nakamaru, M. & Levin, S. A. 1998. Allelopathy of bacteria in a lattice population: competition between colicin-sensitive and colicin-producing starins. *Evol. Ecol.* **12**, 785–802.

[Jacobs et al. 1997] Jacobs, J., Ott, E., Antonsen, T., & Yorke, J. A. 1997.Modeling fractal entrainment sets of tracers advected by chaotic temporally irregular fluid flows using random maps *Physica D* **110**, 1-17.

[Jana et al. 1994] Jana, S. C.; Metcalfe, G. & Ottino, J. M. 1994. Experimental and computational studies of mixing in complex Stokes flows: the vortex mixing flow and multicellular cavity flows. *J. Fluid Mech.* **269**, 199–246.

[Jung & Ziemniak 1992] Jung, C. & Ziemniak, E. 1992. Hamiltonian scattering chaos in a hydrodynamical system. *J. Phys. A* **25**, 3929–3943.

[Jung et al. 1993] Jung, C., Tél, T. & Ziemniak, E. 1993. Application of scattering chaos to particle transport in a hydrodynamical flow. *Chaos* **3**, 555-568.

[Kantz & Grassberger 1985] Kantz, H. & Grassberger, P. 1985. Repellers, semi-attractors, and long-lived chaotic transients. *Physica D* **17**, 75.

[Károlyi & Tél 1997] Károlyi, G. & Tél, T. 1997. Chaotic tracer scattering and fractal basin boundaries in a blinking vortex-sink system. *Physics Reports* **290**, 125–147.

[Károlyi et al. 1999] Károlyi, G.; Péntek, Á.; Toroczkai, Z.; Tél, T. & Grebogi, C. 1999. Chemical or biological activity in open chaotic flows. *Phys. Rev. E* **59**, 5468–5481.

[Károlyi et al. 2000] Károlyi, Gy., Péntek, Á., Scheuring, I., Tél, T. & Toroczkai, Z. 2000. Open chaotic flow: the physics of species coexistence. *Proc. Natl. Acad. Sci. USA* **97**, 13661–13665.

[Károlyi et al. 2002] Károlyi, Gy,; Scheuring, I. & Czárán, T. 2002. Metabolic network dynamics in open chaotic flow. *Chaos* **12**, 460–469.

[Kerr et al. 2002] Kerr, B., Riley, M.A., Feldman, M.W. & Bohannan, B.J.M. 2002. Local dispersal promotes biodiversity in real-life game of rock-paper-scissors. *Nature* **418**, 171–174.

[Kifer 1997] Kifer, Y. 1997. Computations in dynamical systems via random perturbations. *Disc. Cont. Dyn. Syst.* **3**, 457–476.

[King & Schaffer 1999] King, A. A. & Schaffer W. M. 1999. The rainbow bridge: Hamiltonian limits and resonance in predator prey dynamics. *J. Math, Biol.* **39**, 439–469.

[King et al. 2002] King, A. A., Deshernais, R. A.,Henson, S. M., Costantino, R. F.,Cushing, J. M. & Dennis, B. 2002. Random perturbation effects in chaotic population dynamics, response *Science* **297**, 2163b

[King et al. 2004] King, A. A., Costantino, R. F., Cushing, J. M., Henson, S. M., Deshernais, R. A. & Dennis, B. 2004. Anatomy of a chaotic attractor: Subtle model-predicted patterns revealed in population data. *Proc. Natl. Acad. Sci.* **101**, 408–413.

[Kirkup & Riley 2004] Kirkup, B.C, & Riley, M A. 2004. Antibiotic-mediated antagonism leads to a bacterial game of rock-paper-scissors in vivo. *Nature* **428**, 412–414.

[Koi & Boer 2003] Koi, B. W. & Boer, M. P. 2003. Chaotic behaviour of a predator-prey system in the chemostat. *Dynam. Contin. Discr. Imp. Syst. B.* **10**, 259–272.

[Kolmogorov 1957] Kolmogorov A.N. 1954. Théorie générale des systémes dynamiques et mécanique classique. In *Proceedings of the International Congress of Mathematicians*, Amsterdam vol1. pp. 315-333. North-Holland Publishing Co., Amsterdam.

[Korn & Korn 1968] Korn, G. A. & Korn, T. M. 1968. *Mathematical handbook for scientists and engineers* McGraw-Hill, New York

[Kraichnan 1967] Kraichnan, R. H. 1967. Inertial ranges in two-dimensional turbulence *Phys. Fluids* **10**, 1417-1423.

[Lamb 1932] Lamb, H. 1932. *Hydrodynamics*. Cambridge University Press, Cambridge.

[Lanford 1998] Lanford, O.E. 1998. Informal remarks on the orbit structure of discrete approximations to chaotic maps. *Experimental Mathematics* **7**, 317–324

[Lathrop & Kostelich 1989] Lathrop, D. P. & Kostelich, E. J. 1989. Characterization of an experimental strange attractor by periodic orbits. *Phys. Rev. A.* **40**, 4028–4031.

[Levins 1979] Levins, R. 1979. Coexistence in a variable environment *Am. Nat.* **114**, 765-783.

[Levy 1937] Levy, P. 1937. *Theorie de l'addition des variables aleatores*. Gauthiere-Villars, Paris.

[Li & Yorke 1975] Li, T.Y. & Yorke, J. A. 1975. Period three implies chaos *Amer. Math. Monthly* **82**, 985–992

[Liverani 2001] Liverani, C. 2001. Rigorous numerical investigations of the statistical properties of piecewise expanding maps. *Nonlinearity* **14**, 463–490.

[López et al. 2001] López, C., Neufeld, Z., Hernández-Garcia, E., & Haynes, P. 2001. Chaotic advection of reacting substances: plankton dynamics on a meandering jet. *Physics and Chemistry of the Earth B* **26**, 313–317

[Lotka 1925] Lotka, A. J. 1925. *Elements of physical biology* Baltimore: Williams and Wilkins.

[Lorenz 1963] Lorenz, E. 1963. Deterministic nonperiodic flow *J. of Atmospheric Sciences* **20**, 130-—141.

[Luckinbill 1973] Luckinbill, L. S. 1973. Coexistance in laboratory populations of *Paramecium aurelia* and its predator *Didinium nasutum*. *Ecology* **54**, 1320-

[Ma & Hellerstein 2001] Ma, S. & Hellerstein, J. L. 2001. Mining partially periodic event pattern with unknown periods. *Proc. Int Conf. on Data Eng.* , 205–214.

[Manly 1991] Manly, B. F. J. 1991. *Randomization and monte carlo methods in biology* Chapman and Hall, London, New York, Tokyo.

[May 1976] May, R. M. 1976. Simple mathematical models with very complicated dynamics. *Nature* **261**, 459–467.

[Maynard Smith 1983] Maynard Smith, J. 1983. Models of evolution. *Proc. Roy. Soc. London B* **219**, 315–325.

[Maynard Smith & Szathmáry 1995] Maynard Smith, J. & Szathmáry, E. 1995: *The major transitions in evolution*. Freeman, Spektrum, Oxford.

[McCann et al. 1998] McCann, K., Hastings, A & Huxel, G. R. 1998. Weak trophic interactions and the balance of nature. *Nature* **395**, 794–798.

[McWilliams 1984] McWilliams, J. C. 1984. The emergence of isolated coherent vortices in turbulent flow *J. Fluid Mech.* **146**, 21-43.

[McWilliams 1990] McWilliams, J. C. 1990. The vortices in two-dimensional turbulence *J. Fluid Mech.* **219**, 361-385.

[Morales 1999] Morales, J. M. 1999. Viability in a pink environment: why "white noise" models can be dangerous. *Ecol. Lett.* **2**, 228-232.

[Moser 1962] Moser, J.K. 1962. On invariant curves of area-preserving mappings of an annulus. *Nachr. Acad. Wiss. Göttingen 11, Math. Phys. Kl.* 1-20.

[Muratori & Rinaldi 1989] Muratori, S. & Rinaldi, S. 1989. Remarks on competitive coexistence *SIAM J. Appl. Math.* **49**, 1462-1472.

[Nakamaru & Iwasa 2000] Nakamaru, M. & Iwasa, Y. 2000. Competition by allelopathy proceeds in travelling waves: colicin-immune strain aids colicin-sensitive strain. *Theor. Pop. Biol.* **57**, 131–144.

[Neufeld & Tél 1998] Neufeld, Z., & Tél, T. 1998. Advection in chaotically time-dependent open flows *Phys. Rev. E* **57**, 2832-42.

[Neufeld et al. 2003] Neufeld, Z., Kiss, I.Z., Zhou, C.S., Kurths, J. 2003. Synchronization and oscillator death in oscillatory media with stirring. *Phys. Rev. Lett.* **91**, 084101.

[Okubo 1980] Okubo, A. 1980. *Biomathematics* Vol. **10** *Diffusion and Ecological Problems: Mathematical Models* Springer, Berlin.

[Ott 2002] Ott, E. 2002. *Chaos in dynamical systems* Cambridge Univ. Press, Cambridge

[Ottino et al. 1988] Ottino, J.M., Leong, C.W., Rising, H., Swanson, P.D. 1988. Morphological structures produced by mixing in chaotic flows. *Nature* **333**, 419–425.

[Ottino 1989] Ottino, J. M. 1989. *The kinematics of mixing: stretching, chaos and transport*. Cambridge University Press, Cambridge.

[Ozden et al. 1998] Ozden, B., Ramaswamy, S. & Silberschatz, A. 1998. Cyclic assotiation rules. In. *Int. Conf. Data Engineering* 412–421.

[Pedlosky 1987] Pedlosky, J. 1987. *Geophysical Fluid Dynamics* New York, Springer-Verlag.

[Philips 1973] Phillips, O. M. 1973. The equilibrium and stability of simple marine biological systems. I. Primary nutrient consumers *Am. Nat.* **107**, 73-93.

[Powell & Richerson 1985] Powell, T. & Richerson, P. J. 1985. Temporal variation, spatial heterogeneity, and competition for resources in plankton systems: a theoretical model *Am. Nat.* **125**, 431–464.

[Provenzale 1999] Provenzale, A. 1999. Transport by coherent barotropic vortices *Ann. Rev. Fluid Mech.* **31**, 55-93.

[Paine 1984] Paine, R.T. 1984. Ecological determinism in competition for space. *Ecology* **65**, 1339–1348.

[Paiva et al. 1999] Paiva, A., Hargrove, J., Chassignet, E. & Bleck, R. 1999. Turbulent behavior of the fine-mesh (1/12 degree) numerical simulation of the North Atlantic *J. Mar. Syst.* **21**, 307–320.

[Paquin & Adams 1983] Paquin, C.E. & Adams, J. 1983. Relative fitness can decrease in evolving asexual populations of *S. cerevisiae*. *Nature* **306**, 368–371.

[Pasquero et al. 2000] Pasquero, C., Provenzale, A. & Babiano, A. 2000. Parameterization of dispersion in two-dimensional turbulence. *Journal of Fluid Mechanics* **439,** 279–303.

[Péntek et al. 1995] Péntek, Á.; Toroczkai, Z.; Tél, T.; Grebogi, C. & Yorke, J. A. 1995. Fractal boundaries in open hydrodynamical flows: Signatures of chaotic saddles. *Phys. Rev. E* **51**, 4076–4088.

[Péntek et al. 1996] Péntek, Á.; Tél, T. & Toroczkai, Z. 1996. Transient chaotic mixing in open hydrodynamical flows. *Int. J. Chaos and Bifurcations* **6**, 2619–2625.

[Pierrehumbert 2000] Pierrehumbert, R.T. 2000. Lattice models of advection-diffusion. *Chaos* **10**, 61–74.

[Poincaré 1894] Poincaré, H. 1894. *Les methods nouwelles de la mécanique celeste I-III* Gauthier-Villars, Paris.

[Poole et al. 1999] Poole, A.; Jeffares, D. & Penny, D. 1999. Early evolution: prokaryotes, the new kids on the block. *BioEssays* **21**, 880–889.

[Putnam & Tang 1986] Putnam, A.R. & Tang, C.S. 1986. *The science of allelopathy.* Wiley, New York.

[Rao 1973] Rao, C. R. 1973. *Linear statistical inference and its applications.* John Wiley & Sons, New York, New York, USA.

[Renshaw 1991] Renshaw, E. 1991. *Modelling biological populations in space and time.* Cambridge, Cambridge Universiy Press.

[Reynolds 1986] Reynolds, C. S. 1986. Experimental manipulations of phytoplankton periodicity in large, limnetic enclosures in Blelham Tarm, English Lake District. *Hydrobiologia* **138**, 43-64.

[Reynolds 1993] Reynolds, C.S. 1993. Scales of disturbance and their role in plankton ecology. *Hydrobiologia* **249**, 157–171.

[Reynolds 1998] Reynolds, C.S. 1998. The state of freshwater ecology. *Freshwater Biology* **39**, 741–753.

[Ricker 1954] Ricker, W. E. 1954. Stock and recruitment. *J. Fish. Res. Board Can.* **11**, 559-663.

[Riley & Gordon 1992] Riley, M.A. & Gordon, D.M. 1992. A survey of Col plasmids in natural isolates of *Escherichia coli* and an investigation into the stability of Col-plasmid lineages. *J. Gen. Microbiol.* **138**, 1345–1352.

[Riley & Gordon 1999] Riley, M.A. & Gordon, D.M. 1999. The ecological role of bacteriocins in bacterial competition. *Trends Microbiol.* **7**, 129–133.

[Richerson et al. 1970] Richerson, P. J., Armstrong, R. & Goldman, C. R. 1970. Contemporaneous disequilibrium: a new hypothesis to explain the paradox of the plankton *Proc. Natl. Acad. Sci. USA* **67**, 1710–1714.

[Ring Group 1981] Ring Group 1981. Gulf Stream cold core rings: their physics, chemistry and biology *Science* **212**, 1091-1100.

[Ripa & Heino 1999] Ripa, J. & Heino, M. 1999. Linear analysis solves two puzzles in population dynamics: the route to extinction and extinction in coloured environments. *Ecol. Lett.* **2**, 219-222.

[Ruelle & Takens 1971] Ruelle, D. & Takens, F. 1971. On the nature of tubulence *Comm. Math. Phys.* **20**, 167–192.

[Sagdeev et al. 1992] Sagdeev, R. Z., Zaslavsky, G. M., Usikov, D. A., & Chernikov, A. A. 1992. *Weak Chaos and Quasi-Regular Patterns*, (Cambridge University Press, Cambridge).

[Santoboni et al. 2002] Santoboni, G.; Nishikawa, T.; Toroczkai, Z. & Grebogi, C. 2002. Auto-catalytic reactions of active particles with phase distribution. *Chaos,* **12**, 408–417.

[Scheffer 1998] Scheffer, M. 1998. *Ecology of shallow lakes*. Chapman and Hall, London.

[Scheuring 2000] Scheuring, I. 2000. Avoiding Catch-22 of early evolution by step-wise increase in copying fidelity. *Selection* **1–3**, 135–145.

[Scheuring et al. 2000] Scheuring, I.; Károlyi, G.; Péntek, Á.; Toroczkai, Z. & Tél, T. 2000. A Model for resolving the plankton paradox: coexistence in open flow. *Freshwater Biology* **45**, 123–133.

[Scheuring 2001] Scheuring, I. 2001. Is chaos due to over-simplification in models of population dynamics? *Selection***2**, 179–191.

[Scheuring et al. 2003] Scheuring, I., Károlyi, Gy., Toroczkai, Z., Tél T. & Péntek, Á. 2003. Competing populations in flows with chaotic mixing. *Theor. Popul. Biol.* **63**, 77–90.

[Schippers et al. 2001] Schippers, P., Verschoor A.M., Vos, M. & Mooij, W.M. 2001. Does "supersaturated coexistence" resolve the paradox of the plankton? *Ecology Letters* **4**, 404–407.

[Shariff et al. 1991] Shariff, K.; Pulliam, T.H. & Ottino, J.M. 1991. A dynamical systems analysis of kinematics in the time-periodic wake of a circular cylinder. *Lect. Appl. Math.* **28**, 613–646.

[Siegel 2001] Siegel, A., Weiss, J. B., Toomre, J., McWilliams, J., Berloff, P. & Yavneh, I. 2001 Eddies and vortices in ocean basin dynamics. *Geophys. Res. Lett.* **28,** 3183–3187.

[Sievers & von Kiedrowski 1994] Sievers, D., & von Kiedrowski, G. 1994. Self-replication of complementary oligonucleotides. *Nature* **369**, 221-224.

[Sinervo & Lively 1996] Sinervo, B. & Lively, C. M. 1996. The rock-scissors-paper game and the evolution of alternative male strategies. *Nature* **340**, 240–243.

[Smith et al. 1996] Smith, C. L., Richards, K. J. & Fasham, M. J. R. 1996 The impact of mesoscale eddies on plankton dynamics in the upper ocean *Deep-Sea Res.* **43**, 1807-1832.

[Sommer 1985] Sommer, U. 1985. Comparison between steady state and non-steady state competition: experiments with natural phytoplankton *Limnology and Oceanography* **30**, 335-346.

[Sommer et al. 1993] Sommer, U.; Padisák, J.; Reynolds C.S. & Juhász-Nagy, P. 1993: Hutchinson's heritage: the diversity disturbance relationship in phytoplankton. *Hydrobiologia* **249**, 1–8.

[Sommer 2002] Sommer, U. 2002. Competition and coexistence in plankton communities. In: Sommer, U. & Worm, B. *Competition and coexistence.* Springer-Verlag, Berlin

[Sommerer et al. 1996] Sommerer, J.C.; Ku, H.-C. & Gilreath, H.E. 1996: Experimental evidence for chaotic scattering in a fluid wake. *Phys. Rev. Lett.* **77**, 5055–5058.

[Spall & Richards 2000] Spall, S. A. & Richards, K. J. 2000. A numerical model of mesoscale frontal instabilities and plankton dynamics. *Deep-Sea Res.* **47**, 1261-1301.

[Starmer et al. 1987] Starmer, W.T., Ganter, P.F., Aberdeen, V., Lachance, M. & Phaff, H.J. 1987. The ecological role of killer yeasts in natural communities of yeast. *Can. J. Microbiol.* **33**, 783–796.

[Steele 1978] Steele, J.H. 1978. *Spatial Pattern in Plankton Communities* (Plenum, New York).

[Stenseth et al. 1998] Stenseth, N. C., Chan, K.S., Framstad, E. & Tong, H. 1998. Phase- and density-dependent population dynamics in Norwegian lemmings: interaction between deterministic and stichastic processes. *Proc. Roy. Soc. B.* **265**, 1957–1968.

[Strogatz 1994] 1994. *Nonlinear dynamics and chaos: With applications to physics, biology, chemistry, and engineering.* Reading, MA: Perseus Books, Cambridge MA.

[Szabó et al. 2002] Szabó, P. Scheuring, I., Czárán, T. and Szathmáry E. 2002. In silico simulations reveal that replicators with limited dispersal evolve towards higher efficiency and fidelity. *Nature* **420**, 360–363.

[Szabó et al. 2004] Szabó, Gy., Szolnoki, A., Izsák, R. 2004. Rock-scissors-paper game on regular small-world networks. *J. Phys. A* **3**7, 2599–2609.

[Szathmáry & Gladkih 1989] Szathmáry, E., & Gladkih, I. 1989. Sub-exponential growth and coexistence of non-enzymatically replicating templates *J. Theor. Biol.* **138**, 55-58.

[Tainaka 1994] Tainaka, K. 1994. Vortices and strings in model ecosystem. *Phys. Rev. E.* **50**, 3401–3409.

[Takeuchi & Adachi 1983] Takeuchi, Y. & Adachi, N. 1983. Existence and bifurcation of stable equlibrium in two-prey-one-predator communities. *Bull. Math. Biol.* **45**, 877–900.

[Tél 1990] Tél, T. 1990. In: Bai-Lin, H. (Ed.): *Directions in chaos*, Vol. 3., pp. 149–211. World Scientific, Singapore.

[Tél et al. 2000] Tél, T.; Károlyi, G.; Péntek, Á.; Scheuring, I.; Toroczkai, Z.; Grebogi, C. & Kadtke, J. 2000. Chaotic advection, diffusion, and reactions in open flows. *Chaos* **10**, 89–98.

[Tél 2002] Tél T. 2002. *Chaotic dynamics* Nemzeti Tankönyvkiadó, Budapest. (In Hungarian)

[Tilman 1994] Tilman, D. 1994. Competition and biodiversity in spatially structured habitats *Ecology* **58**, 338-348.

[Tilman & Pacala 1993] Tilman, D. & Pacala, S. 1993. In: Ricklefs, R.E. & Schluter, D. *Species diversity in ecological communities: The maintenance of species richness in plant communities*. pp. 13–25, Univ. of Chicago Press.

[Toffoli & Margolus 1987] Toffoli, T. & Margolus, N. 1987. *Cellular automata machines: A new environment for modelling*. MIT Press, Cambridge, Mass.

[Toroczkai et al. 1997] Toroczkai, Z.; Károlyi, G.; Péntek, Á.; Tél, T.; Grebogi, C. & Yorke, J.A. 1997. Wada dye boundaries in open hydrodynamical flows. *Physica A* **239**, 235–243.

[Toroczkai et al. 1998] Toroczkai, Z.; Károlyi, G.; Péntek, Á.; Tél, T. & Grebogi, C. 1998: Advection of active particles in open chaotic flows. *Phys. Rev. Lett.* **80**, 500–503.

[Toroczkai et al. 2001] Toroczkai, Z.; Károlyi, G.; Péntek, Á. & Tél, T. 2001. Auto-catalytic reactions in systems with hyperbolic mixing: Exact results for the active baker map. *J. Phys. A*, **34**, 5215 – 5235.

[Truscott &Brindley 1994] Truscott, J. E. & Brindley, J. 1994 Equilibria, stability and exitability in a general class of plankton population models *Phil. Trans. R. Soc. Lond. A* **347**, 703-718.

[Turchin & Taylor 1992] Turchin, P. & Taylor A. D. 1992. Complex dynamics in ecological time-series. *Ecology* **73**, 289–305.

[Ulam 1960] Ulam, S. M. 1960. *Modern problems in mathematics*. Interscience Publ., New York.

[Varosi et al. 1990] Varosi, F., Antonsen, T.M., Ott, E. 1991. The spectrum of fractal dimensions of passively convected scalar gradients in chaotic fluid flows. *Phys. Fluids A* **3**, 1017–1028.

[Volterra 1925] Volterra, V. 1925. Fluctuations in the abundance of a species considered mathematically. *Nature* **118**, 558–560.

[Wächtershäuser 1994] Wächtershäuser, G. 1994: Life in a ligand sphere. *Proc. Natl. Acad. Sci. USA* **91**, 4283–4287.

[Wilson 1990] Wilson, J.B. 1990: Mechanisms of species coexistence: twelve explanations for Hutchinson's 'paradox of the plankton': evidence from New Zealand plant communities. *N. Z. J. of Ecol.* **43**, 17–42.

[Wium-Andersen et al. 1982] Wium-Andersen, S., Christophersen, C. & Houen, G. 1982. Allelopathic effects on phytoplankton by substances isolated from aquatic macrophytes (Charales). *Oikos* **39**, 187–190.

[Young et al. 2001] Young, W.R., Roberts, A.J., Stuhne, G. 2001. Reproductive pair correlations and the clustering of organisms. *Nature* **412**, 328–331.

[Zakharov et al. 1992] Zakharov, V. E., Lvov, V. S. & Falkovich, G. 1992. *Kolmogorov spektra of turbulence.* Springer-Verlag, Berlin.

[Ziemniak et al. 1994] Ziemniak, E.; Jung, C. & Tél, T. 1994. Tracer dynamics in open hydrodynamical flows as chaotic scattering. *Physica D* **76**, 123-146.

[Zielinski & Orgel 1987] Zielinski, W. S., & Orgel, L. E. 1987. Autocatalytic synthesis of a tetranucleotide analogue *Nature* **327**, 346-347.